IJAE

Italian Journal of Anatomy and Embryology

Official Organ of the Italian Society
of Anatomy and Histology

Vol. 127
N. 1
2023
ISSN 1122-6714

FIRENZE
UNIVERSITY
PRESS

IJAE
Italian Journal of Anatomy and Embryology
Official Organ of the Italian Society of Anatomy and Histology

Founded by Giulio Chiarugi in 1901

Journal e-mail: ijae@unifi.it – Web site: http://www.fupress.com/ijae

2022 Firenze University Press
Firenze University Press
via Cittadella, 7
I-50144 Firenze, Italy
E-mail: journals@fupress.com
Available online at
http://www.fupress.com/ijae

Italian Journal of Anatomy and Embryology

IJAE

Vol. 127, n. 1 - 2023

Firenze University Press

Italian Journal of Anatomy and Embryology

Published by
Firenze University Press – University of Florence, Italy
Via Cittadella, 7 - 50144 Florence - Italy
http://www.fupress.com/substantia

Direttore responsabile: **Ferdinando Paternostro, University of Firenze, Italy**
Direttore scientifico: **Domenico Ribatti, University of Bari, Italy**

IJAE
ITALIAN JOURNAL OF ANATOMY AND EMBRYOLOGY

Firenze University Press
www.fupress.com/ijae

Prof. GIOVANNI E. ORLANDINI passed away in Florence on March 5th, 2022

He was born in Florence in 1934, graduated in Medicine and Surgery at the University of Florence in July 1958 and specialised in Cardiovascular and Rheumatic Diseases at the same University in 1962 with top marks and honours.

In 1969 he moved to the University of Sassari, where he became Director of the Anatomical Institute and Full Professor of Anatomy till 1972, when he was asked by the University of Parma as Full Professor (1973) of Histology and General Embryology as well as Director of the Institute of the same name.

In 1974 he returned to the University of Florence as Full Professor of Normal Human Anatomy, where he performed several institutional roles.

From 1986 to 2001 and then again in 2007 until his retirement, he was elected Dean of the Medical Faculty. In 2004 he became Director of the Department of Anatomy, Histology and Forensic Medicine. In 2009 he was appointed Emeritus by the Italian Ministry of University and Research.

He was a member of several scientific societies: Association des Anatomistes, American Association of Anatomists, Anatomische Gesellschaft. In the latter association, he was elected President (1990-93) and then an honorary member. In the Italian Society of Anatomy since 1993, he was a member of the Board of Directors, and since 2005, he has been elected President for two triennia. In the same Society, he received in 2016 an award for his career. From 1997 to 2004, he was the Italian Board of Anatomists' President.

Giovanni Orlandini participated in many national and international congresses and organised and chaired several symposia, including the European Anatomical Congress in Florence (1995).

For more than 20 years, he was on the directory board of the College of Physicians in Florence. He also showed a noticeable civic engagement, elected to the Florence City Council (1999-2004) and vice-president of the public health Committee.

He was the Author of more than 250 publications and co-author of several textbooks in the field of Anatomy with wide national diffusion.

His scientific interests were mainly focused on the cardiovascular system and the male genital tract. His studies on arterial size have been a clear landmark for many researchers. In 1964 Prof. Orlandini started his more than 40-year period of collaboration with Prof. Holstein, Anatomist in Hamburg, on the structure, function and changes of different tracts of the male genital organs, always using innovative methods and paying great attention to the functional implications of morphology.

An expert Dissector and enthusiast of the History of Medicine and Anatomy, he published studies on Tuscan anatomists and the controversial figure of Girolamo Segato, whose national and international fame he significantly contributed to enhance. For many years, he curated and increased the collection of the Anatomy Museum of the University of Florence.

Very clear and passionate Anatomy Lecturer, Prof. Orlandini was Maestro in training, profession and life. I had the honour of assisting him in the drafting of the re-edition of Chiarugi's treatise on splanchnology and to have my signature on his latest publication, *"The anatomical representation of the human body: from epistemological examples deriving from medical history to morphometric imaging performed with the laser scanner technique"*.

At the end of a whole and serene life, surrounded by his closest affections, he left us in 2022 on March 5th.

His scientific, cultural, didactic and high-flying legacy to the Italian University and the International Anatomical and Histological Society is immeasurable; the Professor is still an unsurpassed and shining reference for all his Colleagues and Students.

Prof. Ferdinando Paternostro

ISSN 1122-6714 (print) | ISSN 2038-5129 (online) | DOI: 10.36253/ijae-14466

IJAE
ITALIAN JOURNAL OF ANATOMY AND EMBRYOLOGY

Firenze University Press
www.fupress.com/ijae

OPEN ACCESS

Citation: Francesco Maria Galassi, Elena Varotto, Mauro Vaccarezza, Veronica Papa (2023) Special issue on "Anatomical radiology and morphological studies applied to radiological and palaeoradiological contexts". *Italian Journal of Anatomy and Embryology* 127(1): 5-6. doi: 10.36253/ijae-14520

Data Availability Statement: All relevant data are within the paper and its Supporting Information files.

Competing Interests: The Author(s) declare(s) no conflict of interest.

Special issue on "Anatomical radiology and morphological studies applied to radiological and palaeoradiological contexts"

Francesco Maria Galassi[1,*], Elena Varotto[2,3], Mauro Vaccarezza[4,5], Veronica Papa[3,6,7]

[1] *Department of Anthropology, Faculty of Biology and Environmental Protection, University of Lodz, Lodz, Poland*
[2] *College of Humanities, Art and Social Sciences, Flinders University, Adelaide-SA, Australia*
[3] *Forensic Anthropology, Paleopathology and Bioarchaeology (FAPAB) Research Center, Avola, Italy*
[4] *Curtin Medical School, Faculty of Health Sciences, Curtin University, Bentley, Perth, 6102 Western Australia, Australia*
[5] *Curtin Health Innovation Research Institute (CHIRI), Faculty of Health Sciences, Curtin University, Bentley, Perth, 6102 Western Australia, Australia*
[6] *Department of Economics, Law, Cybersecurity, and Sports Sciences, University of Naples "Parthenope", Naples, Italy*
[7] *School of Science, Engineering and Health, University of Naples "Parthenope", Naples, Italy*
*Corresponding author. E-mail: francesco.galassi@biol.uni.lodz.pl

Keywords: anatomy, anthropology, morphology, mummy studies, palaeoradiology, radiology.

We would like to express our gratitude to the Italian Society of Anatomy and Histology and this journal's Editor-in-Chief, Prof. Dr. Domenico Ribatti, for kindly granting us the opportunity to launch a special monographic issue dedicated to the intersection between the field of morphological studies and that of radiology. Instead of limiting the scope of this issue to the well-studied area of "radiological anatomy", which Italian anatomical scholars know *inter alia* thanks to the masterful translation of Weir et al.'s "An Atlas of Radiological Anatomy" (*Anatomia radiologica di Weir & Abrahams. Atlante di anatomia umana per bioimmagini*, 6th edition, Edra, 2021) by V. Macchi, A. Porzionato, R. De Caro, we have opted to consider the additional applications of this field. This proves true for sub-areas of human anatomy such as palaeopathology, mummy studies and bio-anthropological research. A mini-review by V. Papa and colleagues, for instance, examines the impact of the use of non-invasive radiological techniques in the study of ancient (naturally or artificially) mummified bodies. An original contribution by C. Moraes and co-authors, instead, by re-analysing previously published tomo-

graphic and radiographic images, endeavours to offer a new anatomically grounded facial approximation of the famous Pharaoh Tutankhamun, also critically considering previous attempts presented both in scientific journals and public venues in the past. If palaeoradiology can enhance our knowledge of morphology in past individuals, we should nonetheless remark how it can also be implemented to verify, in close collaboration with the discipline of toxicology, the embalming formulas that were used by famous embalmers to preserve bodies. A reflection of this very topic makes R. Bianucci and colleagues re-open the vexed case of the Salafia embalming formula by further problematising its nature and subsequent reception by scholars.

As the discipline of human anatomy continues to evolve through time, one of the greatest lessons it never fails to teach its students is that by embracing complementary fields it can not only expand its disciplinary boundaries, but it can also increase the quality of discoveries made in closely related fields, to the benefit of learners and teachers alike.

IJAE
ITALIAN JOURNAL OF ANATOMY AND EMBRYOLOGY

Firenze University Press
www.fupress.com/ijae

OPEN ACCESS

Citation: Raffaella Bianucci, Simon T. Donell, Francesco M. Galassi, Tiziana Lanza, Grazia Mattutino, Andreas G. Nerlich, Luca Sineo (2023) The Salafia embalming formula: do it well or don't do it at all. *Italian Journal of Anatomy and Embryology* 127(1): 7-11. doi: 10.36253/ijae-14513

Data Availability Statement: All relevant data are within the paper and its Supporting Information files.

Competing Interests: The Author(s) declare(s) no conflict of interest.

The Salafia embalming formula: do it well or don't do it at all

Raffaella Bianucci[1,2,3], Simon T. Donell[4], Francesco M. Galassi[5], Tiziana Lanza[6], Grazia Mattutino[1], Andreas G. Nerlich[7], Luca Sineo[8]

[1] *Legal Medicine Section, Department of Public and Pediatric Sciences, University of Turin, Turin, Italy*
[2] *Department of Cultures and Societies, University of Palermo, Palermo, Italy*
[3] *Ronin Institute, Montclair, NJ, USA*
[4] *Norwich Medical School, University of East Anglia, Norwich, United Kingdom*
[5] *FAPAB Research Center, Avola SR, Sicily, Italy*
[6] *Istituto Nazionale di Geofisica e Vulcanologia, Rome, Italy*
[7] *Institute of Pathology, Academic Clinic Munich-Bogenhausen, Germany*
[8] *Dipartimento di Scienze e Tecnologie Biologiche Chimiche e Farmaceutiche, Università degli Studi di Palermo, Palermo, Italy*
All authors equally contributed to the paper and are listed in alphabetical order. All authors are corresponding authors. E-mail (Human Embalming Project©): heproject2021@gmail.com

Abstract. Medical imaging allows non-invasive investigation of human remains. While paleoimaging is undoubtedly necessary in mummy studies, it is intrinsically limited in the sense that it cannot provide mummy experts with information on the chemical composition of the embalming substances. This holds particularly true for modern embalmed mummies (19th-20th centuries). Since the end of the 19th century, cadavers were arterially injected with chemicals which varied depending on different methods. One of those embalming methods was Salafia's, which was much advertised in the USA. Since attempts at experimental reproduction of the Salafia method are planned by our team, a re-examination of the published literature on the formula was made. Here we provide evidence that an error in unit conversion from gallons to litres occurred and that the same mistake was repeated in the majority of the published English literature with a single exception which went unnoticed. Furthermore, we provide English speaking embalmers and mummy scholars with the complete and correct translation of the original version of Salafia's formula.

Keywords: medical imaging vs toxicology, embalming formula, Alfredo Salafia, perfection fluid, United States, historical sources

Paleoimaging allows the non-invasive investigation of human remains and is almost routinely applied in mummy studies (Loynes & Bianucci, 2021). This in order to gain both anthropological and paleopathological data and to understand whether a corpse underwent embalming and which type of cavity treatment (if any) was performed.

In modern mummies (19th-20th centuries), medical imaging has allowed scholars to suppose that chemical compounds such as arsenic or mercury were used to embalm corpses (Panzer et al. 2014). However, the information retrieved is intrinsically limited by absence of grounded chemical evidence, which can be reached exclusively via toxicological analysis. Resorting to modern techniques, it is currently possible to perform paleoproteomics and paleometabolomics on mummified and embalmed bodies with no damage to the analysed specimen (Barberis et al., 2022). The chemical data are, then, compared with the available historical sources (if any) and with the radiological ones (Loynes et al., 2017).

In the field of mummy studies, the Human Embalming Project@ team is devoted to the study of modern embalming techniques. When feasible, attempts at experimental reproduction are made (Bianucci & Nerlich, 2022). Since 2021, we have focused on the figure of Alfredo Salafia (1869-1933), a renowned Sicilian embalmer who invented the "Perfection Fluid" (Galassi et al., 2021; Bianucci et al., 2022a-c; Bianucci et al., in press 2023). This embalming fluid is claimed to allow a cadaver to preserve in a permanent fresh state (Nerlich & Bianucci, 2021). Salafia embalmed the bodies of several important Italian personages, politicians, clergymen and notables (Johnson et al., 1993). One of these, the cadaver of the Deputy and Vice-Consul of the United States, Giovanni Paterniti (died on the 1st of May 1911) is still on display at the Capuchin Catacombs of Palermo (Bianucci et al., 2022c) (Figure 1).

In 1910 to gain a reputation in the American embalmers market, Alfredo Salafia, and his nephew, Achille Salomone (1879-1947) [a licensed funeral director who had studied at The Renouard Training School for Embalmers – Founded in New York in 1895 by Auguste Renouard (https://funeraleducation.org/home/about-aami/)] performed successful demonstrations of their embalming method in New York (Johnson et al., 1993).

In order to sell the Perfection Fluid to the American embalmers, Salafia and Salomone also formed the Salafia Permanent Embalming Method Company (20th of June 1910). The company was registered as the Salafia Permanent Embalming Method Company-Achille Salomone 338 East 63Rd St. New York 10021 under Department of State Id 985, as Foreign Business Corporation entity type. The trademark of the Salafia Permanent Embalming Method Co. was filed on the 16th November 1911 [Ser. Number 59, 748 (Class 6. Chemicals, Medicines and Pharmaceutical Preparations); claims use since the 27th of October 1911] (Official Gazette of the United States Patent Office,1912; Galassi et al., 2021). While the trademark was patented, the formula was not disclosed at the time.

In May 1993, the American embalmers Johnson et al. described one of Salafia's demonstrations performed on the 23rd of April 1910 on the unclaimed body of John Flinch [quoted as Robert Flinch by Quigley (Quigley, 1998)]. He was embalmed at the Eclectic Medical College in New York using the *Salafia chemicals and procedures* (Johnson et al.,1993). Flinch *had died about ten days* and had clear signs of putrefaction (*black and green areas on the trunk, face and neck, arms, and legs).* Johnson et al. (1993) wrote that *the embalming procedure was absurdly simple, consisting solely of the injection (distally) of the right common artery with a total of 15 gallons of Salafia embalming fluid (*Johnson et al., 1993). *No blood drainage, cavity treatment, or secondary injections were resorted to. The body, unrefrigerated, was dissected in early November (1910), six months after embalming.* At dissection "*…all discolorations… had virtually disappeared…The body was well preserved, with the skin firm and moderately hard and dry. All tissue, including fat, was firm and dry. No odor of decomposition, or fecal odor, was present, only the chemical odor of the embalming fluid* (Johnson et al., 1993). The same description was reported by Quigley (1998, p. 52): *On April 23,1910, Prof. Salafia embalmed the unclaimed body of John Flinch to demonstrate the efficiency and simplicity of his process… Fifteen gallons of Salafia's embalming fluid were injected (distally) into the right common artery without draining the blood, treating the cavities, or carrying out secondary injections. The body was stored but not refrigerated.*

On the 22nd of September 1910, a second embalming demonstration on the body of David Jenkins took place *using the same procedure as in the Flinch case* (Johnson et al., 1993). Following the content of an advertisement by the American Embalmers' Association dated to 1910, originally published in Johnson et al. (1993), Quigley described the embalming procedure of David Jenkins: *A committee appointed by the New York State Embalmers' Association witnessed the embalming of the body of David Jenkins at their annual meeting in Syracuse, New York. The embalming was done by Professor Achille Salomone by his uncle's method. Jenkins' decomposing body weighed approximately 130 pounds* (58.9 Kg) *and the surface of the abdomen was green. The carotid artery was raised and six quarts of embalming fluid were injected, a difficult task because of arteriosclerosis* (Quigley, 1998, p. 52).

In March 2009, Piombino-Mascali and Johnson-Williams re-enacted the above demonstrations without noticing any difference: *His much-advertised method was characterized by simplicity: one single injection into*

Figure 1. The embalmed body of the Deputy and Vice-consul of the United States Giovanni Paterniti (died May 1st 1911) in a picture dated to the 23rd of February 2008 (Credits: Prof. Luca Sineo).

the carotid artery of 15 gallons of "Salafia Perfection Fluid" – a chemical compound said to contain nonpoisonous ingredients. No other procedure generally adopted in modern embalming, such as blood drainage, cavity treatment, or further injections appeared to be necessary.

In a second paper dated March 2009, Piombino-Mascali et al. further revealed the rest of the Salafia's secret chemical preparation which *included the use of zinc, glycerin, alcohol and salicylic acid-many of the same chemicals we use today in modern embalming preparations, with the exception of zinc* (Piombino-Mascali et al., 2009). This chemical preparation was contained in Salafia's handwritten memoires whose discovery is now attributed to Di Cristina et al. (Di Cristina et al., 2007; Galassi et al., 2021).

Following the English version of the formula published in 2009 by the Sicily Mummy Project team the Perfection Fluid was composed of *one part glycerin, one part formalin saturated with both zinc sulphate and chloride, and one part of an alcohol solution saturated with salicylic acid* (Piombino-Mascali et al., 2009).

If the scientific data provided by Johnson et al. (1993), Quigley (on the embalming of John/Robert Flinch, 1998) and Piombino-Mascali & Johnson-Williams (2009) were correct, the Salafia Perfection Fluid would have consisted of a solution of 15 gallons (1US gallon= 3.8 litres; 15 US gallons= 57 litres) made of 19 litres of glycerin, 19 litres of formalin saturated with both zinc sulphate and chloride and 19 litres of an alcohol solution saturated with salicylic acid.

It is worth noting that, while describing the embalming procedure of David Jenkins, Quigley wrote that the man, whose weight was 130 pounds (58.9 Kg), was embalmed using six quarts (1.5 US gallons) of the Salafia Perfection Fluid.

Although a discrepancy between the number of gallons used in the two demonstrations could be easily identified by reading the original 1910 advertisement, Piombino-Mascali & Johnson-Williams (2009) still reported the use of 15 US gallons while referring to Salafia's demonstrations in the USA.

It is improbable that John/Robert Flinch was really embalmed with 15 US gallons of Salafia's Perfection Fluid (57 litres per 58.9 kg) (Johnson et al., 1993; Quigley, 1998; Piombino-Mascali & Johnson-Williams, 2009) compared to David Jenkins with 1.5 US gallons (5.7 litres pr 58.9 Kg) (Quigley, 1998).

Bryant and Peck (2009) state that *modern arterial embalming involves injecting chemicals (including preservatives and tint) into the circulation system usually via the right carotid artery. The 3 to 4 gallons (1 gallon per 50 pounds of body= 3.8 litres per 22 kg) of embalming solution is injected while the embalmer massages (and perhaps washes) the corpse to ensure proper distribution of the embalming fluid*. This implies that, depending on the weight of the corpse, 11.36 to 15.142 litres are routinely injected. Furthermore, modern embalmers often resort to *a periodic opening of the jugular drain tube to allow blood to escape and prevent too much pressure from building in the vascular system*. However, it has been repeatedly stated that Salafia never resorted to blood drainage although, in case of need, he himself wrote that abdominal cavity treatment had to be performed by two operators (Piombino-Mascali, 2009, third edition 2012, p. 54).

Apparently, Salafia did not resort to multiple washes, a situation which may have justified the use of 15 gallons/57 litres of embalming fluid. It should be noted that the injection of 57 litres of embalming fluid in a corpse without draining any blood would have caused bloating of the cadaver and disruption of the vascular system.

It is evident that Salafia's experimental embalming cannot be reproduced based on the published data in the English language by Johnson et al. (1993), Quigley

(1998 describing the embalming of John/Robert Flinch) and Piombino-Mascali & Johnson-Williams (2009). Therefore, the embalmers and mummy experts cited here must have made a unit conversion error which was repeated in all published English literature with the sole exception of Quigley's description of the embalming of David Jenkins (1998).

The "15 gallons mystery" can be easily solved if the scattered Italian excerpts of Salafia's memoirs published by Piombino-Mascali (2009; third edition, 2012, p. 53) are carefully translated into English: *the operator will check the glass container and will fill it continuously before it empties in order to impede the ingress of air into the liquid and this (has to be done) until at least seven litres of embalming fluid has been introduced; and sometimes a higher quantity is needed: in this rare case, alcohol needs to be added to the glass container until the injection is completed* [Italian translation: *L'operatore avrà cura di sorvegliare la vaschetta di vetro, e riempirla sempre, prima che si svuoti, in modo di non lasciare penetrare dell'aria con il liquido e ciò sino alla introduzione di almeno sette litri di liquido conservativo, e qualche volta occorrendo una quantità maggiore: caso molto raro, si aggiunge dell'alcool nella vaschetta e ciò fino ad iniezione completa*] (Piombino-Mascali, 2009; third edition, 2012, p. 53).

The above paragraph indicates that Salafia used (at least) seven litres of embalming fluid which corresponds to 1.85 US gallons, not to 15 gallons.

Furthermore, the original Italian excerpt regarding the chemical composition of the formula was never correctly translated. Here we provide English speaking embalmers and mummy scholars with the original version of Salafia's formula (Piombino-Mascali, 2009; third edition, 2012, p. 55).

A mixture of at least 1.85 US gallons (1US gallon= 3.8 litres; 1.85 US gallons= 7 litres) made of:
1- ca. 2.33 litres of glycerin
2- ca. 2.33 litres solution of 40% formalin saturated with zinc sulphate and 10% dry chloride
3- an alcohol solution of 2.33 litres saturated with salicylic acid.
First glycerin has to be added to the formalin solution and then the alcohol solution has to be added. The whole solution has to be carefully mixed, filtered and the injection of seven liters (of the embalming solution) guarantees the perfect sterilization of the body.

We strongly encourage the Sicily Mummy Project team, which is composed of both Italian and English native speakers, to double-check the sources so as to confirm this interpretation for the scientific community. Furthermore, we encourage, for the fifth time from 2021 (Galassi et al., 2021; Bianucci et al., 2022a-c; Bianucci et al., 2023), the Sicily Mummy Project team to publish a complete open access version of the Salafia handwritten memoirs.

In case personal details are contained in the unpublished document and the legal owner does not want them to be shared with the scientific community (Piombino-Mascali & Zink, 2023), it would be sufficient to introduce the term *OMISSIS*. Lastly, we express our concerns to the scientific board of the Paleopathology Association (PPA) and to the World Committee on Mummy Studies and kindly invite them to re-analyse the "Salafia case" in the light of this new information. Free accessibility of the scientific sources to all scholars should be customarily provided.

DISCLOSURE

The authors confirm that they are entertaining a scientific debate on the case of Rosalia Lombardo with another team of authors. The references to these exchanges are offered in this article's comprehensive bibliography. The authors also confirm that the information contained in their article is true and can be verified through the references and links provided. They also specify that their study is merely aimed at assessing a scientific issue and no other third-party objectives are involved.

REFERENCES

American Academy McAllister Institute of Funeral Service, Inc. Available at https://funeraleducation.org/home/about-aami/). Accessed on May 26th 2023.

Barberis E., Manfredi M., Ferraris E., Bianucci R., Marengo E. (2022) Non-Invasive Paleo-Metabolomics and Paleo-Proteomics analysis Reveal the Complex Funerary Treatment of the Early 18th Dynasty Dignitary NEBIRI (QV30). Molecules 27 (21): 7208.

Bianucci R., Donell S.T., Galassi F.M., Lanza T., Mattutino G., Nerlich A.G., Sineo L. (2023). On the embalmer Alfredo Salafia (1869-1933) and the mummy of Rosalia Lombardo (1918-1920): science is not a "narrative". Hum. Evol. 38 (1-2).

Bianucci R., Nerlich A.G. (2022) Introducing the Human Embalming Project. Paleopathol. Newsl. 198: 24.

Bianucci R., Donell S.T., Galassi F.M., Nerlich A.G., Lanza T., Mattutino G., Sineo L. (2022a) The mummy of Rosalia Lombardo at the end of 2022: an update on status quaestionis and a reflection on the level of evidence. Hum. Evol. 37(3-4): 229-234.

Bianucci R., Donell S.T., Galassi F.M., Lanza T., Mattutino G., Nerlich A.G., Sineo L. (2022b) The Ethics of Presentation of Scientific Data and Images of Cadavers to a Popular Audience: from the Salafia embalming method to the case of Rosalia Lombardo (1918-1920). Paleopathol. Newsl. 198: 26-30.

Bianucci R., Galassi F.M., Lanza T., Mattutino G., Nerlich A.G. (2022c) What lies behind the embalmed body of Rosalia Lombardo (1918-1920)? Ital. J. Anat. Embryol. 126 (1): 5-13.

Bryant C.D., Peck D.L. (2009) The Encyclopedia of Death and the Human Experience. SAGE: Los Angeles. Pp. 406-407.

Di Cristina A, Gaziano A, Magrì R. (February 2007) La Dimora delle Anime. I Cappuccini nella Val di Mazara e il Convento di Burgio (Agrigento). Officina di Studi Medievali, Palermo. Pp. 87, 90 note 21.

Galassi F.M., Lanza T., Mattutino G., Sineo L., Nerlich, A.G., Donell S.T., Bianucci R. (2021) The discovery of the Salafia handwritten manuscript and formula: chronological and biological considerations. Arch. Antrop. Etn. 151: 1-19.

Johnson E.C., Johnson G.R., Williams-Johnson M. (1993) The Preparation Arts. The Salafia Method. Alfredo Salafia's embalming produced long-term success but how did he do it? American Funeral Director, May issue: 24-28.

Loynes R.D., Charlier P., Froesch P., Houlton T.M.R., Lallo R., Di Vella G., Bianucci R. (2017) Virtopsy shows a high-status funerary treatment in an early 18th Dynasty non-royal individual. Forensic Sci. Med. Pathol. 13 (3): 302-311.

Loynes R.D., Bianucci R. (2021) Medical Imaging in Mummy studies. In: Shin D.H., Bianucci R. (eds), The Handbook of Mummy Studies: New Frontiers in Scientific and Cultural Perspectives. Springer: Singapore, Volume 1, Chapter 12. Pp. 253-268.

Official Gazette of the United States Patent Office, Washington: Government Printing Office, Volume CLXXVI, March 1912, p 26.

Nerlich A.G., Bianucci R. (2021) Mummies in Crypts and Catacombs. In: Shin D.H., Bianucci R. (eds) The Handbook of Mummy Studies: New Frontiers in Scientific and Cultural Perspectives. Springer, Singapore, Volume 2, Chapter 31. Pp. 741-776.

Panzer S., Zink A.R., Piombino-Mascali D. (2014) Arterial angiography of "catacomb mummy" from Palermo, Sicily. J. Paleopathol. 24: 25-27.

Piombino-Mascali D., Johnson-Williams M. (2009) Alfredo Salafia: Master Embalmer. American Funeral Director, March issue: 42-45.

Piombino-Mascali D. (2009; Third edition: 2012). *Il Maestro del Sonno Eterno*. La Zisa: Palermo. Pp. 54-55.

Piombino-Mascali D., Aufderheide A.C., Johnson-Williams M., Zink A.R. (2009) The Salafia method rediscovered. Virchows Arch. 454 (3): 355-357.

Piombino-Mascali D., Zink A. (2023) Alfredo Salafia's handwritten memoir and the embalming of Rosalia Lombardo: a commentary. Anthropol. Anz. 80 (1): 113-118.

Quigley C. (1998). Modern Mummies: The Preservation of the Human Body in the Twentieth Centur*y*. McFarland Publishing: North Carolina. Pp. 50-54.

IJAE
ITALIAN JOURNAL OF ANATOMY AND EMBRYOLOGY

Firenze University Press
www.fupress.com/ijae

OPEN ACCESS

Citation: Cicero Moraes, Michael E. Habicht, Francesco M. Galassi, Elena Varotto, Thiago Beaini (2023) Pharaoh Tutankhamun: a novel 3D digital facial approximation. *Italian Journal of Anatomy and Embryology* 127(1): 13-22. doi: 10.36253/ijae-14514

Data Availability Statement: All relevant data are within the paper and its Supporting Information files.

Competing Interests: The Author(s) declare(s) no conflict of interest.

Pharaoh Tutankhamun: a novel 3D digital facial approximation

Cicero Moraes (BSc PhD h.c.)[1], Michael E. Habicht (PhD)[2], Francesco M. Galassi (MD PhD)[3,*], Elena Varotto (PhD)[3], Thiago Beaini (PhD)[4]

[1] *Arc-Team Brazil, Sinop-MT, Brazil*
[2] *College of Humanities, Art and Social Sciences, Flinders University, Adelaide-SA, Australia*
[3] *Forensic Anthropology, Paleopathology and Bioarchaeology (FAPAB) Research Center, Avola, Italy*
[4] *Faculty of Dentistry, Federal University of Uberlândia, Uberlândia-MG, Brazil*
*Corresponding author. E-mail: francescom.galassi@fapab.com

Abstract. This article offers a novel and original facial reconstruction of pharaoh Tutankhamun based on data published in the biomedical and Egyptological literature. The reconstruction adopts the Blender 3D software, running the add-on OrtogOnBlender, which allows for a refined presentation of the soft tissues. The present reconstruction is also compared to other approaches produced in the past.

Keywords: anatomy, anthropology, facial reconstruction, 3D, endocast, palaeoradiology, pharaoh, Tutankhamun.

INTRODUCTION

Born Tutankhaten (the living image of Aten) in ca. 1325 BC, in the 11th year of the reign of Pharaoh Akhenaten, his probable father, succeeded him under the name "Tutankhamun" at the age of 9, until his death approximately a decade later (Hawass & Saleem, 2016). His reign took place during the 18th Dynasty, between the years 1333/1336/1356 BC-1324/1327/1346 BC (Hawass et al., 2010, Hawass & Saleem, 2011, Rühli & Ikram, 2014). Still young he may have married his half-sister Ankhesenamun with whom he supposedly had two stillborn foetuses, one at 5-6 and the other at 9 months of gestation, both mummified and present in his tomb, KV62, found by the British Egyptologist Howard Carter (1874-1939) in 1922 in the Valley of the Kings, Egypt (Hawass et al., 2010, Hawass & Saleem, 2011, Rühli & Ikram, 2014, Hussein et al., 2013).

From the first autopsy, performed in 1925 to the present, the life and death of the young pharaoh have been shrouded in mystery, doubt, and speculation (Derry 1927). A series of hypotheses were raised about the pharaoh's state of health, some with more robust evidence, such as a diagnosis of malaria and Köhler's disease that could have contributed to the death of

the young man (Hawass & Saleem, 2016, Hawass et al., 2010), to others with less to no hard anatomo-pathological evidence such as murder due to brain injury, gynecomastia, Fröhlich Syndrome, Antley Bixler Syndrome, Marfan Syndrome and even an occasional hippopotamus attack (Rühli & Ikram, 2014, Hussein et al., 2013). More complex familial neurological conditions have also been hypothesised linking, in particular, Akhenaten and Tutankhamun (Ashrafian, 2012).

When he carried out the first analysis on Tutankhamun's body, Howard Carter did not indicate what could be the cause of the pharaoh's death: it was only in 1968 that the first X-ray images were made on that body, revealing more data and along with these, also new speculations, such as the one that attributed the death to a possible blow to the head (Boyer et al., 2003). It was then in 2005 that a computed tomography scan was performed on the body, bringing more internal structural information and, once again, highlighting the debate about the findings, since, if on the one hand the team agreed on the exclusion of the assassination hypothesis, on the other hand there was no consensus about a possible knee fracture that could have been caused in a time near Tutankhamun's death (Guardians, 2005a). In 2010, a new study, this time with the DNA of some pharaohs and family members, brought new information about the health status and potential family ties between these individuals. Thanks to this study, it was known, for example, that Tutankhamun suffered from malaria and Köhler's disease and that he was closely related to Akhenaten (KV55) and to the two foetuses found in his tomb (Hawass et al., 2010).

THE FACIAL APPROXIMATIONS OF TUTANKHAMUN (1983-2022)

Because he is a historical figure of great notoriety, Tutankhamun's facial appearance (Fig. 1) has always been a matter of general interest, even more so because of his possible familial relation to Akhenaten, known for breaking with the old religious and artistic tenets of ancient Egypt, which causes fascination and perplexities on the part of scholars and the general public, raising hypotheses ranging from the aforementioned syndromes and conditions linked to endogamy, to sensationalist, unscientific extrapolations.

Precisely because of this popularity, the pharaoh's face has been the target of a series of facial approximations using forensic techniques over the last few decades. In 1983, forensic artist Betty Pat Gatliff (1930-2020) reconstructed Tutankhamun's face from a plaster skull moulded from radiographs taken of the skull by physical anthropologist Joe Young. The face was revealed during a meeting of the Miami Society of Egyptology and published in *Life magazine* in June of that year (Sandomir, 2020, Taylor, 2001).

In 2005 the then Secretary General of the Supreme Council of Antiquities of Egypt, Dr. Zahi Hawass, presented to the world the result of the work coordinated with three teams that individually developed three facial reconstructions of Tutankhamun, based on the segmented skull from the computed tomography that had been carried out that same year. The Egyptian group was led by biomedical engineer Khaled Elsaid, who performed the reconstruction digitally with the aid of a 3D editor and was aware of the pharaoh's identity. The French team, on the contrary, was led by forensic specialist Jean-Noel Vignal and the face was modelled analogously by anthropological sculptor Elisabeth Daynes. Both also knew that it was the young pharaoh, while the American team, made up of physical anthropologist Susan Antón and forensic sculptor Michael Anderson, carried out the work completely blindly, without knowing who it was and generating, like the French team, an analogue sculpture of the face. Even though there were slight variations between the faces, the final result was very pleasing to Dr. Hawass, in his own words: "*In my opinion, the shape of the face and skull are remarkably similar to a famous image of Tutankhamun as a child, where he is shown as the sun god at dawn rising from a lotus blossom*" (Guardians, 2005b).

Furthermore, Pausch and colleagues created a bidimensional facial approximation of the profile of Tutankhamun performed from X-ray images, with the aid of the MorphMan 4.0 software (Pausch et al., 2015).

Finally, in the year 2022, Andrew Nelson, segmented and printed the skull of Tutankhamun, based on his computed tomographic scans, passing it on to the sculptor Christian Corbet so that he could proceed with the analogue facial reconstruction. The work was presented in December of that year and served as the basis for a documentary made by the North American broadcaster PBS (Havis & Murray, 2022).

MATERIALS AND METHODS

Biological anthropology is the branch of science that aims to study humankind and its biological characteristics. Primarily performed on real anatomical specimens, in recent decades it has been possible to act on volumetric digital records or images. Current technology allows producing three-dimensional material from photographs

and bidimensional images of CT scans, which significantly increases the possibilities of analysis. Therefore, none of the conclusions of this article are final and are intended only to present the techniques used, as well as to foster new questions about this person of unique historical importance. For this, the analysis by digital deformation of a skull with characteristics similar to those recorded by the Pharaoh are proposed, a facial approximation using forensic techniques was also performed, and analyses of the peculiar characteristics of the shape of this skull, as well as an approach regarding the brain capacity estimated by the volume of the skull were made. Facial approximation is an auxiliary facial recognition technique that uses the skull as a basis to approximate the face of the individual in life. The history of this technique has always been shrouded in controversy (Stephan, 2003) mainly due to the difficulty in defining what is scientific (objective) and what is art (subjective) in its approach. The present work avoids the use of the term reconstruction, replacing it with another one more consistent with its reality, that is, forensic facial approximation (Stephan, 2015), or simply facial approximation (FA). It is not just a question of adapting the name, but of using complementary approaches, based on the analysis of data extracted from living individuals, as will be explained later, in order to obtain a face supported by the maximum of objective references, leaving little room for subjective interventions by the researchers.

3D Reconstruction of the Skull

As mentioned above, the FA technique requires a skull to be made, thus the researchers sought spatial references for it so that it could be reconstructed in 3D. The team that composed this work has a broad and long experience in the structural reconstruction of scenarios from a single photo (Moraes, 2013b) and skulls from several photos (Moraes, 2013c) or orthographic images (Moraes, 2013a). Two works carried out by the authors of this publication used skulls modelled from the intersection of two-dimensional data (photos), such as the case of the pseudo-Sophocles in 2020 (Galassi et al., 2020) and Saint Vincent de Paul in 2022 (Moraes et al., 2022a).

Seeking a more robust and reliable base to provide skull structural data, the researchers searched for articles that offered capture data from tomographic slices and skull X-rays, complemented with some anthropometric measurements. Thus, a vast collection of X-ray captures was studied in the work of Boyer et al. (2003), where proportions could be raised from semi-orthographic images, but without available scale parameters. The visual observations and measurements were adjusted by the publication of Hawass and Saleem (2016), which reported the general dimensions of the skull in the X and Y axes. The study by Habicht et al. (2021) reinforced the available measures, complementing with others, providing a general adjustment for the three axes: X, Y and Z.

Two other materials, even though they are not peer-reviewed publications, were shared by the creators who had access to the tomography performed on Tutankha-

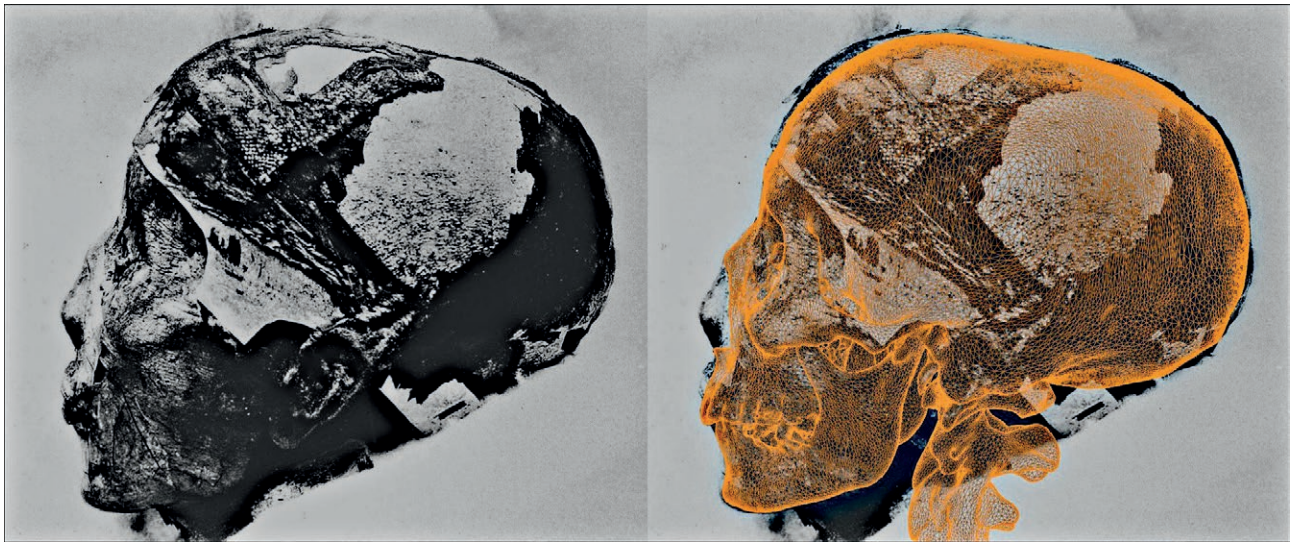

Figure 1. Photograph of Tutankhamun's head (left) and 3D skull test overlay over it. Base image credit: L0019350 A mummified human skull (Creative Commons): https://commons.wikimedia.org/wiki/File:Tutankhamun%27s_mummified_head.jpg

mun's skull and offer potential two- and three-dimensional references to the skull. One of them is a video on YouTube (https://youtu.be/HKnG5W7fvTc) made available by Corbet where, at a given moment, it is possible to see the projection of the eyeball. Knowing that, according to Taylor (2001) the diameter of such a structure is 25 mm, it would be enough to convert the pixels into millimeters and an important measure in the X axis can be found, since the deformation of perspective does not change the measurement in that region drastically. The important measure in this case is the distance between the frontomalar orbital points (fmo-fmo). Another even more precise reference is present in an article on the PHYS.org website (https://bit.ly/3Bqv1W0) about the same approximation performed by Corbet and Nelson (Havis & Murray, 2022), where there is a screenshot with the visualisation of the pharaoh's skull in the axial, sagittal and coronal planes, accompanied by the measurements in millimeters of the frames, thus a conversion from pixels to millimeters would be enough to know the measurements of such structures.

The presence of all the aforementioned materials, formally published or not, demonstrates the abundance of data available on Tutankhamun. It is thus possible to join the fragmented data, in order to reconstruct three-dimensionally, with a good degree of compatibility with the real anatomical structures, what would be the skull of the young pharaoh.

With all the data of proportions and measurements available, a skull resulting from the CT scan of a virtual donor underwent a process known as anatomical deformation (to be explained below), so that the segmented bone structure adapted to the configurations of the skull of Tutankhamun, generating the model that would be used in the facial approximation (Fig. 1).

3D Facial Approximation

Forensic facial reconstruction (FFR) or forensic facial approximation (FFA), or simply facial approximation (FA) (Stephan, 2015) is an auxiliary recognition technique, which reconstructs/approximates the face of an individual from his skull and is used when there is little information for the identification of a subject (Pereira et al., 2017). It should be noted that the technique is not about identification, such as those offered by DNA or comparative analysis of dental arches, but about recognition that can lead to subsequent identification.

The present work uses the same step-by-step approach discussed in Abdullah et al. (2022), starting with the complementation of the missing regions of the skull, followed by the projection of the profile and structures of the face from statistical data, generating the volume of the face with the aid of the anatomical deformation technique and finishing with the details of the face, configuration of the hair and generation of the final images.

The modeling process was performed in Blender 3D software, running the add-on OrtogOnBlender (http://www.ciceromoraes.com.br/doc/pt_br/OrtogOnBlender/index.html) and its submodule ForensicOnBlender. The program and its add-on are free, open source and cross-platform, hence they can run on Windows (≥ 10), MacOS (≥ BigSur) and Linux (=Ubuntu 20.04).

In the case of this work, a desktop computer with the following characteristics was used:

- Intel Core i9 9900K 3.6GHZ/16M processor; 64 GB of RAM memory
- GPU GeForce 8 GB GDDR6 256-bit RTX 2070
- Gigabyte 1151 Z390 motherboard; SSD SATA III 960 GB 2.5"
- SSD SATA III 480 GB 2.5"
- Water Cooler Masterliquid 240V
- Linux 3DCS (https://github.com/cogitas3d/Linux3DCS), based on Ubuntu 20.04.

OrtogOnBlender has cephalometry tools, for which it is necessary to distribute a series of anatomical points on the surface of the skull (S, N, A. B, t11, t21, t16, t26, Go R, Go L, Gn ans Me) and proceed with the calculation of the angles. The cephalometry chosen was that of the Universidade de São Paulo (USP) (https://bit.ly/3pKzP5Q).

RESULTS AND DISCUSSION

The results (Table 1) suggest maxillary prognathism (class II) and mandibular retrognathism, corroborating the findings of Pausch et al. (2015).

Initially, the skull was aligned to the Frankfurt horizontal plane and received a series of projections for the middle limits of regions belonging to the bones (distance between gonions on the X axis, nasospinale point on the Z axis, position of the incisors on the Z axis and position of the chin on the Z axis) and soft tissue (eyeball positioning on the X, Y and Z axes, border of the nasal wings on the X and Z axes, lips on the X axis, eyelids on the X axis and size of the ears on the Z axis) (Moraes & Suharschi, 2022). The projections covering the orbit downwards show a lower region within the expected proportions, with the dimension on the X axis between the gonion slightly larger than the average pro-

Table 1. Acronyms based on craniometric points are summarised at this link: https://bit.ly/3pKzP5Q .

Angle	Result (°)	Observation
Maxillary occlusion	22.03	10 degrees above normal
SNA	87.91	Maxillary prognathism (Class II)
SNB	79.24	Mandibular retrognathism
ANB	8.67	Skeletal class II
SNGn	70.62	Clockwise rotation of the mandible
Mandibular plane	34.73	
SNGoGn	36.81	Vertical growth trend

portion, but still within normal limits. The positions of the average and proportion of the ns point (nasospinale) coincided with that of the skull, the incisors as well, although, in general, they projected slightly downwards, which may indicate that the teeth are slightly larger than the average and projection. The mental region was positioned a little above the markers, indicating that the mandible may be smaller than the expected average/proportional structure (Fig. 2A), such characteristics corroborate the results of the USP cephalometry. A series of 36 (18 symmetrical) soft tissue thickness markers, based on measurements performed with ultrasound in 204 adult Egyptians, were distributed on the frontal portion of the face, in order to trim the limits of the skin in such regions (Fig. 2B). For the tracing of the nose, statistical data from 110 adult individuals of various ancestries were used. A base template for the projection is available at OrtogOnBlender/ForensicOnBlender, based on the work of Moraes and Suharschi (2022). Once the projection of the nose was established, a profile line was drawn using the limits of the pronasal point and the soft tissue thickness markers as a reference (Fig. 2C). To cover the regions not contemplated by the soft tissue thickness markers and to complement the volumetric approximation, the mesh of a virtual donor, composed of the soft tissue, skull and endocranium, was imported and positioned in the same space as the skull of Tutankhamun (Fig. 2D). Structural deformations are performed on the mesh, in order to convert the donor's skull into the skull of the individual to be approximated: as a side effect, the soft tissue mesh also suffers such deformation, resulting in a face with the characteristics of Tutankhamun (Fig. 2E). Although the neck region did not undergo major changes, the most important part of the process generated a profile that was very compatible with the projection made from the soft tissue thickness markers and the nasal projection (Fig. 2F). As discussed in Abdullah et al. (2022), the pre-configured face of another approximated individual is imported into the scene and deformed to fit the current face (Fig. 2G). Such a face already has hair that are adjusted according to the intended configuration (Fig. 2H) and the same applies to the material and texturing, which receives a complementary pigmentation, according to the historical data gathered and the individual's ancestry (Fig. 2I).

Two approaches related to facial approximation were worked on, one more objective and scientific and the other more subjective and artistic.

The scientific approach consisted of a bust equipped with elements closely linked to the statistical aspects of the approximation and, since the initial stage of the process was composed only of data collected from CT scans and measurements of living individuals and a compatible population, it was possible to generate an anatomically coherent image. In addition, to reduce the incompatibility in the region of the orbit, images were generated with closed eyes, as well as to avoid speculations about skin tone, the color chosen was the gray scale (Figs. 3-5).

The most artistic approach consists of a colour image, with open eyes, eyebrows and face painting (Figs. 6-8), based on data present in the press release of the approximations carried out in 2005 (Guardians, 2005b), where Dr. Hawass cites the JE 60723 sculpture (https://bit.ly/3W7SaWI). Although it contains speculative elements about the individual's appearance, as it is one aspect of this work that will be also presented to the general public, it provides the necessary elements for a complete humanisation, very difficult to achieve with just exposing the skull and deficient in the objective image in grayscale with eyes closed.

As mentioned above, when the structure of the virtual donor was deformed, a segmentation corresponding to the endocranium was also adapted to the skull of Tutankhamun (Fig. 9A, B), hence that it was possible to raise its volume to ≈1587 cm^3/ml. The measurement of head circumference resulted in 58.45 cm.

Such data were plotted as a graph, containing the volume of endocrania and circumferences of the heads of another 40 facial approximations, resulting in 41 samples (Fig. 10). It is evident that in this sample the endocranium, combined with the circumference of Tutankhamun's head, is positioned among the largest volumes. The work by Neubauer et al. (2018) with the measurement of modern endocrania, presents a general average (men and women, n=89) of 1328±164 ml, therefore the endocranium studied in this article is 259 ml above, corresponding to +1.58 SD. The volume of the endocranium is different from the volume of the brain, so that, in order to identify a factor to be used for the conversion, the virtual donor's brain was reconstructed directly from its computed tomography, with the aid of semi-automatic and manual

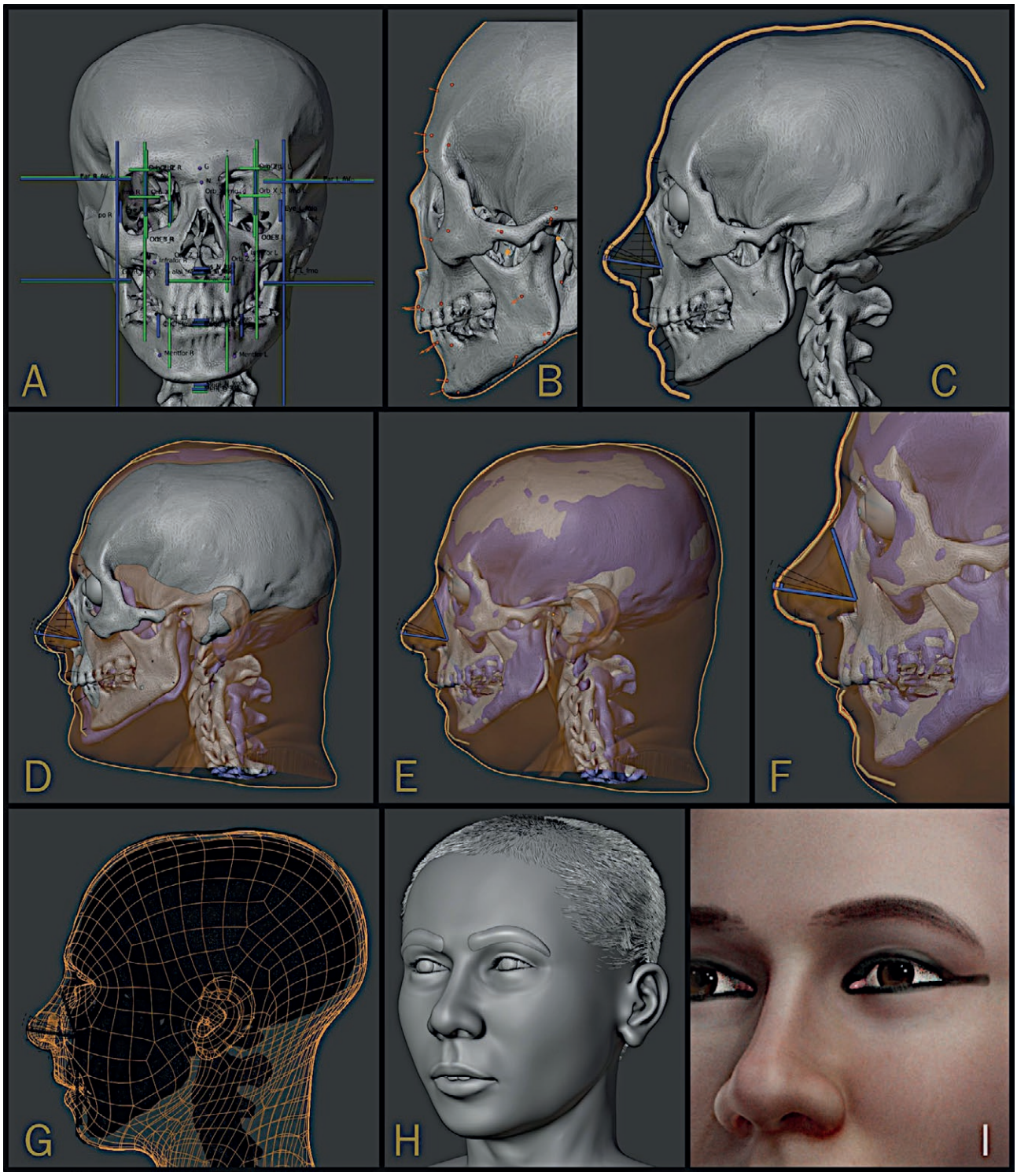

Figure 2 A-I Steps of the forensic facial approximation process.

segmentation tools in the free, open source and cross-platform software Slicer 3D (https://www.slicer.org/), using as a reference the structure presented in the work by Ritchie et al. (2018). According to the calculations raised, the volume of the brain is 9.81% smaller than that of the endocranium, so if the endocranium resulted in

Figure 3. Objective version - 3/4 view face.

Figure 5. Objective version - frontal face.

Figure 4. Objective version – face profile.

Figure 6. Coloured version – 3/4 face.

1587 cm^3, the brain would have a volume of 1431.21 cm^3. Knowing that the average for men (n=2466) is 1233.58 cm^3, Tutankhamun's brain is 197.73 cm above it, therefore, at +2.01 SD, a significantly large brain volume.

When observing the population cluster (Moraes et al. 2022b), based on midface measurements (fmo-fmo, ec, G and N), it can be seen that the skull of Tutankhamun has more affinity with the population of artificially remodeled skulls (Fig. 11), which can be explained by its atypical structure.

Figure 7. Coloured version – face profile (lateral view).

Figure 8. Coloured version – frontal view.

CONCLUSIONS

This new facial reconstruction of Tutankhamun adds to the body of Egyptological and anatomical-anthropological literature on the famous pharaoh and can be of help to both fields of research by highlighting the possibility of a new modelling technique based on the use of digitised graphic information.

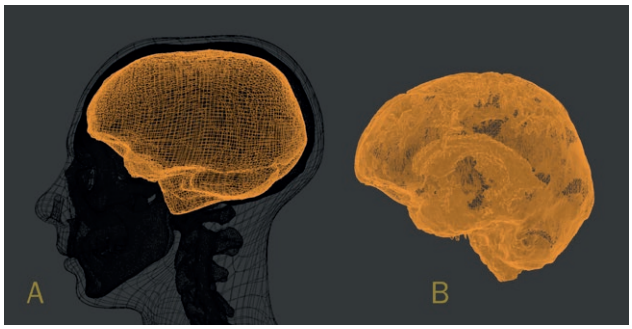

Figure 9. Tutankhamun's endocranium segmented (left) and virtual donor brain segmented (right).

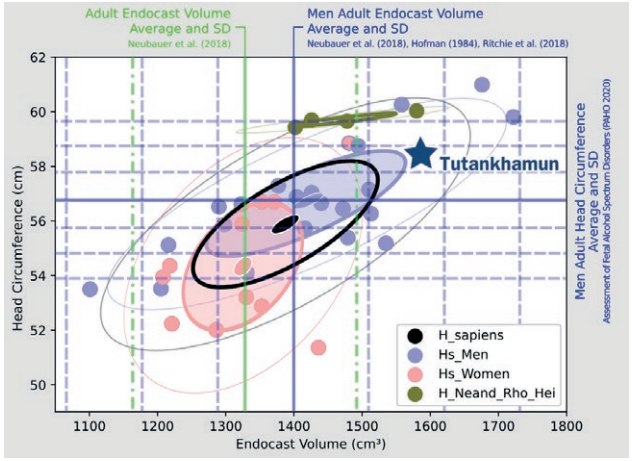

Figure 10. Distribution chart with data on endocranial volume (horizontal) and head circumference (horizontal), with means based on the work of Neubauer et al. (2018), Ritchie et al. (2018), Hofman (1984) and PAHO (2020).

ACKNOWLEDGEMENTS

To Dr. Richard Gravalos for providing the virtual donor CT scan used in this study.

REFERENCES

Abdullah J.Y., Moraes C., Saidin M., Rajion Z.A., Hadi H., Shahidan S., Abdullah J.M. (2022) Forensic Facial Approximation of 5000-Year-Old Female Skull from Shell Midden in Guar Kepah, Malaysia. Appl. Sci. 12 (15): 7871.

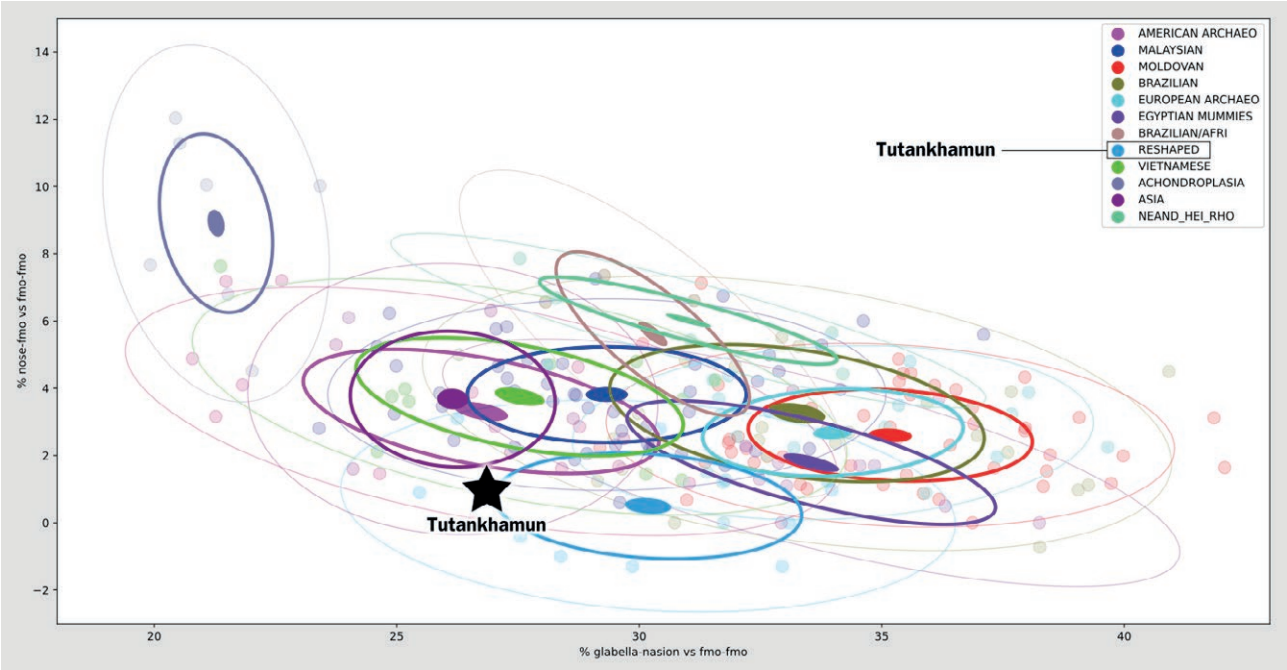

Figure 11. Population cluster with the placement of Tutankhamun in black.

Ashrafian H. Familial epilepsy in the pharaohs of ancient Egypt's eighteenth dynasty. Epilepsy Behav. 2012;25 (1): 23-31.

Boyer R.S., Rodin E.A., Grey T.C., Connolly R.C. (2003) The Skull and Cervical Spine Radiographs of Tutankhamen: A Critical Appraisal. Am. J. Neuroradiol. 24 (6): 1142-1147.

Derry D.E. (1927) Report upon the Examination of Tut-Ankh-Amen's Mummy. In: Carter H. The Tomb of Tut.ankh.Amen. Vol 2. Pp. 143-161.

Galassi F.M., Habicht M.E., Moraes C., Varotto E. (2020). The Alleged Skull of Sophocles: Anthropological and Paleopathological Confutation of a 19th Century Myth. In: Congiu M., C. Miccichè, Modeo S. (Eds.). Atti del XV Convegno di studi sulla Sicilia antica. Edizioni Lussografica, Caltanissetta. Pp. 253-268.

Guardians. (2005). Press release - 8 March 2005 -Tutankhamun CT scan results - Dr. Zahi Hawass - the Plateau - official website of Dr. Zahi Hawass. http://guardians.net/hawass/press_release_tutankhamun_ct_scan_results.htm

Guardians. (2005). Press release May 2005 - king tut facial reconstruction - Dr. Zahi Hawass - the Plateau - official website of Dr. Zahi Hawass.

Habicht M.E., Galassi F.M., Henneberg M. (2021) Cranial variation in Egyptian Pharaohs: Ancestry or microevolution? : Suggestions of family interrelations. Acta Palaeomedica 1: 61-77.

Havis M., Murray G. (2022, December 8). Face of Tutankhamun seen for the first time in over 3,300 years reconstruction. mirror. https://www.mirror.co.uk/news/world-news/face-tutankhamun-seen-first-time-28684112

Hawass Z, Gad YZ, Ismail S, et al. (2010) Ancestry and Pathology in King Tutankhamun's Family. JAMA 303 (7): 638-647.

Hawass Z., Saleem S. (2018) The CT Scan of the Mummy of Tutankhamun: New Evidence on the Life and Death of the King. In: Scanning the Pharaohs CT Imaging of the New Kingdom Royal Mummies. The American University in Cairo Press, Cairo.

Hawass Z., Saleem S.N. (2011) Mummified Daughters of King Tutankhamun: Archeologic and CT Studies. Am. J. Roentgenol. 197 (5): W829-W836.

Hofman M.A. (1984) A Biometric Analysis of Brain Size in Micrencephalics. J. Neurol. 231: 87-93.

Hussein K., Matin E., Nerlich A.G. (2013) Paleopathology of the juvenile Pharaoh Tutankhamun—90th anniversary of discovery. Virchows Arch. 463 (3): 475-479.

Moraes C. (2013.) Homo floresiensis (parte 1 de 2) – modelagem do crânio. Cicero Moraes. http://www.ciceromoraes.com.br/blog/?p=1025.

Moraes C. (2013). Convertendo Uma Pintura em Uma Cena 3D.Cicero Moraes. http://www.ciceromoraes.com.br/blog/?p=840

Moraes C. (2013). Triangulação de Pontos em 3D Por Fotografias.Cicero Moraes. http://www.ciceromoraes.com.br/blog/?p=1461

Moraes C., Suharschi I. (2022). Mensuração de Dados Faciais Ortográficos em Moldavos e Comparação com Outras Populações. figshare. https://doi.org/10.6084/M9.FIGSHARE.20089754

Moraes C., Lira J.L., Dias P.E.M., Machado M.P.S., Beaini T.L., Guimarães M.A., Dornelles R., Bueno P.H., da Silva R.H.A., da Rosa E. (2022). The 3D Aproximação Facial 3D de São Vicente de Paulo. https://doi.org/10.6084/M9.FIGSHARE.18092717.

Moraes C., Suharschi I., Abdullah J.Y., Quang D.N., Santos M.E., Machado M.P.S., Beaini T.L. (2022). Agrupamento em Clusters de Populações a partir de Comparações com a Distância Orbital Frontomalar (fmo-fmo). figshare. https://doi.org/10.6084/M9.FIGSHARE.20161013

Neubauer S., Hublin J.-J., Gunz P. (2018). The evolution of modern human brain shape. Sci. Adv. 4 (1): eaao5961.

PAHO. Assessment of Fetal Alcohol Spectrum Disorders. (2020). Pan American Health Organization. https://doi.org/10.37774/9789275122242

Pausch N.C., Naether F., Krey K.F. (2015). Tutankhamun's Dentition: The Pharaoh and his Teeth. Braz. Dent. J. 26 (6): 701-704.

Pereira J.G.D., Magalhães L.V., Costa P.B., da Silva R.H.A. (2017). Three-Dimensional Forensic Facial Reconstruction: Manual Technique vs. Digital Technique. Rev. Bras. Odontol. Leg. 4 (2): 46-54.

Ritchie S.J., Cox S.R., Shen X., Lombardo M.V. Reus L.M. Alloza C. Harris M.A. Alderson H.L. Hunter S. Neilson E. et al. (2018) Sex Differences in the Adult Human Brain: Evidence from 5216 UK Biobank Participants. Cereb. Cortex 28 (8): 2959-2975.

Rühli F.J., Ikram S. (2014) Purported medical diagnoses of Pharaoh Tutankhamun, c. 1325 BC. HOMO 65 (1): 51-63.

Sandomir R. (2020, January 14). Betty Pat Gatliff, 89, whose forensic art solved crimes, dies. The New York Times. https://www.nytimes.com/2020/01/14/science/betty-pat-gatliff-dead.html

Stephan C.N. (2003). Anthropological facial 'reconstruction' – recognizing the fallacies, 'unembracing' the errors, and performing method limits. Sci. Justice. 43 (4): 193-200.

Stephan C.N. (2015). Facial Approximation-From Facial Reconstruction Synonym to Face Prediction Paradigm. J. Forensic Sci. 60 (3): 566-571.

Taylor K.T. (2001) Three-Dimensional Facial Reconstruction on the Skull. In: Forensic art and Illustration. CRC Press, Boca Raton, Fla. Pp. 466.

IJAE
ITALIAN JOURNAL OF ANATOMY AND EMBRYOLOGY

Firenze University Press
www.fupress.com/ijae

Mini review

Discover the anatomy of the mummies: how imaging techniques contribute to understanding disease in the past

Veronica Papa[1,2,3,*], Mauro Vaccarezza[4,5], Francesco M. Galassi[6,a], Elena Varotto[1,7,a]

[1] *Forensic Anthropology, Paleopathology and Bioarchaeology (FAPAB) Research Center, Avola, Italy*
[2] *Department of Economics, Law, Cybersecurity, and Sports Sciences, University of Naples "Parthenope", Naples, Italy*
[3] *School of Science, Engineering and Health, University of Naples "Parthenope," Naples, Italy*
[4] *Curtin Medical School, Faculty of Health Sciences, Curtin University, Bentley, Perth, 6102 Western Australia, Australia*
[5] *Curtin Health Innovation Research Institute (CHIRI), Faculty of Health Sciences, Curtin University, Bentley, Perth, 6102 Western Australia, Australia*
[6] *Department of Anthropology, Faculty of Biology and Environmental Protection, University of Lodz, Lodz, Poland*
[7] *Archaeology, College of Humanities, Arts and Social Sciences, Flinders University, Adelaide, SA, Australia*
*Corresponding author. E-mail: veronica.papa@uniparthenope.it
[a] Shared last (senior) authorship.

Abstract. Mummies are the well-preserved remains of humans or animals in which non-bony tissue has been maintained naturally or artificially. Their significance lies in their contribution to paleopathological research, which involves understanding the history and evolution of diseases and providing insights into past populations' cultural and social practices. In recent years, mummies studies used nondestructive methods, including modern imaging techniques, to assess the main pathological features of these unique human remains. This mini-review focuses on the role of paleoradiology in mummies' studies and describes the history of mummy radiography and CT scanning over the last fifteen years. The search strategy was conducted between January and April 2023. One thousand one hundred twenty-four records (1124) were initially identified, and 52 studies were assessed for qualitative synthesis. Three main themes and four subthemes were identified, providing a general overview of the role of paleoradiology or offering methodological guidelines. Also, subthemes assessed the role that the use of radiology has in the diagnosis of specific pathologies. Therefore, imaging techniques in ancient human remains might help understand the history and evolution of past and present diseases and their risk factors.

Keywords: computed tomography, magnetic resonance, paleoradiology, radiography, mummies, paleopathology, review.

OPEN ACCESS

Citation: Veronica Papa, Mauro Vaccarezza, Francesco M. Galassi, Elena Varotto (2023) Discover the anatomy of the mummies: how imaging techniques contribute to understanding disease in the past. *Italian Journal of Anatomy and Embryology* 127(1): 23-34. doi: 10.36253/ijae-14549

Data Availability Statement: All relevant data are within the paper and its Supporting Information files.

Competing Interests: The Author(s) declare(s) no conflict of interest.

INTRODUCTION

The word "mummy" has a fascinating history that evolved over time. Initially, it was used to describe a black, tarry substance that was thought to have healing properties. This substance, first reported by Pliny the Elder (AD 23-79), the Roman scholar, was called "múmiyá" by the Persians, likely because it resembled wax, which the Arabs called "mum" (Aufderheide, 2003). Moreover, bitumen and asphalt, inducing dehydration, have been utilized by the ancient Egyptians in their mummification procedures and resulted in the dark or blackened appearance of the mummies' skin. Therefore, substituting this black, crystalline resin found in mummified Egyptian bodies for bitumen in medicine was made possible due to its chemical similarity in later centuries (Monge and Rühli, 2015). Consequently, the term "mumiyá" was extended to include these resins and to describe embalmed bodies. Moreover, in the eighteenth century, its clinical efficacy was demonstrated to be due to the desiccated, light-brown muscle fragments discovered in mummies' resin (Lynnerup, 2010). This evidence resulted in the word "mummy" being used to refer to any form of mummified human remains, including preserved non-skeletal tissues of the human body. Typically, soft tissue preservation happens when natural circumstances or human interventions, such as mortuary practices that might mimic environmental conditions, hinder taphonomic processes (Lynnerup, 2007). Furthermore, the outcome of soft tissue preservation varies greatly due to the collagen levels in the matrix. Generally, muscles and tendons are the soft tissues most commonly preserved. At the same time, organs of the digestive system are often entirely decomposed, and their description might anyhow be challenging due to their desiccation. Also, funerary rites might involve embalming and evisceration procedures and completely remove internal organs and the brain (Lynnerup, 2010). The study of mummies began in the late 18th century and has been intimately linked to the paleopathology of non-bony tissues. Its evolution has been substantial, and it is currently utilized to investigate the history, change, and patterns of disease in past populations. Although recent concerns have been raised regarding methodological accuracy, reliability (O'Brien et al., 2009; Cox, 2015), and even ethical issues (Kaufmann and Rühli, 2010; Kreissl Lonfat et al., 2015), mummies' studies have undeniably experienced consistent growth over the past 50 years (Nystrom, 2018). From the beginning of mummy research, unwrapping and opening mummies's body cavities has been a standard procedure, and autopsies were often performed on Egyptian mummies. Nevertheless, there is no doubt that being an invasive and destructive procedure, an autopsy undermines the integrity of the mummy as an archaeological and cultural-historical specimen. Moreover, when handling human remains, ethical, moral, and even religious issues arise since mummies, like body donors, are not merely research material (Shin and Bianucci, 2021). They do have to be considered human beings and have to be treated accordingly, including acknowledging and honoring their religious beliefs and burial traditions. (Holm, 2001; Lynnerup, 2009; Papa and Vaccarezza, 2013; Papa et al., 2022). Consequently, in more recent years, the trend in mummies studies has shifted to a clinical and medical approach based on nondestructive methods, including especially modern imaging techniques such as radiography (X-rays), computed tomography (CT scan), and magnetic resonance imaging (MRI) David and Tapp, 1984; Aufderheide, 2003; O'Brien et al., 2009; Cox, 2015) [1, 5].

Standard radiographies are non-invasive techniques commonly used to examine the internal structures of mummies. First discovered by William Röntgen (1845 –1923) in 1895, X-rays were then used by Petrie and Moodie, who, in 1931, published the first systematic analysis of a mummy collection based on radiography (Lynnerup, 2010). Furthermore, these techniques are used for both archaeological and medical purposes, such as studying amulets within mummy wrappings and estimating age and sex based on skeletal features, whenever possible. Other pathological signs eventually diagnosed by X-rays include diseases affecting skeletal or calcified structures, such as arthritis, atheroma, bone fractures, and infection-induced changes such as Pott's disease. In more recent years, a crucial improvement in the accuracy of mummies studies came from the advent of Computed Tomography (CT) scanners that allow the study of 3D skeletal and soft tissues without overlapping juxtaposed structures as in 2D radiograms. In addition, computed tomography provides paleopathologists with a sectional view of a scanned body, enabling them to non-invasively examine mummies' complete skeletons and soft tissues without disrupting their wrapping or encasement. Moreover, CT scans might be used to confirm eventual morphological similarities, prompters of family relationships or diseases, and putative causes of death (Habicht et al., 2015). Initially developed for medical imaging, CT imaging was applied to a mummy study two years after its development in 1975 (Cox, 2015). The first CT scanning of mummies was performed in 1977 by Lewin and Harwood-Nash (1977) who CT scanned an Egyptian mummy named Nakht from the Royal Ontario Museum with the purpose to evaluate the mor-

phology of the brain and eventually its pathological features (Lewin and Harwood-Nash, 1977). Since then, CT has been performed on mummies for almost 40 years and has become an increasingly popular method in mummy studies in the 21st century (Harwood-Nash, 1979). Although CT scan still represents the diagnostic gold standard for mummy studies, recent evidence demonstrated successful application of magnetic resonance with allows more effective tissue discrimination on ancient specimens compared to CT (Rühli, 2015). In addition, CT scan imaging allows 3D virtual reconstructions and the analysis on different planes.

Therefore, the aim of this study was to provide a short examination of the literature to evaluate how paleoimaging contributes to studying the history of both past and present diseases.

METHODS

A literature review was performed between January and April 2023. The steps have been assessed in the identification of the research question, the identification of relevant studies, the selection of specific studies, and finally, reporting of the results. The search strategy was designed by V.P. and E.V., validated by the senior author (F.M.G), and included the terms "Paleoradiology AND human remains OR Mummies". It was carried out in PubMed (U.S. National Library of Medicine, National Institutes of Health, Bethesda, MD), Biomed Central (BioMed Central Ltd., Springer Nature, London, UK), Scopus (Elsevier B.V., Amsterdam, the Netherlands), and Google Scholar (Google Inc., Mountain View, CA) search engines. Inclusion criteria enclosed any article published in English-language and peer-reviewed journals in the last 15 years (from 2008-2023) that focused on the role of modern imaging techniques in the paleopathology of ancient human remains and mummies. Titles, abstracts, keywords, and full texts were reviewed by two authors (V.P. and M.V.). Eventually, conflicts between reviewers were discussed until a consensus was reached, and the senior author (F.M.G.) was involved if needed. Afterward, the included records were screened, and a thematic analysis was performed. A total of 1124 records were initially identified; after duplicate removal, 332 records were further processed. Afterward, abstracts, keywords, and the complete reference list were analyzed for all articles. Only items whose abstract unequivocally discussed the topic were included. Therefore, 250 records were excluded with reason, and 82 were finally assessed for full-text screening and qualitative analysis.

The Preferred Reporting Items for Systematic Reviews and Meta-Analysis (PRISMA) flowchart was utilized for the reporting of findings (Aromataris and Riitano, 2014; Moher et al., 2015; Tricco et al., 2018) [39–41], and it is available in the Results section (see below). The records included in this study are listed in Table 1. All the authors agreed on the final number of studies included. Finally, the enrolment of records in the qualitative synthesis was made using the online Research Screener machine learning tool for systematic reviews (Chai et al., 2021). The sample in this qualitative analysis was represented by the records assessing the role of radiological techniques in the paleopathology of human remains and mummies.

Initially, the data set imported into the Research Screener machine learning tool was represented by the 82 records assessed for qualitative analysis. Credibility and reliability were ensured by debriefing and triangulation.

After extensive discussion among team members, eight (n = 8) seed articles were identified (Lynnerup, 2007, 2009, 2010; O'Brien et al., 2009; Cox, 2015; Monge and Rühli, 2015; Nystrom and Tilley, 2019; Nystrom, 2020). Moreover, 30 missing abstracts were automatically removed by the tool. Therefore, a final set of 52 abstracts was further screened. Two reviewers (V.P. and E.V.) independently flagged the abstract and coded the data into themes and subthemes, which were discussed on a regular basis.

Themes and subthemes were generated using the trial version of NVivo qualitative data analysis software package (QSR International Pty, Ltd., Melbourne, VIC, Australia). Moreover, when available, non-narrative data were extracted, categorized, and imported to Excel (Microsoft Corp., Redmond, WA) for further evaluation.

RESULTS AND DISCUSSION

The authors extensively discussed the foundations of their query. Moreover, they reviewed the pools to ensure they were consistent with the research question. Any further discrepancy was discussed to minimize bias. The authors will address three main themes and four subthemes that were used to analyze the included records. Moreover, non-narrative data were analyzed in terms of type of publication (letter to the editor, original research, review, etc.), and the radiological technique that was utilized. Fifty-two records (n=52) were finally included in the qualitative synthesis. Of those, twenty-eight (n=28; 53,8%) were categorized as original articles, 18 (34,6%) as reviews, 2 (3,84%) as letters, 1 (1,92%) as an editorial, 1 (1,92%) as a perspective, 1 (1,92%) as a note and 1 (1,92%) as a brief report. With regards to the

radiological technique that was used or discussed, CT scan was most widely exploited (n=28; 53,8%); X-rays were utilized and appraised in 7 studies (n=7; 13,46%); ultrasound and magnetic resonance in 2 studies each (n=2; 3,77%). Only one study (n=1;1,92%) used a combination of CT scans and X-rays, while in 12 (n=12; 23%) studies, this sorting criteria was not applicable. Three main themes were identified: the first related to a general review assessing the role of paleoradiology in mummies studies, the second containing methodological guidelines, and the third related to the ability of paleoradiology to diagnose or review specific pathologies in mummified remains. From the latter, three subthemes were further identified. They were related to specific diseases such as cardiovascular diseases, bone of spine diseases, and infectious, cancer and other diseases.

Themes and subthemes have been included in Table 1. Additionally, a flowchart depicting the 'Reporting items for systematic reviews' adapted from the 'Preferred reporting items for systematic reviews (PRISMA)' statement has been provided. Please refer to Figure 1 below for the flowchart.

Paleoradiography has been widely acknowledged as a crucial non-invasive method for studying ancient human remains (Lynnerup, 2007, 2009, 2010; O'Brien et al., 2009; Beckett, 2014; Cox, 2015; Lynnerup and Rühli, 2015; Moissidou et al., 2015; Rühli, 2015, 2015; Garvin and Stock, 2016; Giovannetti et al., 2016, 2022; Habicht et al., 2016; Licata et al., 2019; Nystrom, 2020), and several guidelines have been issued on its use (Panzer et al., 2015, 2017, 2018, 2019; Tanti et al., 2021). Moreover, Cramer and coworkers (Cramer et al., 2018) performed a systematic review to summarize artificial changes and detectable paleopathologies diagnosed by CT scans. Although the systematic review only included published records in PubMed, the authors demonstrated that CT analyses might be used to confirm previous conventional studies of paleopathologies and eventually identify traumatic injuries. Moreover, consistent with other findings (Jackowski et al., 2008; Panzer et al., 2010; Öhrström et al., 2021), the authors demonstrated the prevalence the typical destruction of the nasal skeleton due to the removal of the brain and identified traumatic fractures as well as chronic degenerative changes of skeletal bones and arteriosclerosis were reported in a subfraction. Finally, general consensus has been expressed in favor of using three-dimensional visualization in mummy studies. It is also worth mentioning that 14 records evaluated the presence of skeletal diseases (Jackowski et al., 2008; Panzer et al., 2010; Dalchow et al., 2012; Schamall et al., 2012; Schmidt et al., 2013; Saleem and Hawass, 2014; Fritsch et al., 2015; Márquez et al., 2015, 2015; Piombino-Mascali et al., 2015; Villa et al., 2015; Traversari et al., 2016; Beckett et al., 2020; Yatsishina et al., 2020; Öhrström et al., 2021), although some of them were heavily criticized (Beckett et al., 2020, Bianucci et al., 2021a, Bianucci et al., 2021b, Bianucci et al., 2021c). Of note, the majority of the records categorized in this subtheme, described and evaluated common and uncommon bone pathologies while Fritch and coworkers described severe rotator cuff arthropathy and rotator cuff impingement (Fritsch et al., 2015). The authors conducted a study on 52 ancient Egyptian mummies to determine the occurrence of orthopedic diseases. They systematically reviewed orthopedic diseases observed on CT scans of ancient mummies and demonstrated a higher frequency of osteoarthritic changes in the spine than in the large joints. Moreover, these authors reported for the first time a case of Perthes disease, the juvenile aseptic necrosis of the hip, and diagnosed severe rotator cuff arthropathy and rotator cuff impingement.

Seventeen records evaluated chronic, infectious, or neoplastic diseases. Cardiovascular diseases were demonstrated in 10 studies (Allam et al., 2011; Chandrashekhar and Narula, 2011; Thompson et al., 2013, 2014; Clarke et al., 2014; Wann and Thomas, 2014; Wann et al., 2015; Gabrovsky et al., 2016; Panzer et al., 2021; Herrerín et al., 2022), while 7 (Friedrich et al., 2010; Hussein et al., 2013; Lacout et al., 2016a, 2016b; Herrerin et al., 2018; Ventura et al., 2021) assessed the aforementioned pathological conditions. Today, CVD represents the leading cause of death worldwide in both men and women, accounting for at least one-third of all deaths in women and half of deaths in women over 50 years in developing countries (Vaccarezza et al., 2020). Although atherosclerosis was first identified in the mummy of an elderly Egyptian woman in 1852 and diagnosed in ancient in a calcific aortic atherosclerosis, it is still often wrongly thought to be a disease of the modern era, related to contemporary lifestyles, diet, environmental factors, and chronic inflammatory diseases (Thompson et al., 2013; Wann and Thomas, 2014). Nevertheless, CT scans on ancient mummies clearly demonstrated that atherosclerosis was prevalent even in ancient populations and suggested that this disease was present and commonplace in ancient Egypt. Therefore, challenging questions arise about the nature and extent of human predisposition to the development of atherosclerosis. Furthermore, ancient human populations had a different range of diets and lifestyles; thus, the incidence of atherosclerosis in these populations cannot be explained by traditional and modern risk factors. Instead, inhaling cooking fire smoke and chronic infection or inflammation is likely to have been crucial in developing atherogenic plaques in ancient populations. In 2016, Gabrovsky et al. (Gabrovsky et al., 2016), suggested that the chew-

Table 1. List of the included records: the table details the main features of the included records: authors, type of the study, keywords, country, and eventually, the radiological technique that has been appraised. The indication of theme and subthemes has been provided. Abbreviation: DVI, disaster victim identification; MDCT, multidetector computed tomography; CT scan, computer tomography scan; aDNA, ancient DNA; TIRADS, thyroid imaging reporting and database system; CVD, cardiovascular disease(s).

Study details	Title	Type of study	Key words	Radiological technique	Theme and subtheme
Allam AH et al. JACC: Cardiovascular imaging (2011)	Atherosclerosis in Ancient Egyptian Mummies	Original Article	Not available	CT scan	Specific pathologies-CVD
Beckett RG. Forensic Imaging (2014)	Paleoimaging: a review of applications and challenges	Review	Paleoimaging; bioarchaeology; paleoradiology; endoscopy; mummies	Not available	General review
Beckett RG et al. Forensic Imaging (2020)	A paleoimaging study of human mummies held in the mother church of Gangi, Sicily: Implications for mass casualty methodology	Original Article	Paleoimaging; paleopathology; mass casualty; DVI Sicily	X-Rays	Specific pathologies-skeletal system
Chandrashekhar Y and Narula J. JACC: Cardiovascular Imaging (2011)	Medical Imaging: The New Rosetta Stone	Editorial	Not available	Not available	Specific pathologies-CVD
Clarke EM et al. Journal of Cardiology (2014)	Is atherosclerosis fundamental to human aging? Lessons from ancient mummies	Review	Mummies; atherosclerosis; aging; paleopathology; coronary artery disease	Not available	Specific pathologies-CVD
Cox SL.The Anatomical Records (2015)	Critical Look at Mummy CT Scanning	Review	Mummy; CT scan; paleopathology	CT scan	General review
Cramer L et al. Current Problems in Diagnostic Radiology (2018)	Computed Tomography–Detected Paleopathologies in Ancient Egyptian Mummies	Review	Not available	CT scan	General review
Dalchow CV et al. Eur Arch Otorhinolaryngol (2012)	Imaging of ancient Egyptian mummies' temporal bones with digital volume tomography	Original Article	Temporal bone; computed tomography; radiology; paleoradiology; mummy; digital volume tomography; middle ear	CT scan	Specific pathologies-skeletal system
Friedrich KM et al. European Journal of Radiology (2010)	The story of 12 Chachapoyan mummies through multidetector computed tomography	Original Article	Chachapoyas Peru; mummies; computed tomography; MDCT	CT scan	Specific pathologies-other diseases
Gabrovsky AN et al. International Journal of Cardiology (2016)	Paleopathology of cardiovascular diseases in South American mummies	Original Article	Mummies;South America; atherosclerosis; cardiomegaly; coca leaf	X-Rays	Specific pathologies-CVD
Garvin HM and Stock MK. Academic Forensic Pathology (2016)	The Utility of Advanced Imaging in Forensic Anthropology	Review	Not available	Not available	General review
Giovannetti G et al. Magnetic Resonance Imaging (2016)	Magnetic resonance imaging for the study of mummies	Review	Mummy; paleoradiology; magnetic resonance; imaging; multinuclear spectroscopy	MRI	General review
Giovannetti G et al. Magnetic Resonance Imaging (2022)	Computer tomography and magnetic resonance for multimodal imaging of fossils and mummies	Review	Fossil; mummy; paleoradiology; computer tomography; magnetic resonance; imaging; multinuclear spectroscopy	CT	General review
Habicht ME et al. Yearbook of Physical Anthropology (2016)	Identifications of Ancient Egyptian Royal Mummies from the 18th Dynasty Reconsidered	Review	Pharaoh; ancient; methods; identification; CT-scan; X-ray; aDNA; molecu- lar genetics; mummy; skeleton; Thutmosis I–III; Amenhotep II; Thutmosis IV; Amenhotep III; Akhenaton; Nefertiti; Yuya; Thuya; Tije; Tutankhamun; Ay; DB 320; KV 55; KV 35; KV 62; KV 21	Not available	General review

Study details	Title	Type of study	Key words	Radiological technique	Theme and subtheme
Herrerin J et al. World Neurosurg (2018)	Syrinx in Spinal Cord in Mummified Individual from West Thebes (Egypt)	Original Article	Egypt; mummies; paleopathology; spinal cord; Syringomyelia	X-Rays	Specific pathologies-other diseases
Herrerin J et al. World Neurosurg (2022)	A Possible Stroke Victim from Pharaonic Egypt	Original Article	Not available	X-Rays	Specific pathologies-CVD
Hussein K et al. Virchows Arch (2013)	Paleopathology of the juvenile Pharaoh Tutankhamun—90th anniversary of discovery	Perspective	Paleopathology; Tutankhamun; Akhenaten; ancient Egypt	Not available	Specific pathologies-other diseases
Jackowski C et al. RadioGraphics (2008)	Common and Unexpected Findings in Mummies from Ancient Egypt and South America as Revealed by CT	Original Article	Not available	CT scan	Specific pathologies-skeletal system
Lacout A et al. American Journal of Roentgenology (2016)	Mummified Thyroid Syndrome	Original Article	Cystic-like thyroid nodule; doppler ultrasound; mummy; thyroid cancer; thyroid nodule shrinkage; thyroid nodule; TIRADS	US	Specific pathologies-other diseases
Lacout A et al. American Journal of Roentgenology (2016)	Reverse Mummified Thyroid Syndrome	Letter	Not available	US	Specific pathologies-other diseases
Licata M et al. Semin Ultrasound CT and MRI (2018)	Radiology of Mummies	Review	Not available	Not available	General review
Lynnerup N. Yearbook of Physical Anthropology (2007)	Mummies	Review	Paleopathology; bog bodies; mummified tissue; mortuary practices	Not available	General review
Lynnerup N. Anthrop. Anz (2009)	Methods in mummy research	Review	Bog bodies; mummified tissue; natural sciences in archaeology	Not available	General review
Lynnerup N.Gerontology (2010)	Medical Imaging of Mummies and Bog Bodies – A Mini-Review	Review	Mummy; bog body; paleopathology; CT scan; radiography	Not available	General review
Lynnerup N and Ruhli F. The Anatomical record (2015)	Short Review: The Use of Conventional X-rays in Mummy Studies	Review	X-rays; attenuation; mummies	X-Rays	General review
Marquez S et al. The Anatomical record (2015)	CT Examination of Nose and Paranasal Sinuses of Egyptian Mummies and Three Distinct Human Population Groups: Anthropological and Clinical Implications	Original Article	Nose; paranasal sinuses; frontal sinus; maxillary sinus; nasal complex; Egyptian mummies; CT examination	CT scan	Specific pathologies-skeletal system
Moissidou D et al. BioMed Research International (2015)	Invasive versus Non Invasive Methods Applied to Mummy Research: Will This Controversy Ever Be Solved?	Review	Not available	Not available	General review
Nystrom KC. International Journal of Paleopathology (2020)	Advances in paleopathology in context: A focus on soft tissue paleopathology	Review	South America; mummies; mummy studies	Not available	General review
O'Brien JJ et al. International Journal of Osteoarchaeology (2009)	CT Imaging of Human Mummies: A Critical Review of the Literature (1979–2005)	Review	Paleoradiology; imaging; human mummies; computerised tomography; critical review	CT scan	General review
O Fritsch K et al. The Anatomical Record (2015)	The Orthopedic Diseases of Ancient Egypt	Original Article	Orthopedic conditions; ancient Egypt mummies; CT scanning	CT scan	Specific pathologies-skeletal system

Study details	Title	Type of study	Key words	Radiological technique	Theme and subtheme
Ohrstrom LM et al. Plos One (2021)	Radiological and histological findings in ancient salt mummies from the salt mine of Douzlākh, Iran	Original Article	Not available	CT scan	Specific pathologies-skeletal system
Panzer S et al. RadioGraphics (2010)	Radiologic Evidence of Anthropogenic Mummification in the Capuchin Catacombs of Palermo, Sicily	Original Article	Not available	X-Rays	Specific pathologies-skeletal system
Panzer S et al. Fortschr Röntgenstr (2017)	Checklist and scoring system for the assessment of soft tissue preservation in CT examinations of human mummies: application to the Tyrolean iceman	Original Article	Mummy, computed tomography, checklist, organ preservation, paleoradiology	CT scan	Guidelines
Panzer S et al. International Journal of Paleopathology (2018)	CT checklist and scoring system for the assessment of soft tissue preservation in human mummies: application to catacomb mummies from Palermo, Sicily	Original Article	Computed tomography; paleoradiology; mummy; soft tissues preservation;checklist	CT scan	Guidelines
Panzer S et al. International Journal of Paleopathology (2019)	How to CT scan human mummies: Theoretical considerations and examples of use	Original Article	Paleoradiology; computed tomography; mummy	CT scan	Guidelines
Panzer S et al. Plos One (2020)	Checklist and scoring system for the assessment of soft tissue preservation in CT examinations of human mummies	Original Article	Not available	CT scan	Guidelines
Panzer S et al. International Journal of Paleopathology (2021)	Correlation of atherosclerosis and osteoarthritis in ancient Egypt: A standardized evaluation of 45 whole-body CT examinations	Original Article	Egyptian mummies; arterial calcifications; cardiovascular disease; degenerative joint disease; paleoradiology;paleopathology	CT scan	Specific pathologies-CVD
Panzer S et al. International Journal of Paleopathology (2022)	Radiological evidence of purulent infections in ancient Egyptian child mummies	Original Article	Multidetector computed tomography; abscess; infectious disease; paleoradiology; paleopathology; ancient Egyptian medicine	CT scan	Specific pathologies-other diseases
Piombino-Mascali D et al. The Anatomical record (2015)	Paleoradiology of the Savoca Mummies, Sicily, Italy (18th–19th Centuries AD)	Original Article	Mummies; paleoradiology; paleopathology; social status; Italy	X-Rays	Specific pathologies-skeletal system
Ruhli FJ. The Anatomical Records (2015)	Short Review: Magnetic Resonance Imaging of Ancient Mummies	Review	Radiology; computed tomography; mummy; paleo-pathology; soft tissue	MRI	General review
Saleem SN and Hawass Z. Arthritis & Rheumatology (2014)	Ankylosing Spondylitis or Diffuse Idiopathic Skeletal Hyperostosis in Royal Egyptian Mummies of the 18th–20th Dynasties? Computed Tomography and Archaeology Studies	Brief Report	Not available	CT scan	Specific pathologies-skeletal system

Study details	Title	Type of study	Key words	Radiological technique	Theme and subtheme
Schamall D et al. Wien Med Wochenschr (2012)	Diagnosis of contact injuries in a mediaeval skeleton analysed by μCT and histology	Original Article	Monteggia fracture; micro-computed tomography; paleopathology; paleoradiology, Bone histology	CT scan	Specific pathologies-skeletal system
Schmidt C et al. Eur Arch Otorhinolaryngol (2013)	Measurement and comparison of labyrinthine structures with the digital volume tomography: ancient Egyptian mummies' versus today's temporal bones	Original Article	Temporal bone; computed tomography; radiology; paleoradiology; mummy; digital volume tomography; semicircular canal; Labyrinth Cochlea Standardized measurement	CT scan	Specific pathologies-skeletal system
Tanti M et al. Plos One (2021)	Automated segmentation of microtomography imaging of Egyptian mummies	Original Article	Not available	CT scan	Guidelines
Thompson RC et al. Lancet (2013)	Atherosclerosis across 4000 years of human history: The Horus study of four ancient populations	Original Article	Not available	CT scan	Specific pathologies-CVD
Thompson RC et al. Global Heart (2014)	Computed Tomographic Evidence of Atherosclerosis in the Mummified Remains of Humans From Around the World	Review	Not available	CT scan	Specific pathologies-CVD
Traversari M et al. BMSAP (2016)	Three cases of developmental dysplasia of the hip on partially mummified human remains (Roccapelago, Modena, 18th Century): a study of paleopathological indicators through direct analysis and 3D virtual models	Note	Paleopathology; DDH; joint pathology; natural mummies; paleoradiology; risk factors	CT scan	Specific pathologies-skeletal system
Ventura L et al. Virchows Archiv (2021)	Giant cell tumor of bone in an eighteenth-century Italian mummy	Original Article	Osteoclastic giant cell–rich tumors; giant cell tumor; non-ossifying fibroma; osteoclastoma; benign fibrous histiocytoma; fibrous cortical defect	CT scan	Specific pathologies-other diseases
Villa C et al. Anthropol. (2015)	The advantage of CT scans and 3D visualizations in the analysis of three child mummies from the Graeco-Roman Period	Original Article	mummies; CT scan; 3D visualization; Graeco-Roman period; hyperdontia.	CT scan	Specific pathologies-skeletal system
Wann S and Thomas GS. Trends in cardiovascular Medicine (2014)	What can ancient mummies teach us about atherosclerosis?	Original Article	Not available	CT scan	Specific pathologies-CVD
Wann S et al. JAMA Network Open (2019)	Atherosclerosis in 16th-Century Greenlandic Inuit Mummies	Letter	Not available	CT scan	Specific pathologies-CVD
Yatsishina EB et al Crystallography Reports (2020)	CT-Scanning Analysis of the Inner Structure of Ancient Egyptian Mummy	Original Article	Not available	CT scan; X-rays	Specific pathologies-skeletal system

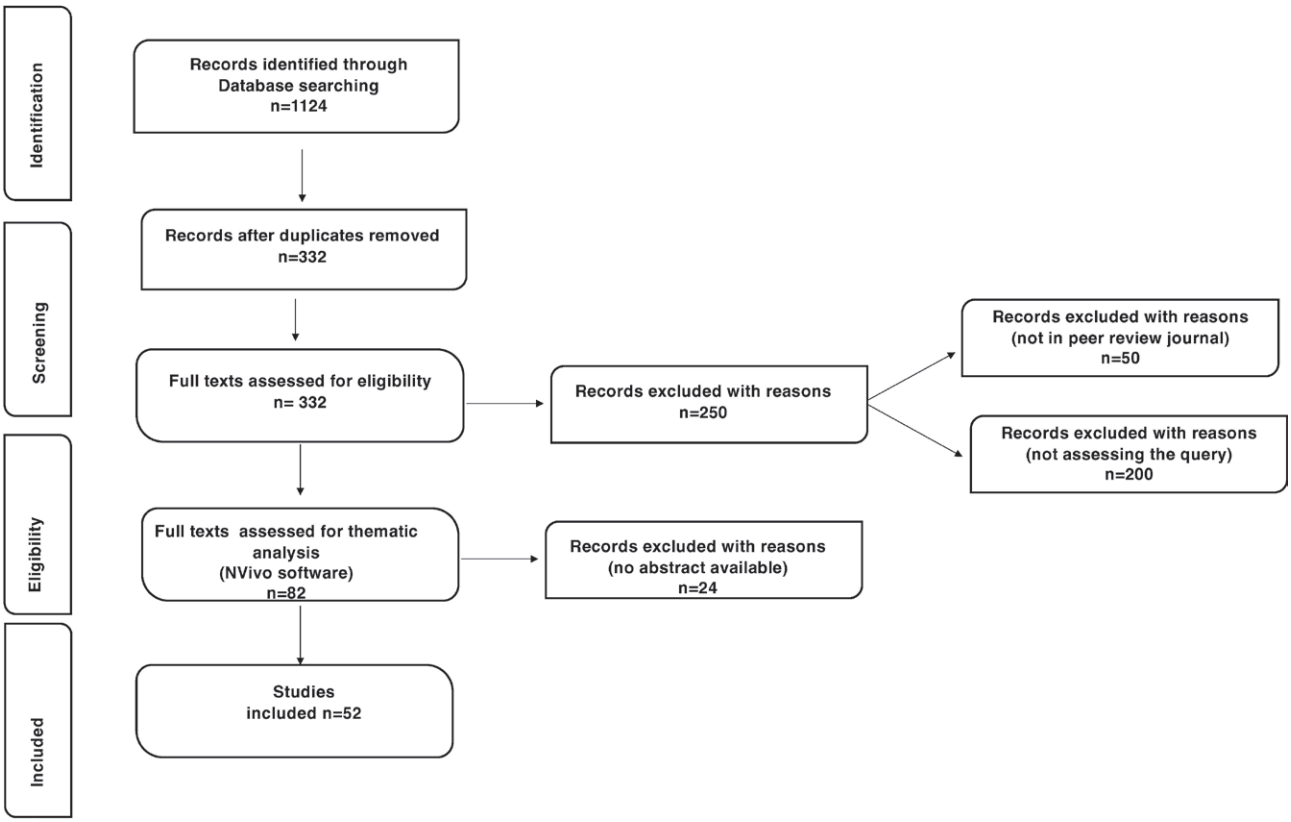

Figure 1.

ing of coca leaves, a habitual cultural practice unique to South American populations might have beneficial effects in decreasing cardiovascular risk among ancient people living in South America. Moreover, Panzer et al. (Panzer et al., 2021), tried to correlate atherosclerosis and osteoarthritis in mummies from ancient Egypt. The authors examined the whole-body CT of 45 mummies and demonstrated for the first time a possible correlation between these diseases with enormous and increasing impacts on public health. The association of atherosclerosis and osteoarthritis was found to be comparable in prevalence to those reported in recent clinical studies, despite the low life expectancy and the different environments and lifestyles of the ancient Egyptians. More recently, studying an ancient female mummy, Herrerın and coworkers (Herrerín et al., 2022) reported the earliest known case of hemiparalysis due to a cerebral stroke, while in previous years the first paleopathological case of stroke was identified by Galassi and colleagues also thanks to CT scan imaging (Galassi et al., 2017, Nerlich et al., 2021). A case of osteoma was reported by Friedrich and coworkers, who assessed the anthropological and paleopathological features of 12 Chachapoyan mummies (Friedrich et al., 2010). More recently, Lacourt and coworkers highlighted the sonographic characteristics of thyroid tumors in mummified tissue (Lacout et al., 2016a, 2016b). Finally, Panzer et al. (Panzer et al., 2022) were the first to describe radiological evidence of purulent infection and skin lesions in ancient Egyptian child mummies.

CONCLUSIONS

According to Monge and coworkers "The raison d'etre for the scientific study of mummies is to understand the evolution of health and disease in previous or extinct populations of humans" (Monge and Rühli, 2015). From this perspective, paleoradiography represents a valuable and crucial non-invasive method to study a broard range of ancient disease and to review modern-day beliefs.

REFERENCES

Allam A.H., Thompson R.C., Wann L.S., Miyamoto M.I., Nur el-Din A el-Halim, Maksoud G.A. el- Al-Tohamy Soliman M., Badr I., Amer H.A. el-Rahman,

Sutherland M.L., Sutherland J.D., Thomas G.S. (2011) Atherosclerosis in Ancient Egyptian Mummies. JACC: Cardiovascular Imaging 4:315–327.

Aromataris E., Riitano D. (2014) Constructing a search strategy and searching for evidence. A guide to the literature search for a systematic review. Am J Nurs 114:49–56.

Aufderheide A.C. (2003) The Scientific Study of Mummies. Cambridge, UK ; New York: Cambridge University Press.

Beckett R.G. (2014) Paleoimaging: a review of applications and challenges. Forensic Sci Med Pathol 10:423–436.

Beckett R.G., Conlogue G.J., Viner M.D., Saleem S.N., Said A.H., Piombino-Mascali D. (2020) A paleoimaging study of human mummies held in the mother church of Gangi, Sicily: Implications for mass casualty methodology. Forensic Imaging 23:200416.

Bianucci R., Sineo L., Miccichè R., Mattutino G., Nerlich A.G., Donell S.T., Galassi F.M. (2021a) A paleoimaging study of human mummies held in the Mother Church of Gangi, Sicily: Implications for mass casualty methodology Forensic Imaging. 24:200426

Bianucci R., Sineo L., Miccichè R., Mattutino G., Nerlich A.G., Donell S.T., Galassi F.M. (2021b) Correspondence re Piombino-Mascali et al on Mummy Research, Ethics and Editorial Comments,

Forensic Imaging. 25, 200447.

Bianucci R., Sineo L., Miccichè R., Mattutino G., Nerlich A.G., Donell S.T., Galassi F.M. (2021c) Beckett RG et al. A Paleoimaging study of human mummies held in the mother church of Gangi, Sicily: Implications for mass casualty methodology. Forensic Imaging.

Volume 24: 200430.

Chai K.E.K., Lines R.L.J., Gucciardi D.F., Ng L. (2021) Research Screener: a machine learning tool to semi-automate abstract screening for systematic reviews. Syst Rev 10:93.

Chandrashekhar Y., Narula J. (2011) Medical Imaging: The New Rosetta Stone. JACC: Cardiovascular Imaging 4:440–443.

Clarke E.M., Thompson R.C., Allam A.H., Wann L.S., Lombardi G.P., Sutherland M.L., Sutherland J.D., Cox S.L., Soliman M.A.-T., Abd el-Maksoud G., Badr I., Miyamoto M.I., Frohlich B., Abdel-Halim Nur eldin, Stewart A.F.R., Narula J., Zink A.R., Finch C.E., Michalik D.E., Thomas G.S. (2014) Is atherosclerosis fundamental to human aging? Lessons from ancient mummies. J. Cardiol. 63:329–334.

Cox S.L. (2015) A Critical Look at Mummy CT Scanning. Anat Rec 298:1099–1110.

Cramer L., Brix A., Matin E., Rühli F., Hussein K. (2018) Computed Tomography–Detected Paleopathologies in Ancient Egyptian Mummies. Curr Probl Diagn Radiol. 47:225–232.

Dalchow C.V., Schmidt C., Harbort J., Knecht R., Grzyska U., Muenscher A. (2012) Imaging of ancient Egyptian mummies' temporal bones with digital volume tomography. Eur Arch Otorhinolaryngol. 269:2277–2284.

David A.R., Tapp E. (1984) Evidence Embalmed: Modern Medicine and the Mummies of Ancient Egypt. Manchester University Press. 198 p.

Friedrich K.M., Nemec S., Czerny C., Fischer H., Plischke S., Gahleitner A., Viola T.B., Imhof H., Seidler H., Guillen S. (2010) The story of 12 Chachapoyan mummies through multidetector computed tomography. Eur J Radiol. 76:143–150.

Fritsch K.O., Hamoud H., Allam A.H., Grossmann A., Nur El-Din A-H., Abdel-Maksoud G., Al-Tohamy Soliman M., Badr I., Sutherland J.D., Linda Sutherland M., Akl M., Finch C.E., Thomas G.S.,

Wann L. S., Thompson R.C. (2015) The Orthopedic Diseases of Ancient Egypt: orthopedic diseases of ancient Egypt. Anat Rec. 298:1036–1046.

Gabrovsky A.N., O'Neill K.D., Gerszten E. (2016) Paleopathology of cardiovascular diseases in South American mummies. I J Cardiol. 223:101–107.

Galassi F.M., Habicht M.E., Rühli F.J., De Carolis S. (2017) A Unique Case of Stroke and Upper Limb Paralysis in a Mid-18th Century Natural Mummy. Circ Res. 121(4):338-340.

Garvin H.M., Stock M.K. (2016) The Utility of Advanced Imaging in Forensic Anthropology. Acad Forensic Pathol. 6:499–516.

Giovannetti G., Guerrini A., Carnieri E., Salvadori P.A. (2016) Magnetic resonance imaging for the study of mummies. Magnetic Resonance Imaging 34:785–794.

Giovannetti G., Guerrini A., Minozzi S., Panetta D., Salvadori P.A. (2022) Computer tomography and magnetic resonance for multimodal imaging of fossils and mummies. Magn Reson Imaging 94:7–17.

Habicht M.E., Bouwman A.S., Rühli F.J. (2016) Identifications of ancient Egyptian royal mummies from the 18th Dynasty reconsidered: Identifications of Ancient Egyptian Royal Mummies. Am J Phys Anthropol. 159:216–231.

Habicht M.E., Henneberg M., Öhrström L.M., Staub K., Rühli F.J. (2015). Body height of mummified pharaohs supports historical suggestions of sibling marriages. Am J Phys Anthropol. 157:519–525.

Harwood-Nash D.C. (1979) Computed tomography of ancient Egyptian mummies. J Comput Assist Tomogr 3:768–773.

Herrerin J., Prats A., Ledesma L., Isidro A. (2018) Syrinx in Spinal Cord in Mummified Individual from West Thebes (Egypt). World Neurosurg.118:230–234.

Herrerín J., Sánchez M.A., Ikram S. (2022) A Possible Stroke Victim from Pharaonic Egypt. World Neurosurg.165:e664–e667.

Holm S. (2001) The Privacy of Tutankhamen – Utilising The Genetic Information In Stored Tissue Samples. Theor Med Bioeth. 22:437–449.

Hussein K., Matin E., Nerlich A.G. (2013) Paleopathology of the juvenile Pharaoh Tutankhamun—90th anniversary of discovery. Virchows Arch. 463:475–479.

Jackowski C., Bolliger S., Thali M.J. (2008) Common and Unexpected Findings in Mummies from Ancient Egypt and South America as Revealed by CT. RadioGraphics 28:1477–1492.

Kaufmann I.M., Ruhli F.J. (2010) Without "informed consent"? Ethics and ancient mummy research. J Med Ethics.36:608–613.

Kreissl Lonfat B.M., Kaufmann I.M., Rühli F. (2015) A Code of Ethics for Evidence-Based Research With Ancient Human Remains. Anat Rec 298:1175–1181.

Lacout A., Chevenet C., Marcy P-Y. (2016a) Reverse Mummified Thyroid Syndrome. AJR Am J Roentgenol 207:W23–W23.

Lacout A., Chevenet C., Marcy P-Y. (2016b) Mummified Thyroid Syndrome. AJR Am J Roentgenol 206:837–845.

Lewin P.K., Harwood-Nash D.C. (1977) Computerized axial tomography in medical archeology. Paleopathol Newsl 8–9.

Licata M., Tosi A., Larentis O., Rossetti C., Lorio S., Pinto A. (2019) Radiology of Mummies. Semin Ultrasound CT MR. 40:5–11.

Lynnerup N. (2007) Mummies. Am J Phys Anthropol. 134:162–190.

Lynnerup N. (2009) Methods in mummy research. Anthranz. 67:357–384.

Lynnerup N. (2010) Medical Imaging of Mummies and Bog Bodies – A Mini-Review. Gerontology 56:441–448.

Lynnerup N., Rühli F. (2015) Short Review: The Use of Conventional X-rays in Mummy Studies: CONVENTIONAL X-RAYS IN MUMMY STUDIES. Anat Rec. 298:1085–1087.

Nerlich A.G., Galassi F.M., Bianucci R. (2021). The Burden of Arteriosclerotic Cardio-vascular Disease in Ancient Populations. In: Shin D., Bianucci R. (Eds). The Handbook of Mummy Studies. Singapore, Springer Nature, pp. 147-162.

Márquez S., Lawson W., Mowbray K., Delman B.N., Laitman J.T. (2015) CT Examination of Nose and Paranasal Sinuses of Egyptian Mummies and Three Distinct Human Population Groups: Anthropological and Clinical Implications. Anat Rec. 298:1072–1084.

Moher D., Shamseer L., Clarke M., Ghersi D., Liberati A., Petticrew M., Shekelle P., Stewart L.A., PRISMA-P Group. (2015) Preferred reporting items for systematic review and meta-analysis protocols (PRISMA-P) 2015 statement. Syst Rev. 4:1.

Moissidou D., Day J., Shin D.H., Bianucci R. (2015) Invasive versus Non-Invasive Methods Applied to Mummy Research: Will This Controversy Ever Be Solved?. Biomed Res Int. 1–7.

Monge J.M., Rühli F. (2015) The Anatomy of the Mummy: Mortui Viventes Docent- When Ancient Mummies Speak to Modern Doctors. Anat Rec. 298:935–940.

Nystrom K.C. (2018) The Bioarchaeology of Mummies. New York: Routledge.

Nystrom K.C. (2020) Advances in paleopathology in context: A focus on soft tissue paleopathology. Int J of Paleopath 29:16–23.

Nystrom K.C, Tilley L. (2019) Mummy studies and the bioarchaeology of care. Int J Paleopathol.25:64–71.

O'Brien J.J., Battista J.J., Romagnoli C., Chhem R.K. (2009) CT imaging of human mummies: a critical review of the literature (1979-2005). Int J Osteoarchaeol. 19:90–98.

Öhrström L.M., Marquez H., Seiler R., Bode B., Aali A., Stöllner T., Rühli F.J. (2021) Radiological and histological findings in ancient salt mummies from the salt mine of Douzlākh, Iran. PLoS ONE 16:e0250745.

Panzer S., Augat P., Sprenger M., Zesch S., Rosendahl W., Sutherland M.L., Thompson R.C., Paladin A., Zink A.R. (2021) Correlation of atherosclerosis and osteoarthritis in ancient Egypt: A standardized evaluation of 45 whole-body CT examinations. Int J Paleopathol.33:137–145.

Panzer S., Augat P., Zink A.R., Piombino-Mascali D. (2018) CT checklist and scoring system for the assessment of soft tissue preservation in human mummies: application to catacomb mummies from Palermo, Sicily. Int J Paleopathol.20:50–59.

Panzer S., Ketterl S., Bicker R., Schoske S., Nerlich A.G. (2019) How to CT scan human mummies: Theoretical considerations and examples of use. Int J Paleopathol.26:122–134.

Panzer S., Mc Coy M.R., Hitzl W., Piombino-Mascali D., Jankauskas R., Zink A.R., Augat P. (2015) Checklist and Scoring System for the Assessment of Soft Tissue Preservation in CT Examinations of Human Mummies. PLoS ONE 10:e0133364.

Panzer S., Pernter P., Piombino-Mascali D., Jankauskas R., Zesch S., Rosendahl W, Hotz G., Zink A.R. (2017)

Checklist and Scoring System for the Assessment of Soft Tissue Preservation in CT Examinations of Human Mummies: Application to the Tyrolean Iceman. Fortschr Röntgenstr 189:1152–1160.

Panzer S., Treitl M., Zesch S., Rosendahl W., Helmbold-Doyé J., Thompson R.C., Zink A.R. (2022) Radiological evidence of purulent infections in ancient Egyptian child mummies. Int J Paleopathol.36:30–35.

Panzer S., Zink A.R., Piombino-Mascali D. (2010) Scenes from the Past: Radiologic Evidence of Anthropogenic Mummification in the Capuchin Catacombs of Palermo, Sicily. RadioGraphics 30:1123–1132.

Papa V., Vaccarezza M. (2013) Teaching anatomy in the XXI century: New aspects and pitfalls. The Scientific World Journal.

Papa V., Varotto E., Galli M., Vaccarezza M., Galassi F.M. (2022) One year of anatomy teaching and learning in the outbreak: Has the Covid-19 pandemic marked the end of a century-old practice? A systematic review. Anat Sci Educ. 15:261–280.

Piombino-Mascali D., Jankauskas R., Zink A.R., Sergio Todesco M., Aufderheide A.C., Panzer S. (2015) Paleoradiology of the Savoca Mummies, Sicily, Italy (18th-19th Centuries AD). Anat Rec. 298:988–1000.

Rühli F.J. (2015) Short Review: Magnetic Resonance Imaging of Ancient Mummies: MRI of Ancient Mummies. Anat Rec. 298:1111–1115.

Saleem S.N., Hawass Z. (2014) Brief Report: Ankylosing Spondylitis or Diffuse Idiopathic Skeletal Hyperostosis in Royal Egyptian Mummies of the 18th-20th Dynasties? Computed Tomography and Archaeology Studies: AS or Dish in Royals of Ancient Egypt. Arthritis Rheumatol 66:3311–3316.

Schamall D., Pietschmann P., Moser D., Dockner M., Teschler-Nicola M. (2012). Diagnosis of contact injuries in a mediaeval skeleton analysed by μCT and histology. Wien Med Wochenschr. 162:386–393.

Schmidt C., Harbort J., Knecht R., Grzyska U., Muenscher A., Dalchow C.V. (2013) Measurement and comparison of labyrinthine structures with the digital volume tomography: ancient Egyptian mummies' versus today's temporal bones. Eur Arch Otorhinolaryngol. 270:831–840.

Shin D.H., Bianucci R. (2021) The Handbook of Mummy Studies. Singapore; Springer.

Tanti M., Berruyer C., Tafforeau P., Muscat A., Farrugia R., Scerri K., Valentino G., Solé V.A., Briffa J.A. (2021) Automated segmentation of microtomography imaging of Egyptian mummies. PLoS ONE 16:e0260707.

Thompson R.C., Allam A.H., Lombardi G.P., Wann L.S., Sutherland M.L., Sutherland J.D., Soliman MA-T., Frohlich B., Mininberg D.T., Monge J.M., Vallodolid C.M., Cox S.L., Abd el-Maksoud G., Badr I., Miyamoto M.I., el-Halim Nur el-din A., Narula J, Finch C.E., Thomas G.S. (2013) Atherosclerosis across 4000 years of human history: the Horus study of four ancient populations. The Lancet 381:1211–1222.

Thompson RC, Allam AH, Zink A, Wann LS, Lombardi GP, Cox SL, Frohlich B, Sutherland ML, Sutherland JD, Frohlich TC, King SI, Miyamoto MI, Mongeyy J.M., Valladolid C.M., Abd el-Halim Nur el-din, Narula J., Thompson A.M., Finch C.E., Thomas G.S. (2014). Computed Tomographic Evidence of Atherosclerosis in the Mummified Remains of Humans From Around the World. gHERITAGE. 9:187.

Traversari M., Feletti F., Vazzana A., Gruppioni G., Frelat M.A. (2016) Three cases of developmental dysplasia of the hip on partially mummified human remains (Roccapelago, Modena, 18th Century): a study of paleopathological indicators through direct analysis and 3D virtual models. BMSAP 28:202–212.

Tricco AC, Lillie E, Zarin W, O'Brien KK, Colquhoun H, Levac D, Moher D, Peters MDJ, Horsley T, Weeks L, Hempel S, Akl EA, Chang C., McGowan J., Stewart L., Hartling L., Aldcroft A., Wilson M.G., Garritty C., Lewin S., Godfrey C.M., Macdonald M.T., Langlois E.V., Soares-Weiser K., Moriarty J., Clifford T., Tuncalp O., Straus S.E. (2018) PRISMA Extension for Scoping Reviews (PRISMA-ScR): Checklist and Explanation. Ann Intern Med. 169:467–473.

Vaccarezza M., Papa V., Milani D., Gonelli A., Secchiero P., Zauli G., Gemmati D., Tisato V. (2020) Sex/gender-specific imbalance in CVD: Could physical activity help to improve clinical outcome targeting CVD molecular mechanisms in women? Int J Mol Sci. 21:1–16.

Ventura L., Petrella E., Piciucchi S., Cilli E., Luiselli D., Feeney R.N.M., Traversari M. (2021) Giant cell tumor of bone in an eighteenth-century Italian mummy. Virchows Arch. 479:1255–1261.

Villa C., Davey J., Craig P.J.G., Drummer O.H., Lynnerup N. (2015). The advantage of CT scans and 3D visualizations in the analysis of three child mummies from the Graeco-Roman Period. Anthranz. 72:55–65.

Wann L.S., Lombardi G., Ojeda B., Benfer R.A., Rivera R., Finch C.E., Thomas G.S., Thompson R.C. (2015) The Tres Ventanas Mummies of Peru: Tres Ventanas Mummies of Peru. Anat Rec. 298:1026–1035.

Wann S, Thomas GS. 2014. What can ancient mummies teach us about atherosclerosis? Trends Cardiovasc Med 24:279–284.

Yatsishina E.B., Vasilyev S.V., Vasilieva O.A., Galeev R.M., Dyuzheva O.P., Kovalchuk M.V. (2020) CT-Scanning Analysis of the Inner Structure of Ancient Egyptian Mummy. Crystallogr Rep. 65:1064–1072.

IJAE
ITALIAN JOURNAL OF ANATOMY AND EMBRYOLOGY

Firenze University Press
www.fupress.com/ijae

Citation: Antonio Centofanti, Michele Runci Anastasi, Angelo Favaloro, Francesco Saverio De Ponte, Luciano Catalfamo, Giuseppina Cutroneo, Giovanna Vermiglio (2023) Effects of low dose bisphosphonates treatment on the mandibular bone in rats with and without mini-implants application: an experimental model. *Italian Journal of Anatomy and Embryology* 127(1): 35-44. doi: 10.36253/ijae-14217

Data Availability Statement: All relevant data are within the paper and its Supporting Information files.

Competing Interests: The Author(s) declare(s) no conflict of interest.

Effects of low dose bisphosphonates treatment on the mandibular bone in rats with and without mini-implants application: an experimental model

Antonio Centofanti[1], Michele Runci Anastasi[2,*], Angelo Favaloro[1], Francesco Saverio De Ponte[1], Luciano Catalfamo[1], Giuseppina Cutroneo[1], Giovanna Vermiglio[1]

[1] *Department of Biomedical and Dental Sciences and Morphofunctional Imaging, University of Messina, 98124 Messina, Italy*
[2] *I.R.C.C.S. Neurolesi "Bonino-Pulejo". Messina, Italy*
*Corresponding author. E-mail: michele.runci@gmail.com

Abstract. Bisphosphonate-Related Osteonecrosis of the Jaw (BRONJ) is a pathological condition observed in patients underwent oral surgical procedures during bisphosphonates treatment. Although several studies have focused on the BRONJ, the exact pathophysiological pathways remain still unclear. In this study we aimed to observe the effects of the low-dose bisphosphonates administration on mandibular bone of rats with and without mini-implants application. For this study we used 28 male Wistar rats, divided in in two groups: 1) control group, treated with saline solution (n = 14 rats); 2) ZA group, treated with low dose zoledronic acid (n=14 rats). After 6 weeks of treatment, the half of each group underwent mini-implant application. All rats were sacrificed and their mandibles were analyzed by light microscopy and scanning electron microscopy (SEM). Our data have shown a healthy bone tissue of control group both with and without mini-implant application. In the treated group empty osteocyte lacunae have been observed and they slightly increase in rats with mini-implant application. Although that, no bone exposition has been observed. By that, during low dose zoledronic acid treatment we can observe the presence of empty osteocytes lacunae, also called "primary lesion", that not seem to be sufficient alone to determine osteonecrosis of the jaw spontaneously or even after mini-implant application.

Keywords: mandibular bone, osteonecrosis, bisphosphonate, mini-implant, osteocytes lacunae.

1. INTRODUCTION

Bisphosphonates (BPs) is a category of drugs that are widely used in various pathological conditions such as hypercalcemia associated with malignancy, Paget's disease, Gorham-Stout syndrome, lytic bone metastasis, breast cancer and for treating osteoporosis [1-9]. This category of drugs plays a role

in regulating bone cells behavior acting directly on bone remodeling. On the basis of their chemical properties are divided into two groups: no nitrogen-containing and nitrogen-containing BPs [10-13]. The non-nitrogen group, such as etidronate and clodronate, is mainly used for metabolic disorders. The nitrogen-containing BPs, such as zoledronate (ZA) and pamidronate, are the gold standard for neoplastic bone diseases [14].

Although the use of BPs determines positive effects in various pathological conditions, their use could be associated to high risk of jaw or maxillary bone necrosis; more often it could involve in osteonecrosis of the jaw (ONJ). The ONJ in a very low percentage of cases could occur spontaneously while in the most cases it is triggered by certain factors such as the use of zoledronic acid [15], the cumulative dose of bisphosphonates, dentoalveolar surgery [16-19] or trauma [20]. According to Advisory Task Force on Bisphosphonate-Related Osteonecrosis of the Jaws (BRONJ), osteonecrosis is commonly described as exposed jaw bone condition without heal within 8 weeks after identification in patients undergoing treatment with BPs and without irradiation therapy to the craniofacial region [21].

Despite the BRONJ is a severe condition, especially in cancer patients, the exact pathophysiological mechanisms are still unknown; for these reasons, it is necessary to understand what the mechanisms are underlying the BRONJ to choose the best preventions and /or curation therapy.

The most discussed hypothesis about the pathophysiological mechanisms of the BRONJ during BPs treatment considers severe the suppression of bone turnover that in turn lead to necrotic bone, depending on the drug type, dosage and other trigger events as trauma application [22-28]. Our previous studies performed on animal model have shown that in rats treated with low dose bisphosphonates (zoledronic acid), the first signs that could lead to bone death, such as empty osteocytes lacunae, appear only after 30 days of treatment and we did not observe spontaneous bone exposure [28,29]. For this reason, we have hypothesized that the presence of empty lacunae may be a predisposing condition to the death of the bone just in case of a trauma application. On this basis, we have repeated the experiment on animal model to observe the low-dose bisphosphonates effects on bone in which a mini-implant has been inserted, comparing it to rats treated with BPs without dental implants, to understand if the presence of empty osteocytes lacune during low dose zoledronate treatment could represent an accelerator of necrotic lesion in case of trauma application.

2. MATERIALS AND METHODS

2.1. Animals and inoculation

In our experiment we used 28 male Wistar rats (each weighing 250g. And aged 7 weeks) coming from Janvier Labs (Saint Berhevin, France). All the rats were placed in individual cages, where they had food and water ad libitum for the duration of the experimental phase. The protocol required the rats to be kept at a constant temperature (22 °), under a 12-h light /dark cycle. The protocol complied with the guidelines of the European Parliament and of the Council on the protection of animals used for scientific purposes, ARRIVE (Animal Research: Reporting of In Vivo Experiments) [30] and Directive 2010/63 / EU. The protocols have been authorized by the Ethics Committee of the University of Messina. Two groups of rats have been tested: 1) control group, treated with saline solution injection, (n = 14); 2) ZA group treated with zoledronic acid (ZA), (n = 14). The ZA group was treated with 0.1 mg / kg zoledronate via intraperitoneal injection, three times a week for 6 weeks, while the control group have been treated with saline solution. The methods and timing of the experimental phase followed the designs of previous studies [29]. After a week from the end of BP and saline solution treatment, 7 rats for each group underwent to mini-implants application in two sides of mandible by a surgical protocol that will be described below while the other 7 rats for each group didn't undergo to mini-implant application. After 4 weeks from the surgical positioning procedure, all rats (with and without mini-implant) were euthanized under general anesthesia and were perfused with 4% paraformaldehyde (Sigma-Aldrich) and each mandible has been divided into two parts, one part direct for histological analyses and the second part for SEM [31-34].

2.2. Mini-implant Positioning Technique

The placement of the mini-implants was performed on the rat under intraperitoneal general anesthesia (Ketamine 100 mg/kg, Atropine 0.4 mg/kg, Diazepam 8 mg/kg) simulating the surgical procedures applied for human. A mucosa anesthesia was performed in the posterior mandibular region using as local anesthetics articaine with adrenaline diluted at 2%. The inoculums were performed in the periosteal region using an insulin syringe with a 30gauge needle. A mucotomy was performed using a blade 11, the bone was mixed at a speed of 1100 rpm using a 1.2 mm diameter drill bit, titanium mini-implant (1.5-mm diameter and 3-mm length) was positioned manually using a dedicated screwdriver.

2.3. Histological preparation

Bone samples were post-fixed with 4% paraformaldehyde (Sigma-Aldrich) at room temperature for 4 hours and then rinsed in 13 M phosphate buffer (pH 7.3); subsequently, they have been decalcified in ethylenediaminetetraacetic acid (pH 7.2; Hach Company, Loveland, CO, USA) for 30 days, dehydrated in ethanol (from 50% to 100% alcohol) and embedded in paraffin. Paraffin block were cut in 8 um sections with the Leica RM2255 microtome (Leica Microsystems GmbH). After coating the sections into lysinated slides, hematoxylin and eosin staining has been performed at room temperature (H&E; Abbey Color, Philadelphia, PA, USA) [35-38].

2.4. SEM analysis

Bone samples were post-fixed with 2% glutaraldehyde (Santa Cruz Biotechnology, Inc., Dallas, TX, USA) in 0.1 M phosphate buffer (Sigma-Aldrich) and then they were dehydrated with ethanol and amyl acetate. After critical point dryer process (Leica Microsystems GmbH, Wetzlar, Germany), the fractured surfaces were coated with a Plasma Sciences CrC-100 Turbo-Pumped sputtering system and observed using a Phenom G2 Pro scanning electron microscope (Phenom-World B.V., Eindhoven, The Netherlands).

2.5. Statistical analysis

We have observed 100 lacunae for ZA group and 100 for ZA group with mini-implant. We observed 10 lacunae taken from 10 random microscopic fields at 20x magnification and we counted how many empty lacunae there were using ImageJ software. After that, we calculated the mean of empty osteocytes lacunae for ZA-group and ZA- group with mini-implant application. The means were compared by T-student test to evaluated the possible statistically significant differences. The means were also turned in a percentage shown in a pie-chart.

3. RESULTS

3.1. H&E staining

The mandibular bones of control group (saline solution injections) showed the characteristics of the healthy bone. This compact bone was characterized by the presence of full osteocytes lacunae with osteocytes that occupy the entire space within the lacunae and full haversian and Volkman's canals (Fig. 1A). The mandibular bone of control group (saline solution injection) after mini-implant applications shows a healthy bone tissue with full lacunae and canals with the same characteristics of the bone of control group without mini-

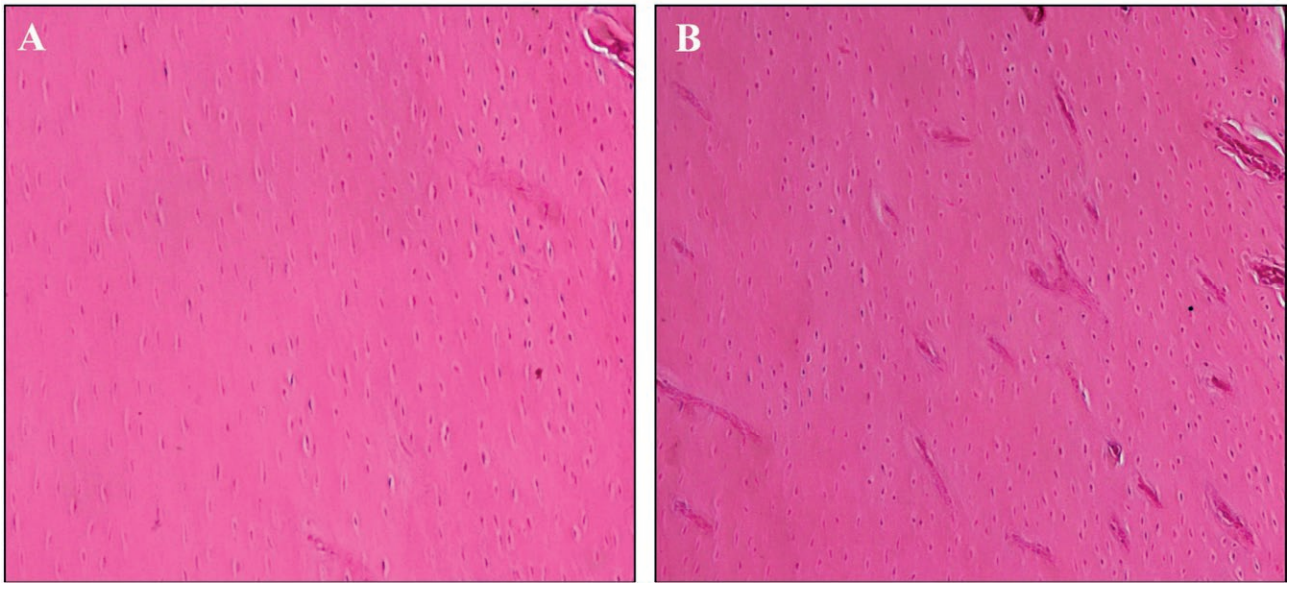

Figure 1. Hematoxylin-eosin staining of bone tissue from rats treated with saline solution (control group) without (A) and with mini-implant application(B). In both cases it is possible to observe a healthy tissue with full osteocytes lacunae and osteocytes that occupy most of the space within the lacunae. No empty osteocyte lacunae and no signs of inflammation have been observed.

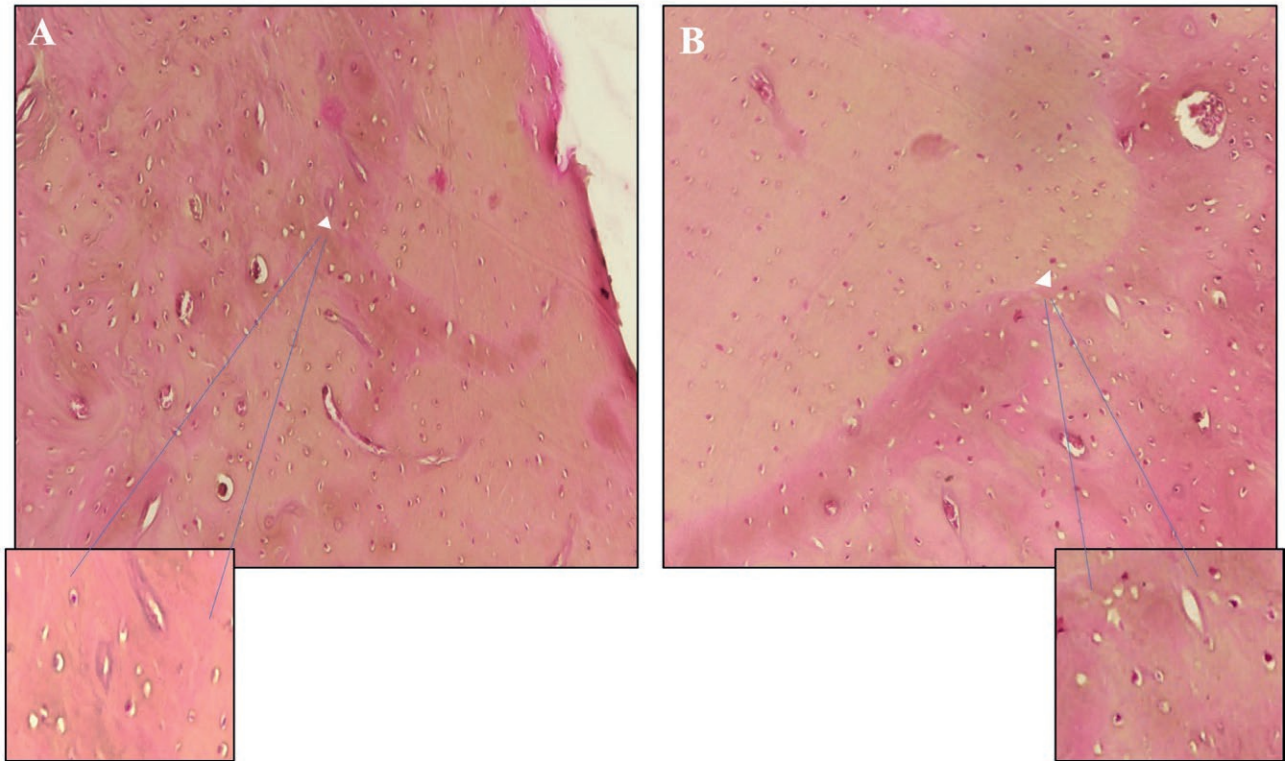

Figure 2. Hematoxylin-eosin staining of bone tissues from rats treated for 6 weeks with zoledronate (0,1 mg/Kg) (ZA group) without (A) and with (B) mini-implant application. The bone of rats without mini-implant application shows the presence of some empty osteocytes lacunae (A, head arrow); in several region of the bone tissue the osteocytes seem to be small and they don't occupy the entire space within the lacunae (A). The bone of rats with mini-implant application shows an increased number of empty osteocytes lacune (B, head arrow). Zoom of empty osteocytes lacunae in the corners of A and B pictures.

implant application; no evidence of inflammatory processes has been observed indicating a total recovery of structural features after 4 weeks of trauma application (Fig. 1B).

In the mandibular bones of rats at 6 weeks of treatment (ZA group), some empty osteocytes lacunae were observed among full osteocytes lacunae where the osteocytes don't occupy the entire space within the lacunae (Fig. 2A).

The ZA group with mini-implants, inserted into the mandibular bone cortex, exhibited a slight increase of empty osteocytes lacunae among full osteocytes lacunae where the osteocytes don't occupy the entire space within the lacunae (Fig. 2B).

3.2. SEM Images

In biopsies of the mandibular bones of control group, the observation of the fracture surface showed the physiological presence of osteocytes lacunae, Haversian systems and Volkmann canals (Fig. 3A).

The bone of control group after mini-implant application showed a full recovered tissue with full lacunae and canals and no evidence of inflammatory processes (Fig. 3B).

In rats group treated with BPs for 6 weeks (ZA group), the fracture surface of biopsy bone fragments frequently showed areas with irregularly spherical or elongated morphology. Moreover, empty osteocytes lacunae were detected (Fig. 4A).

In ZA group with implants placement, an alteration of the morphological structure is visible and empty osteocytes lacunae increased, compared to the mandibular bone of ZA group without mini-implants insertion (Fig. 4B).

3.3. Statistical analysis

Results shows that for every 10 osteocytes lacunae observed we find a mean of 2 and 2,6 of empty osteocytes lacunae, for ZA group and ZA group with mini-implant respectively. The T-student test showed a no statistically significant differences between the ZA without

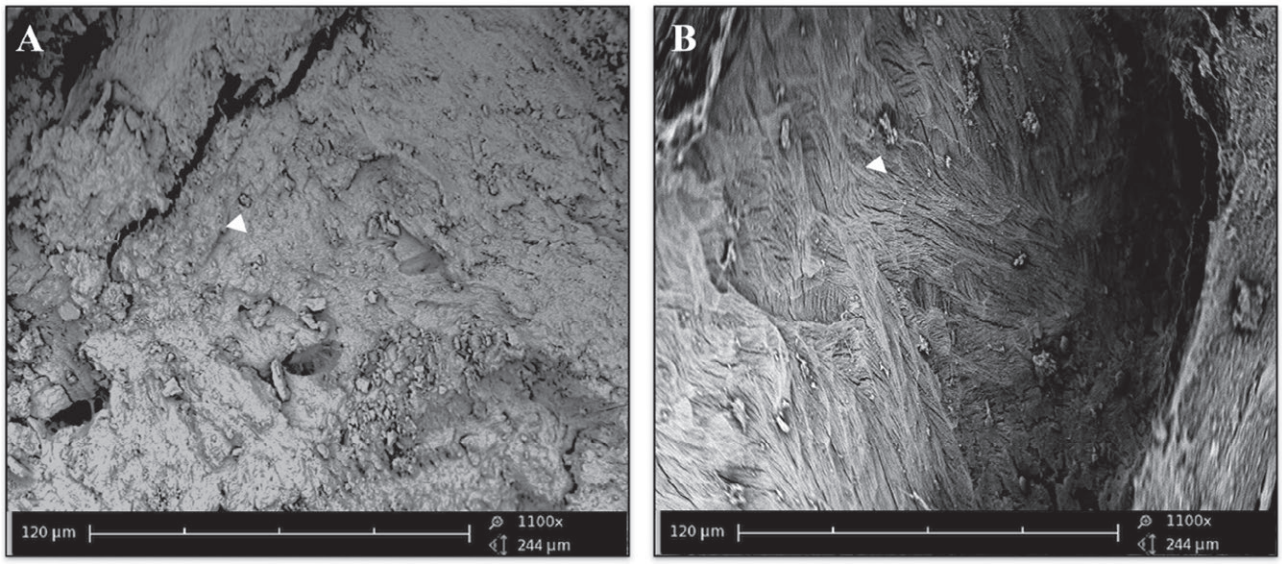

Figure 3. Scanning electron microscopy pictures of bone tissue from rats treated with saline solution (control group) without (A) and with mini-implant application(B). In both cases it is possible to observe a healthy tissue with full osteocytes lacunae and osteocytes that occupy most of the space within the lacunae. No empty osteocyte lacunae and no signs of inflammation have been observed.

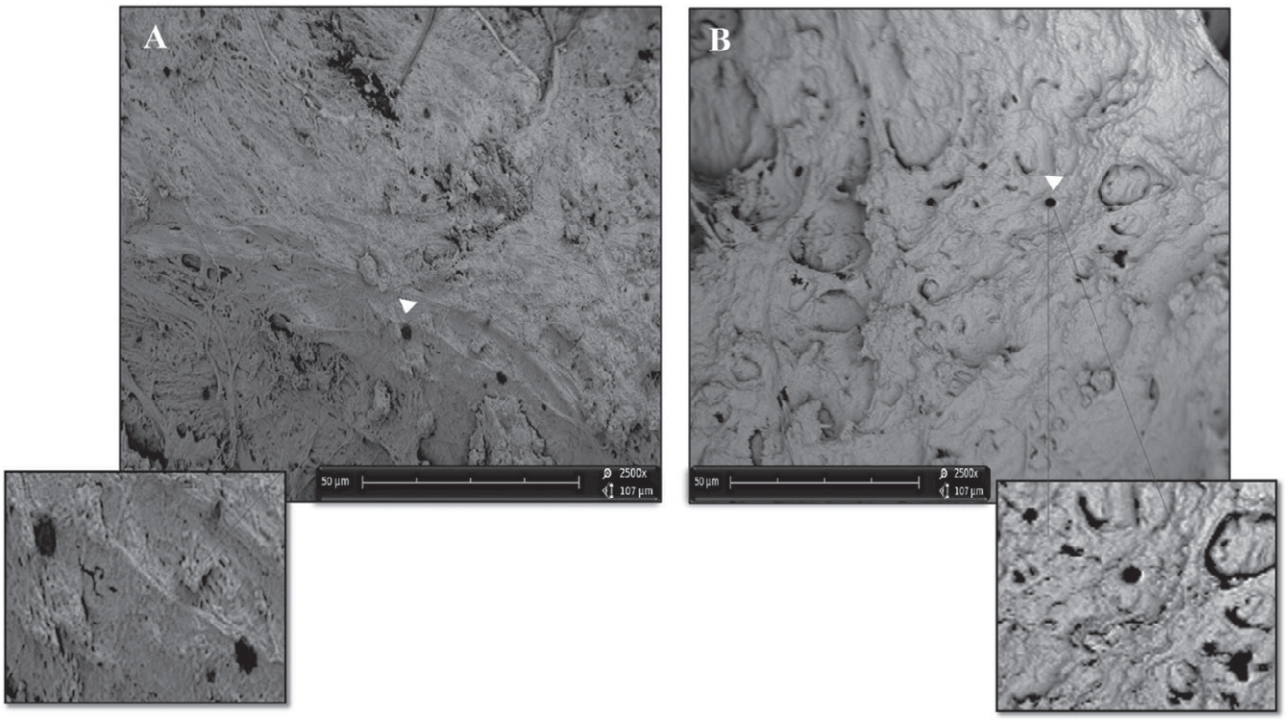

Figure 4. Scanning electron microscopy pictures of bone tissues from rats treated with zoledronate (0,1 mg/Kg) (ZA group) without (A) and with (B) mini-implant application. The bone of rats without mini-implant application shows the presence of some empty osteocytes lacunae (head arrow) (A). The bone of rats with mini-implant application shows an increased number of empty osteocytes lacune as evidenced by head arrow (B). Zoom of empty osteocytes lacunae in the corners of A and B pictures.

ZA-Group	M	DS
ZA-Group without mini implant.	2	1,333333
ZA-Implant-Group	2,6	0,966092

Figure 5. Table that shows the means of empty osteocytes lacunae that we found in 10 microscopic fields both for ZA group without mini-implant application and ZA group with mini-implant application. M= mean; DS= standard deviation. P>0,05.

and ZA with mini-implant application groups. We have turned the means in a percentage shown in a pie-chart (Fig. 5).

4. DISCUSSION

BRONJ is a severe condition that could occur in patients treated with bisphosphonates spontaneously or after trigger events; in fact, tooth extractions and dentoalveolar surgical procedures, such as positioning of dental implants, are represented as precipitating or trigger events for the manifestation of BRONJ in subjects receiving BPs and other antiresorptive drugs [39]. Although several studies have been performed on this severe condition, the etiopathology of BRONJ still remains undefined. BPs are known to have an inhibitory action on bone turnover after surgical procedures [40]. In literature, it was observed that the incidence of BRONJ depends on several factors (the method of administration, the BPs, dose, etc.). Other factors as periodontal diseases and local infection are closely linked to BRONJ [41]. Several authors have observed that the cases of BRONJ increase in patients whose route of administration is intravenous and oral. [42-43]. A study by Henry et al. [44] has shown how the duration of treatment with BPs can lead to an adverse event. Despite that, it is difficult to detect early structural alteration that could lead to necrosis in human. For these reasons, the use of an experimental model seems to be necessary to better understand the structural and molecular mechanism involved in BRONJ. Our previous studies, conducted on bone and gingival tissue samples taken surgically in the perilesional area, showed an alteration of the structural architecture, with the presence of empty lacunae, absence of matrix and disorganization of the fibrillar component. Our results confirm the presence of empty osteocyte lacunae in samples treated with bisphosphonates without mini-implant, and show that in the samples with mini-implant, the number of empty osteocyte lacunae increases slightly [27,28]. The present study has been performed on animal model to evaluate the modification that occur during zoledronic acid treatment with and without the application of trauma such as mini-implant insertion. For this reason, we studied two groups of rats: control group, treated with saline solution and ZA group, treated with zoledronic acid; the half of each group underwent mini-implant application. Our results obtained by Histological and SEM examinations showed that the saline solution injection doesn't causes structural alteration of bone tissue both with and without mini-implant applications. In ZA group, bone tissue structural alterations characterized by the presence of empty osteocyte lacunae have been observed. Moreover, we haven't observed a statistically significant difference in empty osteocytes lacunae between ZA group without and ZA group with mini-implant. No cases of bone exposure have been observed. These results are in accordance with our previous study performed on rats

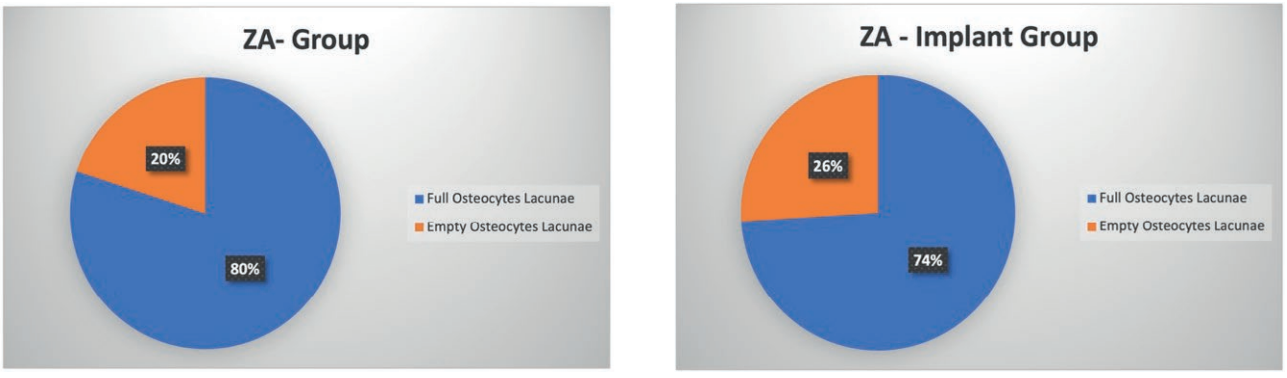

Figure 6. Pie chart showing the percentage of empty and full osteocytes lacunae in bone tissue from rats treated with BPs (ZA group) without (A) and with (B) mini-implant application.

treated with Zoledronate for 45 days without trauma application [29] demonstrating that the mandibular bone at 7 and 15 days of treatment exhibited similar features to those of healthy bone while after 30 and 45 days of treatment a structural alteration in large surface areas of the bone with empty osteocytes lacunae and a marked reduction in the number of osteoblasts and osteoclasts were observed with no cases of bone exposition. Moreover, the present data are also in accordance with Huja et al. [45] that administered a ZA dose of 0.1 mg/kg intraperitoneally without performing extractions and obtained 0% of osteonecrotic lesions and Kobayashi et al. [46] which showed no signs of osteonecrosis (0%) in the jaw bones of experimental animals treated with a ZA dose of 0.250 mg/kg for subcutaneous administration and with extractions. Conversely, Senel et al. [47] detected 20% of ONJ lesions with the same dosage of ZA but in combination with dental extractions and Biasotto et al. [48] showed 100% of ONJ lesions at a ZA dose of 0.04 mg/Kg for intravenous administration; Maahs et al [49] found 80% of osteonecrotic lesions at a ZA dose of 0.6 mg/kg for intraperitoneal administration. The present work shows at morphological level the early bone structural modification, such as empty osteocytes lacunae, that could be involved in BRONJ. Although that, our data support that the existence of these histological features during low dose zoledronic acid treatment is not sufficient to determine osteonecrosis of the jaw spontaneously or even after mini-implant application. By that, the presence of empty osteocytes lacunae could represent the first morphological events, also called "primary lesion" from which, together with other trigger events and/or individual variables, osteonecrosis can occur. It will be interesting to perform future studies to understand how the "primary lesion" can evolve during high dose zoledronic acid treatment.

5. CONCLUSION

Our experimental data obtained by low dose zoledronic acid treatment on rat show "primary lesions" that not lead to osteonecrosis spontaneously or after mini-implant application. Hence, BRONJ should not only be related to a unique factor, but the combination of more factors and more variables would make patients more susceptible to BRONJ. In fact, the bone necrosis and exposure could also depend on long term BP treatment, individual variables or on concomitant oral cavity pathology. That seem to support the possibility of oral surgical intervention in those patients treated with low doses of zoledronic acid.

REFERENCES

1. Fujimoto, N., Nakagawa, K., Seichi, A., Terahara, A., Tago, M., Aoki, Y., Hosoi, Y., Ohtomo, K., 2001. A new bisphosphonate treatment option for giant cell tumors, Oncol. Rep. 8 (3) 643–647. 10.3892/or.8.3.643
2. Hammer, F., Kenn, W., Wesselmann, U., Hofbauer, L.C., Delling, G., Allolio, B., Arlt, W., 2005. Gorham-Stout disease - Stabilization during bisphosphonate treatment, J. Bone Miner. Res. 20 (2) 350–353. 10.1359/JBMR.041113
3. Wells, G.A., Cranney, A., Peterson, J., Boucher, M., Shea, B., Robinson, V., Coyle, D., Tugwell, P., 2008. Etidronate for the primary and secondary prevention of osteoporotic fractures in postmenopausal women, Cochrane Database Syst. Rev. (1) CD003376. 10.1002/14651858.CD003376.pub3
4. Zara, S., De Colli, M., Di Giacomo, V., Zizzari, V.L., Di Nisio, C., Di Tore, U., Salini, V., Gallorini, M., Tetè, S., Cataldi, A., 2015. Zoledronic acid at subtoxic dose extends osteoblastic stage span of primary human osteoblasts, Clin. Oral Investig. 19 (3) 601–611. 10.1007/s00784-014-1280-8
5. Manzano-Moreno, F.J., Ramos-Torrecillas, J., De Luna-Bertos, E., Ruiz, C., García-Martínez, O., 2015. High doses of bisphosphonates reduce osteoblast-like cell proliferation by arresting the cell cycle and inducing apoptosis, J. Craniomaxillofac. Surg. 43 (3) 396–401. 10.1016/j.jcms.2014.12.008
6. Kim, M.K., Hong, J.R., Kim, S.G., Lee, S.K., 2015. Fatal progression of Gorham disease: a case report and review of the literature, J. Oral Maxillofac. Surg. 73 (12) 2352–2360. 10.1016/j.joms.2015.06.154
7. Fleisch, H., 2002. Development of bisphosphonates. Breast Cancer Res., 4(1):30-4. 10.1186/bcr414
8. Watts, N.B., Diab, D.L., 2010. Long-term use of bisphosphonates in osteoporosis. J Clin Endocrinol. Metab. 95(4):1555-65. 10.1210/jc.2009-1947
9. Mhaskar, R., Kumar, A., Miladinovic, B., Djulbegovic, B., 2017. Bisphosphonates in multiple myeloma: an updated network meta-analysis. Cochrane Database Syst Rev., 12(12):CD003188. 10.1002/14651858.CD003188.pub4
10. Smith,M.R., 2003. Antitumor activity of bisphosphonates. Clin Cancer Res. ;9(15):5433-4
11. Bukowski, J.F., Dascher, C., Das, H., 2005. Alternative bisphosphonate targets and mechanisms of action. Biophys Res Commun. ;328(3):746-50. 10.1016/j.bbrc.2004.11.075
12. Maffia, F., Vellone, V., De Quarto, C., Runci Anastasi, M., Cascone, P., 2019. Synovial chondromatosis

of the temporomandibular joint with glenoid fossa erosion: Disk preservation for spontaneous anatomical recovery. J Craniomaxillofac Surg. , 47(12),1898-1902. 10.1016/j.jcms.2019.10.005
13. Rodan, G.A., 1997. Alendronate: preclinical studies. J Clin Rheumatol. ;3(2 Suppl):34-6
14. Anesi, A., Generali, L., Sandoni, L., Pozzi, S., Grande, A., 2019. From Osteoclast Differentiation to Osteonecrosis of the Jaw: Molecular and Clinical Insights. Int J Mol Sci., 20(19):4925. 10.3390/ijms20194925
15. Dimopoulos, M.A., Kastritis, E., Anagnostopoulos, A., Melakopoulos, I., Gika, D., Moulopoulos, L.A., Bamia, C., Terpos, E., Tsionos, K., Bamias, A., 2016. Osteonecrosis of the jaw in patients with multiple myeloma treated with bisphosphonates: evidence of increased risk after treatment with zoledronic acid. Hematologica, 91(7):968-71
16. Sher, J., Kirkham-Ali, K., Luo, J.D., Miller, C., Sharma, D., 2021. Dental Implant Placement in Patients with a History of Medications Related to Osteonecrosis of the Jaws: A Systematic Review. J Oral Implantol, 47(3):249-268. 10.1563/aaid-joi-D-19-00351
17. Cuozzo, A., Iorio-Siciliano, V., Vaia, E., Mauriello, L., Blasi, A., Ramaglia, L., 2022. Incidence and risk factors associated to Medication-Related Osteo Necrosis of the Jaw (MRONJ) in patients with osteoporosis after tooth extractions. A 12-months observational cohort study. J Stomatol Oral Maxillofac Surg 2022 , S2468-7855(22)00086-6. 10.1016/j.jormas.2022.03.020
18. Picciolo, G., Mannino, F., Irrera, N., Minutoli, L., Altavilla, D., Vaccaro, M., Oteri, G., Squadrito, F., Pallio, G., 2022. Reduction of oxidative stress blunts the NLRP3 inflammatory cascade in LPS stimulated human gingival fibroblasts and oral mucosal epithelial cells. Biomed Pharmacother. , 146:112525. 10.1016/j.biopha.2021.112525
19. Picciolo, G., Mannino, F., Irrera, N., Altavilla, D., Minutoli, L., Vaccaro, M., Squadrito, V., Picciolo, G., Squadrito, F., Pallio, G., 2021. PDRN, a natural bioactive compound, blunts inflammation and positively reprograms healing genes in an “in vitro” model of oral mucositis. Biomed Pharmacother. , 138, 111538. 10.1016/j.biopha.2021.111538
20. Ruggiero, S.L., 2008. Bisphosphonate-related osteonecrosis of the jaws. Compend Contin Educ Dent., 29(2):96-8, 100-2, 104-5.
21. Advisory Task Force on Bisphosphonate-Related Osteonecrosis of the Jaws, American Association of Oral and Maxillofacial Surgeons, American Association of Oral and Maxillofacial Surgeons position paper on bisphosphonate-related osteonecrosis of the jaws, J. Oral Maxillofac. Surg. 65 (3) (2007) 369–376. 10.1016/j.joms.2006.11.003
22. Khan. A.A., Morrison, A., Hanley, D.A., Felsenberg, D., McCauley, L.K., O’Ryan, F., Reid I.R., Ruggiero, S.L., Taguchi, A., Tetradis, S., Watts, N.B., Brandi, M.L., Peters, E., Guise, T., Eastell, R., Cheung, A.M., Morin, S.N., Masri, B., Cooper, C., Morgan, S.L., Obermayer-Pietsch, B., Langdahl, B.L., Al Dabagh, R., Davison, K.S., Kendler, D.L., Sándor, G.K., Josse, R.G., Bhandari, M., El Rabbany, M., Pierroz, D., Sulimani, R., Saunders, D.P., Brown, J.P., Compston, J., 2015. Diagnosis and management of osteonecrosis of the jaw: a systematic review and international consensus. J Bone Miner Res., 30(1):3-23. 10.1002/jbmr.2405
23. Fliefel, R., Tröltzsch, M., Kühnisch, J., Ehrenfeld, M., Otto, S., 2015. Treatment strategies and outcomes of bisphosphonate-related osteonecrosis of the jaw (BRONJ) with characterization of patients: a systematic review. Int J Oral Maxillofac Surg., 44(5):568-85. 10.1016/j.ijom.2015.01.026
24. Kawahara, M., Kuroshima, S., Sawase, T., 2021. Clinical considerations for medication-related osteonecrosis of the jaw: a comprehensive literature review. Inter J Implant Dent. 14;7(1):47. 10.1186/s40729-021-00323-0
25. Jacobsen, C., Metzler, P., Rössle, M., Obwegeser, J., Zemann, W., Grätz, K.W., 2013. Osteopathology induced by bisphosphonates and dental implants: clinical observations, Clin. Oral Investig. , 17 (1), 167–175. 10.1007/s00784-012-0708-2
26. Pichardo, S., Van der Hee, J.G., Fiocco, M., Appelman-Dijkstra, N.M., van Merkesteyn, J.P.R., 2020. Dental implants as risk factors for patients with medication-related osteonecrosis of the jaws (MRONJ). Bra J Oral Maxillofac Surg., 58(7):771-776. 10.1016/j.bjoms.2020.03.022
27. Nastro Siniscalchi, E., Cutroneo, G., Catalfamo, L., Santoro, G., Allegra, A., Oteri, G., Cicciù, D., Alonci, A., Penna, G., Musolino, C., De Ponte, F.S., Anastasi, G., Favaloro, A., 2010. Immunohistochemial evaluation of sarcoglycans and integrins in gingival epithelium of multiple myeloma patients with bisphosphonate-induced osteonecrosis of the jaw, Oncol. Rep. 24 (1) 129–134. 10.3892/or_00000837
28. De Ponte, F.S., Favaloro, A., Siniscalchi, E.N., Centofanti, A., Runci, M., Cutroneo, G.,Catalfamo, L., 2013. Sarcoglycans and integrins in bisphosphonate treatment: Immunohistochemical and scanning electron microscopy study, Oncol. Rep. 30 (6) 2639–2646. 10.3892/or.2013.2766
29. De Ponte, F.S., Catalfamo, L., Micali, G., Runci, M., Cutroneo, G., Vermiglio, G., Centofanti, A., Rizzo,

G., 2016. Effect of bisphosphonates on the mandibular bone and gingival epithelium of rats without tooth extraction, Exp. Ther. Med. , 11 (5), 1678–1684. 10.3892/etm.2016.3168

30. Kilkenny, C., Browne, W.J., Cuthill, I.C., Emerson, M., Altman, D.G., 2010. Improving Bioscience Research Reporting: The ARRIVE Guidelines for Reporting Animal Research, PLoS Biol. , 8 (6), e1000412. 10.4103/0976-500X.72351
31. Arco, A., Favaloro, A., Gioffrè, M., Santoro, G., Speciale, F., Vermiglio, G., Cutroneo, G., 2012. Sarcoglycans in the normal and pathological breast tissue of humans: an immunohistochemical and molecular study, Cells Tissues Organs 195 (6) 550–562. 10.1159/000329508
32. Vermiglio, G., Centofanti, A., Ramieri G., Tepedino, M., Anastasi Runci, M., Micali, A., Arco, A., Piancino, M. G. Immunofluorescence evaluation of Myf5 and MyoD in masseter muscle of unilateral posterior crossbite patients. JFMK 2020 Volume 5, Issue 47 November Article number jfmk5040080
33. Lo Giudice R., Rizzo G., Centofanti A., Favaloro A., Rizzo D., Cervino G., Squeri R., Costa B.G., La Fauci V., Lo Giudice G. Steam Sterilization of Equine Bone Block: Morphological and Collagen Analysis. 2018 BioMed Res.Int. Volume 20182018 Article number 9853765.
34. Rosa, M.A.,Gugliandolo, P., Favaloro, A., Vermiglio, G., Centofanti, A., Bruschetta, D., Rizzo, G., 2015. Morpho-structural alterations of sub-chondral bone tissue in patients with osteoarthritis: A scanning electron microscopy study, Ital. J. Anat. Embryol. 2015, 120, 71–81.
35. Vermiglio, G, Piancino, M.G., Runci Anastasi, M., Picciolo, G., Centofanti, A., Santoro, G., Malandrino, M.C., Cutroneo, G., Anastasi, G., 2021. Use of immunofluorescence technique to perform a quantitative analysis of masseter mucle fibers in unilateral posterior crossbite. Appl. Sci., 11 (12), 5350.
36. Runci Anastasi, M., Centofanti, A., Arco, A., Vermiglio, G., Nicita, F., Santoro, G., Cascone, P., Anastasi, G., Rizzo, G., Cutroneo, G., 2020. Histological and Immunofluorescence Study on Discal Ligaments in Human Temporomandibular Joint, J. Funct. Morphol. Kinesiol., 5 (4), 90. 10.3390/jfmk5040090
37. Puleio, F., Rizzo, G., Nicita, F., Giudice, F., Tamà, C., Marenzi, G., Centofanti, A., Raffaele, M., Santonocito, D., Risitano, G. Chemical and mechanical roughening treatments of a supra-nano composite resin surface: SEM and topographic analysis. 2020 Appl. Sci (Switz.) Volume 10, Issue 131, Article number 4457
38. De Ponte, F.S., Falzea, R., Runci, M., Nastro Siniscalchi, E., Lauritano, F., Bramanti, E., Cervino, G., Cicciu, M., 2017. Histomorhological and clinical evaluation of maxillary alveolar ridge reconstruction after craniofacial trauma by applying combination of allogeneic and autogenous bone graft. Chin. J. Traumatol., 20(1),14-17. 10.1016/j.cjtee.2016.10.005
39. Otto, S., Pautke, C., Van den Wyngaert, T., Niepel, D., Schiødt, M., 2018. Medication-related osteonecrosis of the jaw: Prevention, diagnosis and management in patients with cancer and bone metastase. Cancer Treat Rev., 69:177-187. 10.1016/j.ctrv.2018.06.007
40. Ruggiero, S.L., Dodson, T.B., Fantasia, J., Joodday, R., Aghaloo, T., Mehrotra, B., O'Ryan, F., 2014. American Association of Oral and Maxillofacial Surgeons, American Association of Oral and Maxillofacial Surgeons position paper on medication-related osteonecrosis of the jaw-2014 update. J. Oral. Maxillofac. Surg., 72 (10), 1938-1956. 10.1016/j.joms.2014.04.031
41. Li, C.L., Seneviratne, C.J., Huoa, L., Lu, W., Zheng, L.W., 2015. Impact of Actinomyces naeslundii on bisphosphonate-related osteonecrosis of the jaws in ovariectomized rats with periodontitis, J. Craniomaxillofacial Surg., 43 (8), 1662–1669. 10.1016/j.jcms.2015.07.001
42. Pozzi, S., Marcheselli, R., Sacchi, S., Baldini, L., Angrilli, F., Pennese, E., Quarta, G., Stelitano, C., Caparotti, G., Luminari, S., Musto, P., Natale, D., Broglia, C., Cuoghi, A., Dini, D., Di Tonno, P., Leonardi, G., Pianezze, G., Pitini, V., Polimeno, G., Ponchio, L., Masini, L., Musso, M., Spriano, M., Pollastri, G., Rotondo, G., 2007. Bisphosphonate-associated osteonecrosis of the jaw: a review of 35 cases and an evaluation of its frequency in multiple myeloma patients, Leuk. Lymphoma., 48 (1), 56–64. 10.1080/10428190600977690
43. Diniz-Freitas, M., López-Cedrún, J.L., Fernàndez-Sanromàn, J., Garcìa-Garcia, A., Fernàandez-Feijoo, J., Diz-Dios, P., 2012. Oral bisphosphonate-related osteonecrosis of the jaws: Clinical characteristics of a series of 20 cases in Spain, Med. Oral Patol. Oral Cir. Bucal., 17 (5), e751–e758. 10.4317/medoral.18041
44. Henry, D.H., Costa, L., Goldwasser, F., Hirsh, V., Hungria, V., Prausova, J., Scagliotti, G.V., Sleeboom, H., Spencer, A., Vadhan-Raj, S., Von Moos, R., Willenbacher, W., Woll, P.J., Wang, J., Jiang, Q., Jun, S., Dansey, R., Yeh, H., Henry, D., 2011. Randomized, Double-Blind Study of Denosumab Versus Zoledronic Acid in the Treatment of Bone Metastases in Patients With Advanced Cancer (Excluding Breast and Prostate Cancer) or Multiple Myeloma, J. Clin. Oncol., 29, 1125–1131. 10.1200/JCO.2010.31.3304

45. Huja, S., Fernandez, S., Phillips, C., Li, Y., 2009. Zoledronic acid decreases bone formation without causing osteocyte death in mice, Arch. Oral Biol. , 54 (9), 851–856. 10.1016/j.archoralbio.2009.06.002
46. Kobayashi, T., Hiraga, A., Ueda, A., Wang, L., Matsumoto-Nakano, M., Hata, K., Yatani, H., Yoneda, T., 2010. Zoledronic acid delays wound healing of the tooth extraction socket, inhibits oral epithelial cell migration, and promotes proliferation and adhesion to hydroxyapatite of oral bacteria, without causing osteonecrosis of the jaw in mice. J. Bone Miner. Metab., 28 (2), 165-175. 10.1007/s00774-009-0128-9
47. Senel, F.C., Kadioglu Duman, M., Muci, E., Cankaya, M., Pampu, A., Ersoz, S., Gunhan, O., 2010. Jaw bone changes in rats after treatment with zoledronate and pamidronate, Oral Surgery, Oral Med. Oral Pathol. Oral Radiol. Endodontology, 109 (3), 385–391. 10.1016/j.tripleo.2009.10.011
48. Biasotto, M., Chiandussi, S., Zacchigna, S., Moimas, S., Dore, F., Pozzato, G., Cavalli, G., Zanconati, F., Contardo, L., Giacca, M., Di Lenarda, R., 2010. A novel animal model to study non-spontaneous bisphosphonates osteonecrosis of jaw, J. Oral Pathol. Med., 39 (5), 390–396. 10.1111/j.1600-0714.2009.00878.x
49. Maahs, M.P., Azambuja, A., Campos, M., Salum, F.G., Cherubini, K., 2011. Association between bisphosphonates and jaw osteonecrosis: A study in Wistar rats, Head Neck. , 33 (2), 199–207. 10.1002/hed.21422

IJAE
ITALIAN JOURNAL OF ANATOMY AND EMBRYOLOGY

Firenze University Press
www.fupress.com/ijae

OPEN ACCESS

Citation: Maria Grazia Poerio, Michele Runci Anastasi, Giovanna Vermiglio, Antonio Centofanti, Piero Cascone (2023) The Auriculotemporal Nerve and TMJ region: anatomy and function. *Italian Journal of Anatomy and Embryology* 127(1): 45-50. doi: 10.36253/ijae-14487

Data Availability Statement: All relevant data are within the paper and its Supporting Information files.

Competing Interests: The Author(s) declare(s) no conflict of interest.

The Auriculotemporal Nerve and TMJ region: anatomy and function

Maria Grazia Poerio[1,*], Michele Runci Anastasi[2,*], Giovanna Vermiglio[3], Antonio Centofanti[4], Piero Cascone[5]

[1] *DDS Student; Graduand, School of Dentistry, Department of Oral and Maxillofacial Sciences, "Sapienza" University of Rome, 00100 Rome, Italy*
[2] *MD, Resident; IRCCS (Istituto di Ricovero e Cura a Carattere Scientifico) Centro Neurolesi "Bonino-Pulejo" IRCCS Messina, 98100 Messina, Italy*
[3] *PhD, Research Fellow; Department of Biomedical and Dental Sciences and Morphofunctional Imaging, University of Messina, 98100 Messina, Italy*
[4] *DDS, PhD, Research Fellow; Department of Biomedical and Dental Sciences and Morphofunctional Imaging, University of Messina, 98100 Messina, Italy*
[5] *MD, Full Professor; Saint Camillus International University of Health Sciences, University in Rome, 00131 Rome, Italy*
*Corresponding author. E-mail: michele.runci@gmail.com

Abstract. The studies on the auriculotemporal nerve in humans are limited. However, we considered crucial to investigate the topographic relation between the auriculotemporal nerve and the TMJ region that can explain some of the symptoms in TMDs. The results derived from our experience in the anatomic dissection on 16 adult cadaveric heads were compared with what literature describes from 1971 to 2023. The results confirm the existence of a particular anatomic position of the ATN within the infratemporal fossa in direct contact with the lateral pterygoid muscle and the TMJ capsular region. Therefore, there is evidence of a potential entrapment mechanism involving the ATN caused by an internal derangement of TMJ or a spastic condition of the lateral pterygoid muscle. Through a detailed anatomical description of the ATN the present study aims to offer an explanation to the main sensory and otological symptoms that patients with TMJ disorders often complaint, from facial pain and paresthesias to external ear pruritus.

Keywords: auriculotemporal nerve, TMJ, pterygoid muscle.

1. INTRODUCTION

The auriculotemporal nerve (ATN) origins within the infratemporal fossa and it is in direct contact with the TMJ capsular region and the lateral pterygoid muscle. For these reasons we suggest the involvement of the ATN in a potential entrapment mechanism. The ATN anatomy has been described in textbooks and paper as a nerve that origins form a single root that splits into two segments surrounding the middle meningeal artery (MMA) before reuniting, such as a 'button hole' (Wilson 1857; Chung 1995; Netter 1997; Sinnatamby

1999; Gosling et al. 2002; Snell 2004). After reuniting the ATN runs 1) posteriorly to the the lateral pterygoid muscle and between the sphenomandibular ligament and neck of the mandible, 2) laterally to the temporomandibular joint and then 3) splitting into the auricular and temporal components. The straight interaction of the ATN with the Temporomandibular Joint (TMJ) suggest the involvement of the nerve with some TMJ pathologies, such as potential entrapment mechanism. Given the close relationship with the aforementioned anatomical structures, it is crucial to define the precise origin and precise course of the nerve. Although that, many anatomy texts frequently provide stereotyped descriptions and neglect pertinent features of the auriculotemporal nerve; moreover, the existent anatomical descriptions are not representative of all individual and ethnic variables (Toni et al. 2003, 2005). By that, the aim of the present report was to give a detailed description of the anatomy and functions of this nerve in order to attribute an etiology to the main neurosensory and otological symptoms associated with TMJ disorders.

2. MATERIAL AND METHODS

Sixteen adult cadaveric heads (32 sides) were dissected. On each side, the TMJ region was approached laterally. A preauricular incision was extended to the superior aspect of the temporal region; the skin, subcutaneous tissue, and muscle were reflected. It was performed an osteotomy of mandibular ramus from the mandibular angle to the sigmoid notch to expose the infratemporal fossa and identify the exit of the third branch of the trigeminal nerve at the level of the middle cranial fossa (foramen ovale) [3, 16]. The mandibular nerve was followed from its origin to the medial aspect of TMJ capsule. The auriculotemporal nerve was identified at its point of origin off the mandibular nerve and was observed along his course. The results derived from our experience in the anatomic dissection of the mandibular nerve were compared with what literature describes. This paper includes experimentations on human cadavers approved by the local Ethics Committee (prot. n. 33/2020 approved on 30 July 2020).

3. RESULTS

3.1 Descriptive anatomy

The ATN arises in the infratemporal fossa from the posterior trunk of the mandibular nerve (V3), which is the third division of the trigeminal nerve (CN V). The mandibular nerve exits the middle cranial fossa through the foramen ovale and splits up into two divisions, the anterior and posterior trunk. The posterior trunk comprises the lingual, inferior alveolar and auriculotemporal nerve. Although many variations have been described about the formation and the configuration of the auriculotemporal nerve, in most specimens analyzed in the entire literature two are the anatomical patterns that occur most frequently. The first one is the ATN with two roots that envelope the middle meningeal artery, the second one is the ATN with a single root. Other patterns are three-, four-,and five-roots variants, but they are beyond our aim. Fernandes et al. (7) describe a case in which the ATN arises as a single root and then it divides into two segments that travel around the middle meningeal artery to rejoin again on the opposite side of this vessel. We had a doubt in deciding which category it belongs to, and because its relative high frequency we have thought it belongs to the first pattern. We infer there is no clear distinction about the pattern with two roots and the pattern with one root that splits up into two segments to become again a single trunk. A review of the literature revealed that the study by Baumel presents the most complete quantitative data on the ATN. We compared our findings with those of Baumel and observed no differences in the results regarding variations. ATN roots are usually long (15 mm) and when they converge they form a short trunk (6mm) that divides into a spray of branches which abruptly diverge (Fig 1). Moreover, roots length and trunk length are inversely correlated [1]. The principal named branches are: the superficial temporal ramus, communicating rami with the facial nerve, nerves to the external acoustic meatus, the anterior auricular nerve, parotid branches, articular branches to TMJ, and communicating branches with otic ganglion [1].

3.2 Topographic anatomy

The roots of the ATN run postero-inferiorly beneath the infratemporal surface of the great wing of the sphenoid bone. They lie on the lateral surface of the spine of the sphenoid bone, in the plane between the posterior fasciculi of the tensor veli palatini muscle and the lateral pterygoid muscle. The trunk formed by the joining of the roots is in direct contact with the medial aspect of the capsular region of the TMJ. According to Schimdt's study, the horizontal distance between the nerve and the condyle was 0 mm in all cases at the posterior border of lateral pterygoid muscle. Moreover, Loughner sug-

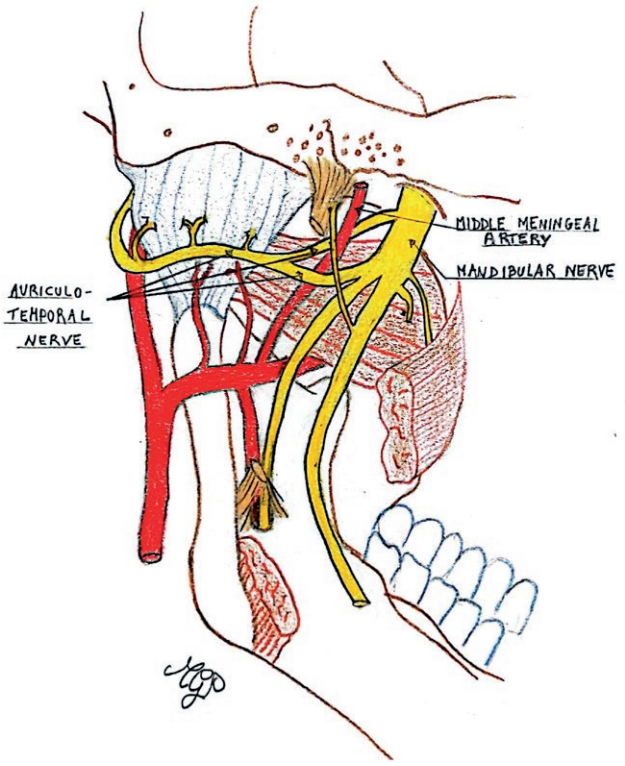

Figure 1. The antero-medial disk displacement. (FO: disk displacement; I: inferior alveolar nerve; AT: auricolo-temporal nerve; D: articular disk).

gested that ATN runs between fibers of the lower belly of the lateral pterygoid muscle (13). The nerve enters the parotid fascia, and then the retro-mandibular process of the parotid gland, and breaks up into smaller terminal branches. The terminal branches are mostly in line with the posterior border of the mandible above the bifurcation of the external carotid into the maxillary and superficial temporal arteries, regardless of the length of the trunk. The cluster of branches is divided into three sagittal levels by two arteries. The superficial temporal artery separates the lateral and intermediate levels; the deep auricular artery separates the intermediate and deep levels (1).

3.3 Terminal branches and related functions

The superficial temporal ramus is the largest terminal branch; it runs laterally and typically supplies fine twigs to the TMJ, passing posterior to it. Getting more superficial, it turns superiorly lying postero-medial to the superficial temporal artery, then diverges into anterior and posterior divisions. The posterior division rises in front of the ear and sometimes splits up into several twigs supplying the anterior part of the external ear above the intertragal notch (1). The divisions ramify to the skin of the temporal region. It carries only general somatic afferent fibers (sensory fibers).

Two communicating rami with the facial nerve are usually present (22). Both rami pass postero-laterally and connect with the facial nerve near to the posterior border of the mandible. They join the temporofacial division of the facial nerve and were observed to supply the upper muscles of facial expression, i.e. frontalis, orbicularis oculi and zygomaticus major. According to Namking's study (14), these fibers convey proprioceptive impulses from orbicularis oculi. This finding has special significance, since it has not been clearly established which nerve carries the proprioceptive impulses from the muscles of facial expression. It is believed that proprioception is conveyed via the same cutaneous nerves (i.e. branches of the trigeminal nerve) which innervate the skin over the muscles of facial expression and form multiple communications with the branches of the facial nerve (12). Normally, blinking occurs every six seconds and proprioception from the orbicularis oculi should therefore be important for its precise action (14). It is possible that these fibers provide proprioceptive impulses from these muscles to the trigeminal nuclei of the brainstem. Knowledge about that may be of special importance for ophthalmic, oral and maxillofacial surgeons, as lesions of communicating rami with the facial nerve may compromise proprioceptive feedback and therefore the function of orbicularis oculi.

The anterior auricular nerve at first courses laterally, then turns posteriorly and runs deep to the superficial temporal artery. It pierces the interval between the tragus and crus of the helix and supplies the skin above and below its point of entry (1). It carries only sensory fibers.

Nerves to the external acoustic meatus: deep level of the terminal spray is represented by two branches, the superior and inferior nerves to the external acoustic meatus that form neuro-vascular bundles with branches of the deep auricular artery (1). The posteromedial region of the TMJ capsule receives two to four fine branches from the superior nerve. At the level of osseocartilaginous junction of the external acoustic canal, both nerves enter. The superior nerve enters the canal by the lateral extent of the squamotympanic fissure in the bony incisure directly behind the postglenoid tubercle.

The inferior nerve pierces the antero-inferior part of the canal. Each of them gives off a medially directed ramus membranae tympani which basically supply skin of the osseous segment of the acoustic canal and the out-

er surface of the tympanic membrane. The lateral twigs of each nerve connect to the superficial temporal ramus and anterior auricular nerve to supply the skin lining the cartilaginous portion of the auditory canal. Typically, the nerve supplies the anterior and superior walls of the meatus, whereas the auricular branches of the vagus, facial, and glossopharyngeal nerves innervate the postero-inferior half of the canal (1).

The parotid rami are numerous terminal branches that provide secretomotor innervation for the parotid gland; they may also carry sensory fibers from the capsule of the gland and perhaps to myoepithelial cells and smooth muscle of the parotid gland. Parotid rami arise in two ways: as independent terminal branches or as collaterals of the major branches such as the superficial temporal ramus and the communicating rami with the facial nerve (1).

The articular rami to the posteromedial portion of the TMJ capsule originate from the superior nerve of the external acoustic meatus; the posterolateral part of the capsule is supplied by rami from the superficial temporal ramus (1).

The vascular rami carry vascular sensory fibers from the vessels. Communication between the peri-arterial nerve plexuses of the maxillary, middle meningeal, superficial temporal and accessory meningeal arteries with the ATN have been found.

Communicating rami with otic ganglion: the otic ganglion is commonly considered to contain cell bodies of postganglionic parasympathetic, secretomotor fibers for the parotid gland, but also parasympathetic vasodilator fibers for the glandular vessels and motor fibers for myoepithelial cells and smooth muscle of the duct system of the gland. The otic ganglion receives preganglionic fibers from the glossopharyngeal nerve via the tympanic plexus and the small superficial petrosal nerve. The auriculotemporal nerve, which connects to the otic ganglion through a communicating branch, carries postganglionic parasympathetic secretomotor and sympathetic vasomotor fibers for the parotid gland. In summary, the general visceral efferent fibers of the glossopharyngeal nerve (CN IX), that originate in the inferior salivatory nucleus, provides parasympathetic innervation of the parotid gland via the otic ganglion.

4. DISCUSSION

The present study aimed to emphasize the existence of topographic relations in the infratemporal fossa for mechanical influence upon the ATN. The peripheral nervous system may be injured in different ways such as nerve entrapment, especially if the nerve runs in anatomical districts where nearby anatomical structures can compress it (20).

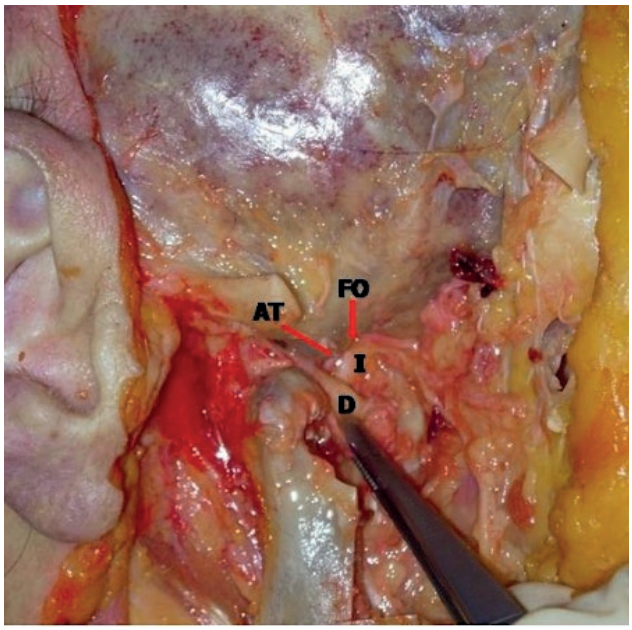

Figure 2: In this figure, the ATN is represented with two roots converging in a single trunk. I, the undersigned, Maria Grazia Poerio, being the creator of the figure 2, hereby give permission to have my artwork submitted with this article.

One of the sites that has the potential of compressing the nerves is the infratemporal fossa, a space behind the maxilla that contains several structures, including the lateral pterygoid muscle (21); these specific anatomical regions are also referred to as "points of entrapment." (21).

Entrapment process occurs when a peripheral nerve is caught and subjected to persistent mechanical trauma that triggers irritation and inflammation by means of compression, rubbing, traction or friction (9, 30,31,32). At the level of the roof of the infratemporal fossa, the mandibular nerve exits the middle cranial fossa through the foramen ovale and then immediately bifurcates, in close association with the lateral pterygoid muscle, into two divisions that originate terminal branches. The anterior division contains the anterior deep temporal, posterior deep temporal, and masseteric nerves and travels between the roof of the infratemporal fossa and the LPM. The posterior division contains the lingual, inferior alveolar, and auriculotemporal nerves and descends medial to the LPM. Of these, the auriculotemporal nerve is at greatest risk for entrapment (18, 23, 24, 25, 27).

Because of its close anatomic relation with the lateral pterygoid muscle and the TMJ capsular region described above, it was speculated that a spastic condi-

tion of the lateral pterygoid muscle or other local changes in this muscle such as myositis or myofibrositis and an internal derangement of the TMJ, such as an anteromedial disk displacement (Fig. 2), could cause nerve compression or impingement. (13, 9).

The outstanding feature of this condition is pain, probably related to focal ischemia effecting the local nervi nervorum, followed by paresthesias, hypesthesias, and dysthesias (13, 9). During jaw movements, symptoms are local sharp, shooting pains within the cutaneous preauricular area over the condyle often spreading upward into the temple or along the zygomatic arch, sometimes in conjunction with a burning sensation in the anterior half of the external ear (9). Other symptoms are otalgia, characterized by absence of aural pathology that radiates to the auricle or the temple, and itching of the external auditory meatus (ear pruritus). Therefore, sensory disturbances affect the TMJ-ear region as well as the temporal region. Furthermore, secretomotor fibers innervating the parotid gland also may be compressed and this compression could result in ipsilateral impairment of salivation (20).

Moreover, through its communicating branch, the ATN is strictly related to the facial nerve. For this reason, ATN entrapment could lead to discomfort and impaired functions in the muscles that control facial expression because of this anatomical connection.

These findings could offer an explanation to the sensory and otological disturbances that patients with TMJ disorders often complaint (26, 28,29).

5. CONCLUSIONS

The anatomical study of the ATN is pivotal since it opens the door to attributing the right etiological meaning to the symptoms reported by patients with TMJ disorders so as to direct the clinician towards the correct diagnosis and treatment. In addition, our contribution aims to underline the importance of sensory disturbances of TMJ region in order to not overlook them as etiological factors in analyzing cases. We suggest that knowledge about the topographic relationship between the TMJ and the ATN and the existence of an entrapment mechanism involving the ATN may be of special interest for otolaryngologist and oral and maxillo facial surgeons as well as for dentists.

ETHICAL APPROVAL

This paper includes experimentations on human cadavers approved by the local Ethics Committee (prot. n. 33/2020 approved on 30 July 2020).

REFERENCES

1. Algieri G.M.A., Leonardi A., Arangio P., Vellone V., Paolo C.D., Cascone P. (2017) Tinnitus in Temporomandibular Joint Disorders: Is it a Specific Somatosensory Tinnitus Subtype? Int Tinnitus J. , Apr 19;20(2):83-87. doi: 10.5935/0946-5448.20160016. PMID: 28452718.
2. Baumel J.J., Vanderheiden J.P., McElenney J.E. (1971) The auriculotemporal nerve of man. Am J Anat. Apr;130(4):431-40. doi: 10.1002/aja.1001300405. PMID: 5581228.
3. Block L.S. (1947) Diagnosis and treatment of disturbances of the temporomandibular joint especially in relation to vertical dimension. J Am Dent Assoc. Feb 15;34(4):253-60. doi: 10.14219/jada.archive.1947.0067. PMID: 2028-2523.
3. Cascone P., Fatone F.M., Paparo F., Arangio P., Iannetti G. (2010) Trigeminal impingement syndrome: the relationship between atypical trigeminal symptoms and anteromedial disk displacement. Cranio. Jul;28(3):177-80. doi: 10.1179/crn.2010.024. PMID: 20806735.
4. Costen J.B. A syndrome of ear and sinus symptoms dependent upon disturbed function of the temporomandibular joint. (1997) Ann Otol Rhinol Laryngol. Oct;106 (10 Pt 1):805-19. doi: 10.1177/000348949710601002. PMID: 9342976.
5. Davidson J.A., Metzinger S.E., Tufaro A.P., Dellon A.L. (2003) Clinical implications of the innervation of the temporomandibular joint. J Craniofac Surg. Mar;14(2):235-9. doi: 10.1097/00001665-200303000-00019. PMID: 12621296.
6. Dias G.J., Koh J.M., Cornwall J. (2015) The origin of the auriculotemporal nerve and its relationship to the middle meningeal artery. Anat Sci Int. Sep;90(4):216-21. doi: 10.1007/s12565-014-0247-9. Epub 2014 Jun 28. PMID: 24973088.
7. Fernandes P.R., de Vasconsellos H.A., Okeson J.P., Bastos R.L., Maia M.L. (2003) The anatomical relationship between the position of the auriculotemporal nerve and mandibular condyle. Cranio. Jul;21(3):165-71. doi: 10.1080/08869634.2003.11746246. PMID: 12889671.
8. Gülekon N., Anil A., Poyraz A., Peker T., Turgut H.B., Karaköse M. (2005) Variations in the anatomy of the auriculotemporal nerve. Clin Anat. Jan;18(1):15-22. doi: 10.1002/ca.20068. PMID: 15597375.
9. Johansson A.S., Isberg A., Isacsson G.A. (1990) Radiographic and histologic study of the topographic relations in the temporomandibular joint region: implications for a nerve entrapment mechanism. J Oral Max-

illofac Surg. Sep;48(9):953-61; discussion 962. doi: 10.1016/0278-2391(90)90008-p. PMID: 2395048.
10. Komarnitki I., Tomczyk J., Ciszek B., Zalewska M. (2015) Proposed classification of auriculotemporal nerve, based on the root system. PLoS One. Apr 9;10(4):e0123120. doi: 10.1371/journal.pone.0123120. PMID: 25856464; PMCID: PMC4391942.
11. Kucukguven A., Demiryurek M.D., Vargel I. Temporomandibular joint innervation: Anatomical study and clinical implications. (2022) Ann. Anat. Feb;240:151882. doi: 10.1016/j.aanat.2021.151882. Epub 2021 Dec 11. PMID: 34906668.
12. Last R.J. (1984) Anatomy: Regional and Applied. Singapore: English Language Book Society & Churchill Livingstone.
13. Loughner BA, Larkin LH, Mahan PE. (1990) Nerve entrapment in the lateral pterygoid muscle. Oral Surg Oral Med Oral Pathol. Mar;69(3):299-306. doi: 10.1016/0030-4220(90)90290-9. PMID: 2314856.
14. Namking M., Boonruangsri P., Woraputtaporn W., Güldner F.H. (1994) Communication between the facial and auriculotemporal nerves. J. Anat. Oct;185 (Pt 2)(Pt 2):421-6. PMID: 7961148; PMCID: PMC1166772.
15. Okeson, J.P., (2020a). In: Okeson, J.P. (Ed.), Signs and Symptoms of Temporomandibular Disorders. Management of Temporomandibular Disorders and Occlusion, 8th ed. Elsevier, Missouri, USA, pp. 132–173.
16. Paparo F., Fatone F.M., Ramieri V., Cascone P. (2008) Anatomic relationship between trigeminal nerve and temporomandibular joint. Eur Rev Med Pharmacol Sci. Jan-Feb;12(1):15-8. PMID: 18401968.
17. Schmid F. (1969) On the nerve distribution of the temporomandibular joint capsule. Oral Surg Oral Med Oral Pathol. Jul;28(1):63-5. doi: 10.1016/0030-4220(69)90194-7. PMID: 5255364.
18. Schmidt B.L., Pogrel M.A., Necoechea M., Kearns G. (1998) The distribution of the auriculotemporal nerve around the temporomandibular joint. Oral Surg Oral Med Oral Pathol Oral Radiol Endod. Aug;86(2):165-8. doi: 10.1016/s1079-2104(98)90119-6. PMID: 9720090.
19. Sicher H. (1948) Temporomandibular articulation in mandibular overclosure. J Am Dent Assoc. Feb;36(2):131-9. doi: 10.14219/jada.archive.1948.0021. PMID: 18906440.
20. Speciali J.G., Gonçalves D.A. (2005) Auriculotemporal neuralgia. Curr Pain Headache Rep. Aug;9(4):277-80. doi: 10.1007/s11916-005-0037-0. PMID: 16004845.
21. Thompson W.A., Kopell H.P. (1959) Peripheral entrapment neuropathies of the upper extremity. N Engl J Med. Jun 18;260(25):1261-5. doi: 10.1056/NEJM195906182602503. PMID: 13666948.
22. Woodburne Rt, Burkel We (1988) Essentials ofHuman Anatomy. New York: Oxford University Press.
23. Runci Anastasi M., et al., (2020) The discomalleolar ligament: anatomical, microscopical and radiological analysis. Surg. Radiol. Anat. May; 42 (5): 559-565
24. Runci Anastasi M., et al. (2020) Microscopic reconstruction and immunihistochemical analysis of discomalleolar ligament. Heliyon, Aug. 11; 6(8)
25. Runci Anastasi M., et al. (2020) Histological and immunofluorescence study of discal ligament in human temporomandibular joint. J. Funct. Morphol. Kinesiol. Dec. 8; 5(4): 90
26. Sindona C., Runci Anastasi M. et al. (2021) Temporomandibular Disorders Slow Down the Regeneration Process of Masticatory Muscles: Transcriptomic analysis. Medicina (Kaunas), Apr. 7; 57(4): 354
27. Runci Anastasi M. et al. (2021) Articular Disc of a Human Temporomandibular Joint: Evaluation through Light Microscopy , Immunofluorescence and Scanning Electron Microscopy. J. Funct. Morphol. Kinesiol. Feb. 25; 6(1):22
28. Maffia F. et al. (2019) Synovial chondromatosis of the temporomandibular Joint with glenoid fossa erosion: Disk preservation for spontaneous anatomical recovery. J.Craniomaxillofac. Surg. Dec.47 (12): 1898-1902
29. Vermiglio G. et al.,(2020) Immunofluorescence Evaluation of Myf5 and MyoD in Masseter Muscle of Unilateral Posterior Crossbite Patients. J. Funct. Morphol. Kinesiol. Nov. 7; 5(4): 80
30. De Ponte F.S. et al. (2013) Sarcoglycans and integrin in bisphosphonate treatment: immunohistochemical and scanning electron microscopy study. Oncol. Rep. (2013) Dec.; 30(6): 2639-46
31. De Ponte F.S. et al. (2016) Effect of bisphosphonates on the mandibular bone and gingival epithelium of rats without tooth extraction. Exp. Ther. Med. May; 11(5): 1678-1684
32. De Ponte F.S. et al. (2016) Histochemical and morphological aspects of fresh frozen bone: a preliminary study. Europ. Journal of Histochemistry Dec. 6; 60(4): 2642.

IJAE
ITALIAN JOURNAL OF ANATOMY AND EMBRYOLOGY

Firenze University Press
www.fupress.com/ijae

OPEN ACCESS

Citation: Cheryl Melovitz-Vasan, Susan Huff, Nagaswami Vasan (2023) Multiple arterial, venous and ureteric manifestations in horseshoe kidney: Developmental analysis and significance. *Italian Journal of Anatomy and Embryology* 127(1): 51-58. doi: 10.36253/ijae-14048

Data Availability Statement: All relevant data are within the paper and its Supporting Information files.

Competing Interests: The Author(s) declare(s) no conflict of interest.

Multiple arterial, venous and ureteric manifestations in horseshoe kidney: Developmental analysis and significance

Cheryl Melovitz-Vasan[1], Susan Huff[2], Nagaswami Vasan[3,*]

[1] *PT, DPT, Ph.D. Associate Professor, Department of Biomedical Sciences, Cooper Medical School of Rowan University, Camden, New Jersey 08103, USA*
[2] *BA, Medical Education Research Collaborator and Instructional Designer, Rowan University, Glassboro, New Jersey 08028, USA*
[3] *D.V.M., M.V.SC., Ph.D. Professor of Anatomy, Department of Biomedical Sciences, Cooper Medical School of Rowan University, Camden, New Jersey 08103, USA*
*Corresponding author. E-mail: vasan@rowan.edu

Abstract. Horseshoe kidney (HSK), the most common type of congenital renal fusion anomaly, is characterized by ectopia, malrotation, and altered vascular changes. Horseshoe kidney in this case is atypical because of multiple ureters, arteries, and veins, as well as how they originated and formed. During the routine dissection of 83-year-old male donor who died of respiratory failure, we observed the presence of horseshoe kidney in which the lower lobes of the left and right kidneys were connected by an isthmus below the level of inferior mesenteric artery (IMA). Furthermore, the presence of arterial, venous, and ureteric anomalies was also observed; these were sequentially dissected and are described here.

Key words: horseshoe kidney, developmental analysis, multiple vasculatures, multiple ureters, isthmus artery.

INTRODUCTION

Horseshoe kidney (HSK), the most common type of congenital renal fusion anomaly, is characterized by ectopia, malrotation, and altered vascular changes. It consists of two normally functioning kidneys connected at the lower poles by an isthmus of functioning renal parenchyma or fibrous tissue that crosses the midline of the body (Natsis et al., 2014). In 80% of the cases, the isthmus contains renal parenchyma with 20% fibrous tissues (Taghavi et al., 2016). HSKs are found in approximately 1 in 400-600 adults and are more frequently encountered in males (M:F 2:1) (Yoshinaga et al., 2002; O'Brien et al., 2008). HSKs in children are diagnosed as part of a combination of malformations or other urological problems (e.g., in Fanconi anemia in males or in diagnosis of delayed menarche seen in Turner syndrome) (Tischkowitz and Hodgson, 2003; Glodny et al., 2009). Adults are

usually asymptomatic and diagnosis is made incidentally during intravenous pyelography, standard ultrasound, or computed tomography (CT) scan performed for other reasons (Boatman et al., 1971). Anatomically, HSK involves three main anomalies: changes in vascular supply, rotation of the fetal kidneys, and abnormal position (Yoshinaga et al., 2002). The ureteropelvic junction has been reported to be higher in HSK patients and their ureters also enter at a higher level into the renal pelvis, which may result in increased incidence of urinary tract complications (Natsis et al., 2014; Yoshinaga et al., 2002; Tischkowitz and Hodgson 2003; Frego et al., 2007; Ramkumar et al., 2009). We observed other abnormalities in this study, including multiple arteries, ureters, and venous structures.

Embryologically, developing kidneys lie close to each other in the pelvis; they attain their mature position in the lumbar region during the fetal period. This "ascent" results from the growth of the embryo's body caudal to the kidneys. In the beginning, the hilum of each kidney faces ventrally; however, as the kidneys reposition, the hilum rotates to face medially. As the kidneys migrate, they are sustained sequentially by branches from the common iliac and abdominal aorta. This migration or ascent occasionally causes the kidneys to develop incorrectly. Ectopic kidney occurs when both kidneys fuse and are located in the pelvis (pancake or discoid); kidneys connect on each side at the lower poles (horseshoe kidney); kidneys remain in the pelvis (pelvic kidney); or both kidneys migrate to the same side (crossed renal ectopia) (Moore et al., 2020).

MATERIALS AND METHODS

Case report

For the present study, we utilized a donated cadaver that had been dissected and studied by the medical students at Cooper Medical School of Rowan University. During the dissection of an 83-year-old Caucasian male who died of respiratory distress, we observed the presence of horseshoe kidney; the lower lobes of the left and right kidneys were connected by an isthmus below the level of inferior mesenteric artery (IMA). The right and left renal mass extended approximately between L1 and L3 and the isthmus was at L4 level. The presence of arterial, venous, and ureteric anomalies was also observed; these were sequentially dissected and described.

The authors state that every effort was made to follow all local and international ethical guidelines and laws that pertain to the use of human cadaveric donors in anatomical research.

RESULTS AND OBSERVATIONS

We measured the length of the isthmus, keeping the crossing of ureters anteriorly as a point of reference. The distance between the two ureters was 6.2 cm. The width varied between 2.9 cm and 4.2 cm (in the middle), depending upon where it was measured. The height of the kidneys was measured superiorly from where the suprarenal gland rested on the kidneys and the beginning of the isthmus where the ureter crossed the renal moiety. The right and left kidneys were 11.1 cm and 12.2 cm long respectively. The kidney lobes were difficult to accurately discern. Due to number of vasculatures and ureters entering and leaving the renal moiety, the hilum was inadequately defined. The ill-defined hilum of the kidneys turned anteriorly and a number of arteries branched from the subdiaphragmatic abdominal aorta. To study ureters and vasculatures in detail, some of the renal medullary tissues were removed to expose and define these structures. After careful dissection of the renal tissues, we were able to discern the pattern of veins, arteries and ureters, as described below.

Renal Veins

On the left renal moiety, a major left renal vein **[a]** from the upper lobe is drained into the inferior vena cava (IVC). Other smaller veins [**a1-a3**] from the middle and inferior lobes, as well as the isthmus, directly reached the IVC, going posterior to the aorta. Both a well-defined left testicular vein **[b]** and the left suprarenal vein **[c]** drained into the left renal vein. The right renal vein from the upper [**1**] and middle lobe (not labeled) of the kidney and the right suprarenal gland [**2**] drained directly into the IVC. A noticeably large right renal vein **[3]** received venous blood from the testicular vein [**4**] and a large venous return from the lower lobe and isthmus **[5]** drained into the right renal vein [See Figure 1]. Glodny reported that the incidence of renal vein anomalies in horseshoe kidneys is high (23%) (Glodny et al., 2009). In the present case, the venous system of the HSK showed multiple variations, compared to what has been previously described (Nikumbh et al., 2014).

Renal Arteries

Both the left and right renal moieties, as well as the isthmus, were dissected to demonstrate several renal arteries that were clearly identified; they are listed below and appear in Figure 2. Additionally, the suprarenal artery from the right and left renal artery was dissected

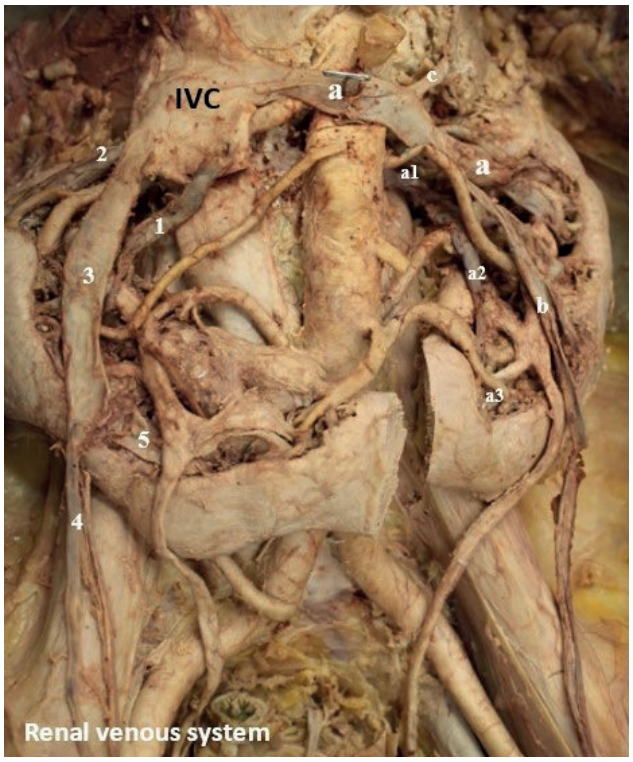

Figure 1. Photograph of a detailed dissection of the venous system of horseshoe kidney studied and presented. IVC. Inferior Vena Cava. The left renal moiety displayed several large and small veins (a, a1-3, b and c) draining into the main left renal vein. The right renal moiety exhibited many large and small veins numbered 1-5.

to show their distributions to the right and left adrenal glands. Unfortunately, the other arteries for the adrenal gland could not be clearly dissected and documented.

Right Renal Arteries

The large right renal artery **[1]** branched from the lateral aspect of the aorta below the superior mesenteric artery [SMA] and supplied the upper and middle lobe of the right renal moiety. Additionally, a branch from right renal artery also supplied the adrenal gland through a well-defined right suprarenal artery **[1a]**. The branch **[2]** that arose from the anterior aspect of the aorta supplied the middle lobe and, through a small branch, the inferior lobe, as well. An arterial branch arose from the lateral aspect of lower part of aorta **[3]**; it supplied the middle and inferior lobe of the right kidney. A branch **[4]** arose from the anterior aspect of the lower part of aorta to supply the inferior lobe and isthmus. The branch **[5]** that originated from the right common iliac **[RCI]** artery bifurcated behind the isthmus to supply the inferior lobe and, through an isthmus artery, the isthmus, as well (Killen et al., 1968; Wilder et al., 1963; Cohn et al., 1969) [See Figure 2 - RK].

Left Renal Arteries

A large left renal artery **[a]** that originated from the lateral aspect of the abdominal aorta below the superior mesenteric artery immediately bifurcated in to a superior and inferior branch. The superior branch supplied primarily the upper lobe and the inferior branch supplied the upper lobe and through a small branch to the middle lobe. Arising from the lateral aspect of the aorta the **[b]** primarily supplied the middle lobe and through a small branch to the lower lobe. A branch **[c]** that originated from the aorta inferior to the IMA provided blood supply to the middle lobe and through a small branch the inferior lobe. The large branch **[d]** began from the anterolateral aspects of the aorta branched to supply the lower lobe and through a well-defined isthmus artery **[d1]** the isthmus [See Figure 2 - LK].

Ureters

Due to the lack of well-defined hilum, dissection was carried out by removing much of the renal medullary tissues to study the ureters in detail. This exposed the major calyceal system from different lobes of the renal mass which entered the hilum independently and contributed to formation of units of a ureter. Extrarenal calyces, wherein the calyces and renal pelvis lie outside the renal parenchyma, is one of the rare anomalies of the collecting system (Raghunath et al., 2012). There is considerable variation in the number of renal calyces and the shape of the renal pelvis, but there is also a marked variation in the position of the renal pelvis. Thus, a pelvis may lie almost entirely within the sinus (an intrarenal pelvis) or its main portion may be a dilated sac and lie outside the kidney proper (an extrarenal pelvis) (Raghunath et al., 2012). Variations in the major calyces and pelvis are more striking. The major calyces may pass downward for some distance beyond the hilum and end by joining to form the ureter without undergoing any obvious expansion. In such cases, the pelvis is absent; if the calyces dilate, one or two pelves may be present (Rao et al., 2012) [See Figure 3].

Right Kidney

From the right kidney, the superior lobe calyx formed a large ureter **[1]** that joined a small ureter **[2]**

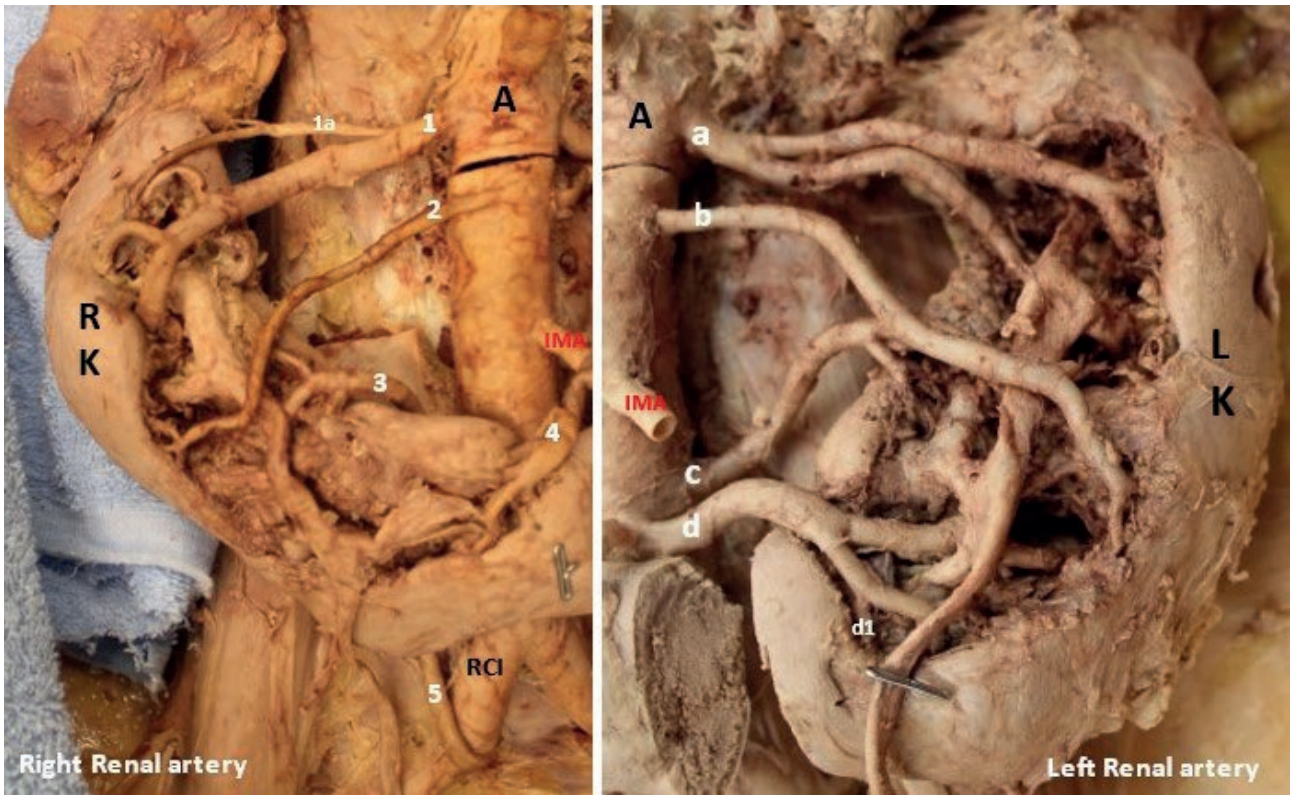

Figure 2. Photograph of a detailed dissection of the horseshoe kidney displaying the heterogeneity of the arterial system of right and left renal moiety and the isthmus studied. RK-Right Kidney, LK-Left Kidney, A-Aorta, IMA- Inferior mesenteric artery, RCI- Right Common Iliac artery. The right renal moiety (RK) is supplied by several large and small arteries labeled [1-4] branching from the aorta, a supra renal artery [1a] branching from artery 1 and a branch 5 from the right common iliac artery [1]. We observed that the isthmus was also supplied by a branch from artery 5 (not displayed in the photograph). The left renal moiety (LK) is also supplied by several arterial branches from the aorta [a-d] and a small 'isthmus artery' [d1] branching from d.

from the middle lobe calyx. A small ureter from the calyx of the lower lobe **[3]** and a large ureter **[4]** from the isthmus joined the longitudinal ureter. In a real sense, 1 through 4 are tributaries that united to distally form the ureter **[Ur]** proper. Unlike in a normal kidney, both the ureters in the HSK reported here did not lie on the ventral surface of the psoas muscle, but crossed the common iliac artery distally and entered the urinary bladder posterolaterally [See Figure 3 – RKur].

Left Kidney

From the left kidney, the superior lobe calyx formed a medium sized ureter **[a]** that joined by a medium sized ureter **[b]** from the middle lobe calyx. A medium sized ureter from the calyx of the lower lobe **[c]** and a large sized ureter **[d]** from the isthmus joined the longitudinal ureter. In a real sense, a through d, are tributaries that united to distally form the ureter [Ur] proper [See Figure 3 – LKur].

DISCUSSION

The development of the kidney begins in the fourth week of gestation by inductive interaction between the ureteric bud and the metanephric blastema. The ureteric bud arising from the mesonephric duct gives rise to the collecting tubules and the pelvicalyceal system; the metanephros develop into an excretory part formed by nephrons. During the sixth to ninth weeks of gestation, the developing kidney ascends due to differential growth of dorsal and caudal regions to reach its mature position in the posterior lumbar region. During ascent, the kidneys sequentially receive arterial supply from iliac arteries and the abdominal aorta. During the ascent, the kidney also undergoes axial rotation, resulting in the hilum which is initially placed anteriorly, but becomes medial. Congenital renal anomalies can occur due to abnormalities of development, migration, and rotation (Moore et al., 2020).

HSK is one of the most common renal anomalies; it occurs approximately 1 in 400-600 individuals and

Figure 3. Photograph of a detailed dissection of the horseshoe kidney displaying the heterogeneity of the ureteric system of right and left renal moiety and the isthmus studied. Please note that the position of the kidney facing anteromedially medially with a poorly defined hilum. The right renal moiety [RK] displayed three ureteric components [1-3] and a large ureteric part from the isthmus [4], all joining to form the ureter [Ur]. From the left renal moiety [LK], there are four ureteric structure [a-d] joined to form the ureter [Ur].

is more frequent in men than women (2:1 ratio) (Yoshinaga et al., 2002). No genetic or ethnic association has been linked with HSK, although siblings within the same family have been reported (Yoshinaga et al., 2002). HSK in adults is usually asymptomatic and discovered during routine imaging studies conducted for other reasons. During the early 1900s, embryologists posited a number of theories to explain HSK. Domenech-Mateu and Gonzalez-Compta examined human embryos (crown-rump lengths of 3-19 mm) from the Ballaterra Collection (Domenech-Mateu and Gonzalez-Compta,1988). They showed that there are two kinds of horseshoe kidneys: one wherein the isthmus is made up of material derived from mesenchyme and the other wherein the isthmus is composed of renal parenchyma. Additionally, they arranged the HSK malformations into three groups: 1) early fusion due to a converging course taken by the ureteric buds, which may force the metanephric blastemas to become closer and eventually merge (Arey, 1974); 2) as a consequence of the relation between the metanephroi and the umbilical arteries during development (Lewis and Papez (1915); and 3) related to the association of several factors.

MECHANISM OF FUSION ANOMALIES

The exact mechanism of the development of renal fusion anomalies is not completely understood and many theories have been advanced to explain this abnormality (Babu et al., 2015).

1. Mechanical Theory proposes that, during cranial migration, the kidneys pass through the fork between the two umbilical arteries and any positional change in these arteries wedge the kidneys close together, resulting in their fusion and in HSK. Fusion of both nephrogenic blastemas with early arrested migration results in a completely fused pelvic kidney. Abnormal position of an umbilical artery can result in abnormal migration of a renal unit to the contralateral side, following the path of least resistance (crossed renal ectopia).

2. Theory of Abnormal Caudal Rotation suggests that fusion occurs due to lateral flexion and rotation of the caudal end of the embryo, disturbing the relative position of the nephrogenic blastema and ureteric bud (Cook and Stephens, 1977). The distal curled end of the vertebral column permits one ureter to cross the midline and enter the opposite nephrogenic blastema or transplant the kidney and ureter to the opposite side during ascent. Association of scoliosis with crossed renal ectopia supports this theory.

3. Ureteral Theory states that crossover is strictly a ureteral phenomenon with the developing ureteral bud wandering to the opposite side and inducing the differentiation of the contralateral metanephric blastema; it is assumed that the metanephric tissue that does not receive a ureteric bud regresses.

4. Teratogenic Theory posits that HSK results from abnormal migration of posterior nephrogenic cells due to teratogenic insult, forming a parenchymal isthmus (Doménech-Mateu and Gonzalez-Compta 1988; Tijerina de la Garza et al.,2009). The increased incidence of malignancies and other organ system anomalies associated with HSK possibly supports this theory (Nastis et al., 2014).

5. Genetic Theory suggests that genetic influence may play a role because some renal fusion anomalies have been reported to occur in identical twins and siblings within the same family. It is suggested that the sonic hedgehog gene signal is critical for kidney positioning along the mediolateral axis and its disruption will result in renal fusion (Shapiro et al., 2012). McPherson suggested that HSK may occur as a previously undescribed autosomal dominant condition (McPherson, 2007). Analysis of patients with Turner syndrome revealed that 33% of patients studied had some renal malformations, with HSK occurring in 7% of these, rendering support to the genetic theory (Lippe et al., 1988).

The following is intended to highlight the uniqueness of the HSK studied and presented here. These include the veins, arteries, and ureters with what was observed and how they compared and differed from the reports available from other studies.

Veins

In an earlier study, Nikumbh et al. reported that two tributary veins, superior and inferior, that originated from the right hilum and formed the right renal vein drained into the IVC (Nikumbh et al., 2014). The right suprarenal vein directly drained into IVC, but the right gonadal vein drained into right renal vein. The left kidney was drained by the left renal vein, which had four tributaries outside the hilum. Normally, the left suprarenal and gonadal veins drain into the left renal vein. Interestingly, we also observed the presence of an "isthmus" vein that drained into IVC [See Figure 1]. However, Nikumbh et al. and Natsis et al. did not observe an isthmus vein (Nikumbh et al., 2014; Natsis et al., 2014). In the present study, we observed multiple variations of veins, including an isthmus vein, and their drainage pattern [See Figure 1].

Arteries

Because of its anomalous embryologic origin, HSK have multiple renal arteries (Boatman et al., 1971). A systematic study by Graves described six basic patterns of arteries in HSK and, more importantly, that each artery supplies its own area, with no collateral circulation between segments (Graves 1969). In our study, an accurate demonstration and description of the arteries was challenging, due to the lack of a well-defined hilum and the way multiple arteries arose not only from the aorta, but also from the common iliac artery to enter the renal moieties [See Figure 2]. Furthermore, each artery also supplied more than one lobe. While much of the arterial distribution in our case followed Graves's six patterns of arteries, it also differed to some extent in how the arteries branched and distributed (Graves 1969).

Clinical significance

HSK has been reported to have a close relationship with vascular, calyceal, and ureteral abnormalities (Nastis et al., 2014). Upper urinary tracts of HSKs are characterized by the great variation in their number and origin. Typically, calyces are located in the upper two-thirds of each kidney, but an external calyx or an independent ureter may drain the isthmus (Pawar et al., 2018). In HSK, the fusion of the lower poles results in abnormal position of the ureter in the renal pelvis and highly placed ureteropelvic junction. Impaired drainage of the collecting system and associated ureteropelvic obstruction may predispose the patient to kidney stones

and hydronephrosis that is usually the result of a urinary tract obstruction. HSK is also common in some genetic diseases, such as Turner syndrome (Ranke and Saenger, 2001) and Trisomy 18 (Cereda and Caret, 2012). Ribs do not protect HSK well; trauma may cause injury across the lumbar vertebral column (O'Brien et al., 2008).

Clinical manifestation of horseshoe kidney

HSK is usually asymptomatic and often discovered as an incidental finding. When symptoms do occur, it is predominantly due to infection, obstruction, or stones. The most common finding in HSK is ureteropelvic junction (UPJ) obstruction; O'Brien estimates that up to 35% of HSK patients may be affected (O'Brien et al., 2008). UPJ obstruction can occur when a high insertion of ureters into the kidney pelvis causes delayed pelvic emptying. Another rare cause of obstruction can be the crossing of the ureter over the HSK isthmus (Costa et al., 2004). A diagnosis of UPJ obstruction is made based on a CT urography or intravenous pyelography with a typical appearance of a large pelvis with a high-riding ureter in the pelvis.

CONCLUSION

HSK is the most common congenital anomaly of the urinary tract. These kidney fusion anomalies are mostly asymptomatic; however, significant symptoms, especially hydronephrosis, kidney stones, and infections, represent causes of death in HSK patients. An abnormal kidney is usually related to a range of anatomical changes. Vessel relations and supply are highly variable. Furthermore, horseshoe kidneys are characterized by various ureteric patterns. All of these abnormalities have important clinical implications. The vascular and ureteral anomalies seen in the case presented here is especially important when surgery is contemplated.

FUNDING

This study was supported by the Faculty Development Funds administered by the Cooper Medical School of Rowan University.

ACKNOWLEDGEMENTS

The authors sincerely thank the donor and his family for their generosity, which made this study possible and facilitated scientific and medical innovations in patient care.

The authors state that every effort was made to follow all local and international ethical guidelines and laws that pertain to the use of human cadaveric donors in anatomical research.

REFERENCES

Arey L.B. (1974) Developmental anatomy: A textbook and laboratory manual of embryology, 7th edition. W.B. Saunders Co., Philadelphia, Pa.

Babu C.S.R., Sharma V., Gupta O.P. (2015) Renal fusion anomalies: a review of surgical anatomy. Anat Physiol. 5:S5-001. doi:10.4172/2161-0940.S5-001

Boatman D.L., Cornell S.H., Kölln C.P. (1971). The arterial supply of horseshoe kidneys. Am J Roentgenol Radium Ther Nucl Med. 113:447-451.

Cereda A., Carey J.C. (2012) The trisomy 18 syndrome. Orphanet J Rare Dis. 7:Article 81. https://doi.org/10.1186/1750-1172-7-81

Cohn L.H., Stoney R.J., Wylie E.J. (1969) Abdominal aortic aneurysm and horseshoe kidney. Ann Surg. 170:870-874.

Cook W.A., Stephens F.D. (1977) Fused kidneys: morphologic study and theory of embryogenesis. Birth Defects Orig Artic Ser. 13:327-340.

Costa R.P., Schaal C.H., Navarro F.C. (2004). Neoplasia in horseshoe kidney with pyelic fusion and crossed single ureter. Int Braz J Urol. 30:319-320.

Doménech-Mateu J.M., Gonzalez-Compta X. (1988) Horseshoe kidney: a new theory on its embryogenesis based on the study of a 16-mm human embryo. Anat Rec. 222:408-417.

Frego M., Bianchera G., Angriman I., Pilon F., Fitta C., Miotto D. (2007) Abdominal aortic aneurysm with coexistent horseshoe kidney. Surg Today. 37:626–30.

Glodny B., Petersen J., Hofmann K.J., Schenk C., Herwig R., Trieb T., Koppelstaetter C., Steingruber I., Rehder P. (2009). Kidney fusion anomalies revisited: clinical and radiological analysis of 209 cases of crossed fused ectopia and horseshoe kidney. BJU Int. 103:224-235.

Graves F.T. (1969) The arterial anatomy of the congenitally abnormal kidney. Br J Surgery. 56:533-541.

Killen D.A., Scott H.W., Rhamy R.K. (1968) Aneurysm and arterial occlusive disease of the abdominal aorta and its major branches associated with horseshoe kidney. Amer J Surg. 116:920-924.

Lewis F.T., Papez J.W. (1915) Variations in the early development of the kidney in pig-embryos with spe-

cial reference to the production of anomalies. Proceedings of the American Association of Anatomists. Abstracts. Anat Rec. 9:105-106.

Lippe B., Geffner M.E., Dietrich R.B., Boechat M.I., Kangarloo H. (1988) Renal malformations in patients with Turner syndrome: imaging in 141 patients. Pediatrics. 82:852-856.

McPherson E. (2007) Renal anomalies in families of individuals with congenital solitary kidney. Genet Med. 9:298-302.

Moore K.L., Persaud T.V.N., Torchia M.G. (2020) Urogenital System. In: Moore K.L., Persaud T.V.N., Torchia M.G.: The Developing Human: Clinically Oriented Embryology, 11th Ed. Elsevier, Edinburgh. Pp 223-262.

Natsis K., Piagkou M., Skotsimara A., Protogerou V., Tsitouridis I., Skandalakis P. (2014) Horseshoe kidney: a review of anatomy and pathology. Surg Radiol Anat. 36:517-526.

Nikumbh R.D., Kazi S., Ughade M.N. (2014) Gross anatomy of the horseshoe kidney: a case report with brief review of literature. Eur J Anat. 18:128-131.

O'Brien J., Buckley O., Doody O., Ward E., Persaud T., Torreggiani W. (2008) Imaging of horseshoe kidneys and their complications. J Med Imaging Radiat Oncol. 52:216-226.

Pawar A.S., Thongprayoon C., Cheungpasitporn W., Sakhuja A., Mao M.A., Erickson S.B. (2018) Incidence and characteristics of kidney stones in patients with horseshoe kidney: A systematic review and meta-analysis. Urol Ann. 10:87-93.

Raghunath B.V., Narendra B.M., Gowrishankar B.C., Ramesh S.. (2012) Extrarenal calyces associated with pelviureteric junction obstruction: A case report of a rare anomaly. J Indian Assoc Pediatr Surg. 17:124-125.

Ramkumar H., Ahmed S.M., Syed E., Tuazon J. (2009) Horseshoe kidney in an 80-year-old with chronic kidney disease. Scientific World Journal 9:1346–1347.

Ranke M.B., Saenger P. (2001) Turner's syndrome. Lancet. 358:309-314.

Rao S., Nikolai O., Avinash J., Tantradi R.R. (2012) Bilateral extrarenal calyces, renal pelvis and associated variations of renal vessels – A rare variation of the renal collecting system. IJAV. 5:62-64.

Shapiro E., Bauer S.B., Chow J.S. (2012) Anomalies of the upper urinary tract. In: Wein A.J. Campbell-Walsh Urology, 10th edition. Elsevier Saunders, Philadelphia. Pp. 3123-3160.

Taghavi K., Kirkpatrick J., Mirjalili S.A. (2016). The horseshoe kidney: Surgical anatomy and embryology. J Pediatr Urol. 12:275-280.

Tijerina de la Garza O., Uresti J., Urrutia de la Vega E., Elizondo-Omana R.E., Guzmán-López S. (2009) Anatomical study of the horseshoe kidney. Int J Morphol. 27:491-494.

Tischkowitz M.D., Hodgson S.V. (2003) Fanconi anaemia. J Med Genet. 40:1-10.

Wilder J. R., Koch J. M., Stein A. (1963) Abdominal aortic aneurysms in association with horseshoe kidney. JAMA. 183:1038-1041.

Yoshinaga K., Kodama K., Tanii I., Toshimori K. (2002) Morphological study of a horseshoe kidney with special reference to the vascular system. Anat Sci Int. 77:134–139.

IJAE
ITALIAN JOURNAL OF ANATOMY AND EMBRYOLOGY

Firenze University Press
www.fupress.com/ijae

OPEN ACCESS

Citation: Midhat Syed, Farah Syed, Masooma Syed (2023) Morphometric analysis of glenoid cavity in adult human scapulae and its clinical importance. *Italian Journal of Anatomy and Embryology* 127(1): 59-62. doi: 10.36253/ijae-14299

Data Availability Statement: All relevant data are within the paper and its Supporting Information files.

Competing Interests: The Author(s) declare(s) no conflict of interest.

ORCID
MiS: 0000 0002 0168 3670
FS: 0000 0002 8811 9211
MaS: 0000 0002 3515 3635

Morphometric analysis of glenoid cavity in adult human scapulae and its clinical importance

Midhat Syed, Farah Syed*, Masooma Syed

Department Anatomy Government Medical College, Srinagar, India
Corresponding author: E-mail: syefar001@gmail.com

Abstract. *Background:* The glenoid cavity of scapula is quite small, which allows space for only limited fixation devices. Appropriate fixation of the glenoid component of shoulder is of key importance in total shoulder arthroplasty to prevent loosening, which is a common indication of revision surgery. Orthopedic surgeons and prosthetic designers must have a thorough understanding of the glenoid's dimensions and shape, in order to create the finest feasible prosthesis. *Aims and objectives:* To determine the glenoid cavity index (GCI) and the form of the glenoid cavity, as well as the supero-inferior diameter, shortest antero-posterior diameter, and longest antero-posterior diameter. *Materials and methods:* The study was conducted on 50 dry unpaired adult human scapulae of North Indian population obtained from GMC, Srinagar. All the important morphometric parameters were studied using a vernier calliper. *Result:* Supero-inferior diameter, shortest antero-posterior diameter, and longest antero-posterior diameter were found to have respective mean values of 35.06 mm, 15.8074 mm, and 23.3814 mm. Glenoid cavity index had a mean value of 66.68. 42% of the glenoid cavities had an inverted comma shape, 36% had a pear shape, and 22% had an oval shape. *Conclusion:* The results showed that mean supero-inferior diameter of glenoid is about 35mm while the average prosthesis for shoulder arthroplasty in the market starts from 40mm. This suggests that while developing and fitting glenoid components for total shoulder arthroplasty in the North Indian population, it may be necessary to take into account the smaller dimensions of the glenoid cavities.

Keywords: clinical anatomy, orthopedics, glenoid, shoulder joint.

INTRODUCTION

The scapula, or shoulder blade, is located in the postero-lateral portion of the chest wall. In the glenohumeral joint, it articulates with the head of the humerus and the distal end of the clavicle. Careful study of the scapula's measurement is necessary to comprehend the mechanics of rotator cuff disease, total shoulder arthroplasty, and recurrent shoulder dislocation (1). The glenoid cavity, also known as the upper and lateral angle of the scapula, is a pyriform, shallow anterior surface for articulation with the head of the humerus (2). Based on the presence of a notch on the front of glenoid rim, the morpholo-

gies of the glenoid cavity have been categorised into pear-shaped, inverted comma-shaped, and oval-shaped cavities (3)(4). The body's most unstable joint is the glenohumeral joint since it can do a wide variety of movements (5).

It has been proven that full thickness rotator cuff tears are related to glenoid inclination (6). In order to comprehend shoulder dislocations, rotator cuff pathology, and to precisely estimate the glenoid component in total shoulder arthroplasty, variations in the form and size of the glenoid cavity are crucial (6). It also plays a vital role as a prognostic factor in primary gleno-humeral osteoarthritis.

Nowadays, the majority of the implants consist of a range of 3 to 5 sizes, with progressive increments in both height (superior inferior) and width (anterior posterior). However, all these sizes share a common radius of curvature at the bone/implant interface. Based on the findings of anatomical investigations conducted on healthy (non-arthritic) glenoid articular surfaces, the sizes and radii of curvature of these implants were chosen (7).

MATERIAL AND METHODS

For the present study, fifty (50) dry, undamaged scapulae were observed in the Department of Anatomy of GMC, Srinagar. Bones with distinct, unaltered traits were used. The age and sex of the scapulae were unknown. Using sliding Vernier callipers, the glenoid cavity's superior-inferior and antero-posterior dimensions were measured. Data was also used to calculate the Glenoid Cavity Index (GCI). Morphological shape of glenoid cavity was recorded as comma shaped, pear shaped and oval shaped. The various dimensions were taken as follows:

Superio-inferior diameter: It was determined to be the greatest distance between the most prominent supraglenoid tubercle point and the most inferior glenoid margin point (designated as AB in Figure 1).

Antero-posterior diameter 1: It was determined to be the maximum width of the articular edge of the glenoid cavity, measured perpendicular to the height (designated as CD in Figure 1).

Antero-posterior diameter 2: Diameter of the superior half of glenoid cavity at mid-point between the superior rim and mid-equator (designated as EF in Figure 1).

Glenoid Cavity Index (GCI): It can be deduced by the following formula:

$$GCI = \frac{\text{Antero-posterior diameter1}}{\text{Superio-inferior diameter}} \times 100$$

Shape of Glenoid: Placing the paper over the glenoid cavity and firmly holding it there while drawing the shape with a pencil allowed the shape to be seen on the plain paper. The three most common shapes seen in the Glenoid are shown in Figure 2.

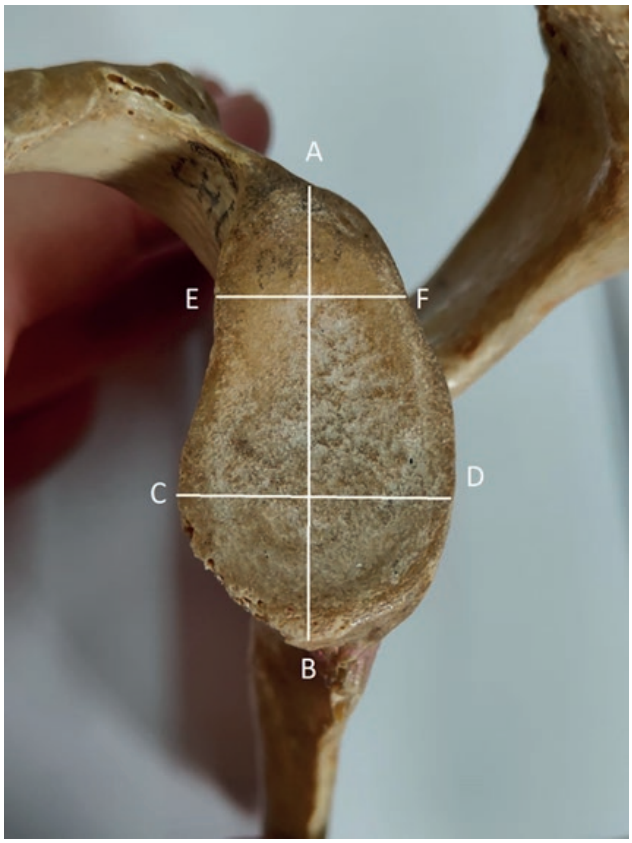

Figure 1. Various parameters of Glenoid cavity taken.

RESULTS

Measurements related to Glenoid cavity dimensions are documented in Table 1. The values observed are presented as mean and standard deviation (mean ± SD).

In the present study, the maximum recorded superoinferior diameter (AB) was 40mm while the minimum diameter was 26mm. The mean diameter came out to be 34.97±3.62mm. The maximum antero-posterior diameter (CD) at the widest breadth was 28mm while the minimum breadth was 17mm. The mean diameter was 23.45±2.69mm. The maximum recorded antero-posterior diameter (EF) was 28mm while the minimum recording was 10mm. The mean diameter was 16.82±3.06mm. The Glenoid Cavity Index was also measured for all the scapulae and the minimum value obtained was 55.2 while the maximum value calculated was 82.3. The shape of glenoid was also observed; the three most common shapes

Figure 2. Various shapes of glenoid seen.

Table 1. Various parameters of Glenoid cavity with their mean and standard deviation.

S. No	Parameters	Number of scapulae	Minimum Value (mm)	Maximum Value (mm)	Mean (mm)	Standard deviation
1.	Supero-inferior diameter (AB)	50	26	40	34.97	3.62315
2.	Antero-posterior diameter 1 (CD)	50	17	28	23.459	2.699162
3.	Antero-posterior diameter 2 (EF)	50	10	28	16.821	3.069968
4.	Glenoid Cavity Index (GCI)	50	55.2	82.3	66.796	6.058884

Table 2. Various shapes of Glenoid cavity with their percentage.

S. No	Shape of the glenoid	Total scapulae	Number	Percentage
1.	Inverted comma shape	50	21	42%
2.	Oval shape	50	11	22%
3.	Pear shape	50	18	36%

seen were inverted comma shaped, pear shaped and oval shaped. Out of 50 scapulae, 21 (42%) were inverted comma shaped, 18 (36%) were pear shaped and 11 (22%) were oval shaped. The various shapes of glenoid recorded are tabulated in Table 2.

DISCUSSION

In present study the Superio-inferior diameter of glenoid cavity varied from 26mm to 40mm with mean of 34.97mm. The antero-posterior diameter 1 of glenoid cavity varied from 17mm to 28mm with mean of 23.45mm. The Antero-posterior diameter 2 varied from 10mm to 28mm with the mean of 16.82mm. These values when compared with the data obtained from other countries show that the supero-inferior diameter and the antero-posterior diameter 1 seen in Indian population is lesser than those counties. Coskun et al. (2006) (8) with their study based in Turkish population, shows a mean supero-inferior diameter of 36.3mm, while von Shroeder et al. (2001) (9) shows the mean supero-inferior diameter as 36.4mm in the Canadian population. Cho et al. (2011)(10) also shows a mean supero-inferior diameter of 35.2mm in the Korean population. The parameters seen in comparison with foreign authors are in Table 3.

CONCLUSION

The glenoid cavity dimensions are required by prosthetic engineers and orthopaedic surgeons to design a

Table 3. Comparison of SI diameter and widest AP diameter with foreign authors.

S. No	Authors	Country	Supero-inferior diameter (mm) [AB]	Antero-Posterior diameter (mm) [CD]
1	Coskun et al. (2006) (8)	Turkey	36.3	24
2	Von Schroeder et al. (2001) (9)	Canada	36.4	29
3	Cho et al. (2011) (10)	Korea	35.2	-
4	Present study	India	34.9	23.4

workable and reliable prosthetic for total shoulder arthroplasty. The mean supero-inferior diameter and mean antero-posterior diameter1 in the present study show a lower value than what is seen in some other countries. This indicates that the prosthetic design for the Indian population needs to be tailored to the specific dimensions to reduce the incidence of failure of the surgery.

BIBLIOGRAPHY

1. Gallino M, Santamaria E, Doro T. Anthropometry of the scapula: Clinical and surgical considerations. J Shoulder Elbow Surg. 1998;7(3):284–91.
2. B Rajput H, K Vyas K, D Schroff B. A Study of Morphological Patterns of Glenoid Cavity of Scapula. National Journal of Medical Research. 2012 Oct; 2(4):504–7.
3. El-Din WAN, Ali MHM. A Morphometric Study of the Patterns and Variations of the Acromion and Glenoid Cavity of the Scapulae in Egyptian Population. J Clin Diagn Res. 2015 Aug 1; 9(8):AC08-11.
4. Prescher A, Klumpen T, Mpen. The glenoid notch and its relation to the shape of the glenoid cavity of the scapula. J Anat. 1997;190:457–60.
5. Saha S, Vasudeva N. Morphological Variations of Glenoid Cavity of Human Scapulae: An Anatomical Study with Clinical Relevance. International Journal of Anatomy and Research. 2020 Feb 5; 8(1.2):7288–93.
6. Hughes RE, Bryant CR, Hall JM, Wening J, Huston LJ, Kuhn JE, et al. Glenoid Inclination is Associated With Full-Thickness Rotator Cuff Tears. Clinical Orthopaedics and related Research . 2003;407:86–91.
7. Moineau G, Levigne C, Boileau P, Young A, Walch G. Three-dimensional measurement method of arthritic glenoid cavity morphology: feasibility and reproducibility. Orthop Traumatol Surg Res. 2012 Oct; 98(6 Suppl).
8. Coskun N, Karaali K, Cevikol C, Demirel BM, Sindel M. Anatomical basics and variations of the scapula in Turkish adults. Saudi Med J. 2006 Sep; 27(9):1320–5.
9. von Schroeder HP, Kuiper SD, Botte MJ. Osseous anatomy of the scapula. Clin Orthop Relat Res. 2001; 383(383):131–9.
10. Cho SH, Cho NS, Rhee YG. Preoperative analysis of the hill-sachs lesion in anterior shoulder instability: How to predict engagement of the lesion. American Journal of Sports Medicine. 2011 Nov; 39(11):2389–95.

IJAE
ITALIAN JOURNAL OF ANATOMY AND EMBRYOLOGY

Firenze University Press
www.fupress.com/ijae

OPEN ACCESS

Citation: Pawel Iwaszkiewicz, Robert Iwanowski, Slawomir Wozniak (2023) Sonographic imaging of the great occipital nerve in the diagnosis and treatment of primary headache disorders. *Italian Journal of Anatomy and Embryology* 127(1): 63-67. doi: 10.36253/ijae-14301

Data Availability Statement: All relevant data are within the paper and its Supporting Information files.

Competing Interests: The Author(s) declare(s) no conflict of interest.

Sonographic imaging of the great occipital nerve in the diagnosis and treatment of primary headache disorders

Pawel Iwaszkiewicz[1], Robert Iwanowski[1,*], Slawomir Wozniak[2]

[1] *STN (Students Scientific Society) ANATOMIA-KLINIKA-NAUKA. Wroclaw Medical University, Department of Human Morphology and Embryology, Division of Anatomy, Chalubinskiego 6a, 50-368 Wroclaw, Poland*
[2] *Wroclaw Medical University, Department of Human Morphology and Embryology, Division of Anatomy, Chalubinskiego 6a, 50-368 Wroclaw, Poland*
*Corresponding author. E-mail: robert.iwanowski@student.umw.edu.pl

Abstract. Primary headaches are a type of headache that occurs independently, without any other underlying medical condition or injury. They are a major concern due to their prevalence in the population and their potential to cause significant disruption to daily life. In past years, new techniques have been developed that utilize sonography in diagnosing and treating headache disorders. Some recent publications have appeared on the use of ultrasound in blocks of the greater occipital nerve and the diagnosis of headaches. For a long time, blocks of the nerve have been performed without target visualization, based on exterior landmarks only. New methods may improve the results of performed procedures. Therefore, this study aims to provide an overview of the applications of ultrasound imaging of the greater occipital nerve in clinical practice.

Keywords: greater occipital nerve, primary headache disorders, sonography.

INTRODUCTION

The greater occipital nerve (GON) is a sensory nerve that arises from the medial division of the dorsal ramus of the second cervical nerve. It emerges under the obliquus capitis inferior muscle (OCI) and then courses along the posterior neck, passing between the OCI and the semispinalis capitis (SSC). In the further course, the nerve pierces the SCC and the trapezius muscle (TP) to enter the scalp. Here, it gives rise to branches that provide cutaneous sensory innervation to the occipital region [1]. Studies have shown that the GON may play a key role in primary headaches, such as migraine and tension-type headaches [2], but the pathophysiology is not entirely understood.

Primary headaches are a type of headache that occurs independently, without any other underlying medical condition or injury. According to ICHD-3 (3rd edition of The International Classification of Headache Disorders), primary headaches include migraines, tension-type headaches, trigemi-

nal autonomic cephalalgias, and other primary headache disorders [3]. They are a major concern due to their prevalence in the population and their potential to cause significant disruption to daily life. Estimates suggest that almost three billion individuals suffer migraines or tension-type headaches [4]. Increasing interest in primary headaches has led to the development of new treatment and diagnostic options, some of which involve ultrasound.

The purpose of this article is to provide an overview of the current applications of ultrasound of the GON in the diagnosis and treatment of primary headaches. We concentrate on the sonographic examination technique, changes in the nerve morphology in pathological states, and sonographic guidance in the GON blockade.

SONOGRAPHIC ANATOMY AND EXAMINATION TECHNIQUE

In clinical practice, the GON is usually visualized at the distal location at the height of the superior nuchal line or the proximal location at the level of the C2 spinous process. In both cases, a patient should be in a prone or sitting position with minimal flexion in the cervical spine. To localize the nerve at the proximal location, a linear transducer is placed in a transverse plane beneath the external occipital protuberance (EOP) and then moved downwards until the C2 bifurcated spinous process is seen. The probe is then moved laterally and oriented towards the mastoid process (MP) (see Figure 1). The view of the OCI and the SSC separated by connective tissue should be obtained. The GON will be seen as a hypoechoic oval within the connective tissue surroundings. To localize the nerve at the distal location, the occipital artery (OA) should be identified using Doppler mode at the level of the superior nuchal line. The GON should be visible in close proximity to the OA as a small hypoechoic oval structure. In patients with long hair, using an excess ultrasound gel may help move the hair away from the examined area.

In a study published by Cho JC. et al. [5], the GON was successfully identified at the proximal location in 49 out of 60 examinations in 30 healthy individuals. They reported that the nerve was hypoechogenic, round to oval structure with a mean cross-sectional area of $2mm^2 \pm 1mm^2$ and a mean circumference of 4.8mm ±1.3mm in both males and females. Greher M. et al. performed a study on cadavers, where they examined the GON in proximal and distal locations [6]. In the proximal site, the median depth of the nerve was and the median distance from the C2 spinous process was 27.6mm. In the distal site, the median depth was 8.0mm

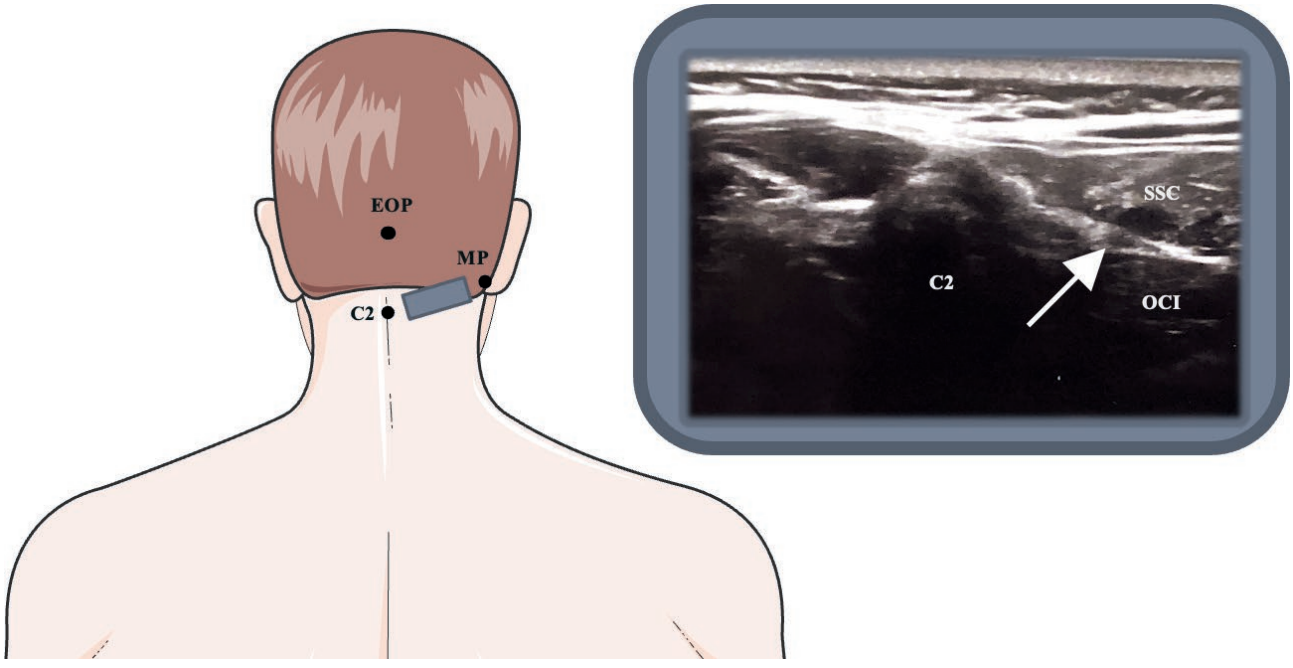

Figure 1. Position of the linear transducer at the proximal location. The GON is indicated by the white arrow. EOP - external occipital protuberance. MP - mastoid process. C2 - the spinous process of C2. OCI - obliquus capitis inferior muscle. SSC - semispinalis capitis muscle. The Figure was partly generated using Servier Medical Art, provided by Servier, licensed under a Creative Commons Attribution 3.0 unported license.

and the median distance from the EOP was 17.4mm. Shim JH. et al. [7] reported that the right nerve was on average 23.1mm away from the EOP, 1.5mm from the OA and 6.8mm from the skin. The left nerve was on average 20.5mm away from the EOP, 1.2mm from the OA and 7.3mm from the skin surface. Measurements were collected in the distal location. They managed to successfully visualize the nerve in 35 out of 40 cases in 20 volunteers. To our knowledge, there are very few publications describing the sonographic anatomy of the GON in the distal location or the position of the nerve in relation to bony landmarks in the proximal location in living patients.

DIAGNOSTIC APPLICATIONS

Sonographic changes in some pathological conditions of peripheral nerves have been well characterized [8]. However, there is still little known about changes in the GON. Cho JC. et al. described a significant increase in cross-sectional area and nerve circumference in patients with occipital neuralgia on the symptomatic sides. The cross-sectional area of the nerve did not depend on the severity of the headaches. Moreover, they showed the correlation of the cross-sectional area with the BMI. Hence, the cross-sectional area and BMI ratio may be more useful in diagnostic applications [5]. A similar mechanism associated with the GON entrapment, as in occipital neuralgia, may have an essential role in the pathogenesis of primary headaches [2]. Therefore, we think similar morphological changes can be seen in sonographic examinations of patients with these conditions. However, we did not find any studies concerning that issue.

THE GON BLOCKADE UNDER SONOGRAPHIC GUIDANCE

The GON block is a procedure of injecting a small dose of local anesthetic (lidocaine, bupivacaine, chirocaine) and/or steroid around the GON.

The GON block is reported to be useful in occipital neuralgia [9]. It has a clinical application in cervicogenic headaches resulting in 2-24 weeks of analgesia depending on the type of block localization [10]. Leinisch-Dahlke E. et al. suggest that this procedure is ineffective in chronic tension-type headaches, but the study was performed on a small sample of 15 patients [11]. The GON block is likely an adequate option for the acute management of migraine headache and proves to be equally effective across different age and gender groups [12].

For a long time, blocks of the GON have been performed without target visualization, based on exterior landmarks only. The ultrasound-guided blockade is likely to be a more effective technique than blind blockade in occipital headache treatment [7]. The conventional visionless technique of GON block just medial to the pulsation of the OA at the level of the superior nuchal line was inadequate due to intramuscular infiltration and blocks of other nearby nerves, such as branches of the lesser and third occipital nerve and even the greater auricular nerve. In patients with diversed anatomy, sightless injection in this area can cause unwanted and alarming complications even such as sudden coma [13]. The base for using a GON block in headache treatment arrives from evidence of the confluence of sensory input to the trigeminal nucleus caudalis neurons from both cervical and trigeminal fibers [14, 15]. There are many ways of GON block under sonographic guidance – the first being a distal block circa ~2–3 cm lateral to the EOP and the second proximal block where GON is superficial to the OCI muscle. In the study published by M. Greher et al., the success rate of a simulated GON block was 80% (95% confidence interval: 58–93%) in the distal and 100% (95% confidence interval: 86–100%) in the proximal approach. The study was carried out on 10 embalmed cadavers placed in a prone position with the head and neck flexed and injected with 0.1 ml of indocyanine green. The imitation block was categorized as successful if it dyed the targeted nerve and this nerve was identified as the GON by anatomical dissection [6]. Other ways include injection into the medial head of the SSC muscle at the C1 level of the cervical vertebra, where both GON and the third occipital nerve enter this muscle, in close proximity, which gives the possibility to block them simultaneously [16]. The study follow-up designed to compare two distinguishable US-guided techniques for blocking the GON demonstrated that both distal and proximal techniques can provide a short-term improvement in headache intensity, reduction in the number of headaches days per week, and an improvement in sleep interruptions. In this study, GON block was performed with bupivacaine and methylprednisolone acetate. The primary outcome was the contrast in the Numerical Rating Score (NRS) for headache intensity at 1 month. There were no significant adverse effects [17]. Another study proved that Ultrasound-guided GON blocks may provide superior pain reduction at 4 weeks when compared with landmark-based GON blocks for patients with occipital neuralgia or cervicogenic headache [18].

CONCLUSION

Primary headaches are an essential issue that should be addressed, as they can severely impact a person's quality of life. In past years new techniques have been developed that utilize sonography. Therefore, the anatomy of the GON has become an important topic. Yet, the sonographic anatomy and variability of the nerve have not been fully explored, especially in the distal location and living patients. Furthermore, to our knowledge, morphological changes in the ultrasound examination of the nerve in primary headaches have not been described in any publications. Evidence of the role of the GON compression in the pathogenesis of primary headaches and the results of the studies on patients with occipital neuralgia suggest that this topic is important.

The GON blocks using anesthetics and/or steroids have been used and are proven to be advantageous in occipital neuralgia, cervicogenic, and migraine headaches resulting in time-limited analgesia, and thus may be used as a medical practice for patients with specific types of headaches. Unfortunately, there is some evidence that GON block is ineffective in chronic tension-type headaches, therefore, other ways to relieve pain must be determined in these patients. Ultrasound-guided block seems to be more advantageous in comparison to the visionless technique primarily due to undesirable complications, among them the most dangerous is a coma. This fact suggests replacing a sightless GON block with an ultrasound-guided block. Furthermore, the topic of ultrasound-guided GON block technique localization should be thoroughly explored. More studies should be performed to determine whether the proximal or distal block is more effective. Likewise, we endorse more research on the intricacies of both ultrasound-guided techniques.

REFERENCES

[1] J. Li and A. Szabova, "Ultrasound-Guided Nerve Blocks in the Head and Neck for Chronic Pain Management: The Anatomy, Sonoanatomy, and Procedure," 2021, [Online]. Available: www.painphysicianjournal.com

[2] P. Blake and R. Burstein, "Emerging evidence of occipital nerve compression in unremitting head and neck pain," *Journal of Headache and Pain*, vol. 20, no. 1, Jul. 2019, doi: 10.1186/s10194-019-1023-y.

[3] J. Olesen, "Headache Classification Committee of the International Headache Society (IHS) The International Classification of Headache Disorders, 3rd edition," *Cephalalgia*, vol. 38, no. 1. SAGE Publications Ltd, pp. 1–211, Jan. 01, 2018. doi: 10.1177/0333102417738202.

[4] L. J. Stovner *et al.*, "Global, regional, and national burden of migraine and tension-type headache, 1990–2016: a systematic analysis for the Global Burden of Disease Study 2016," *Lancet Neurol*, vol. 17, no. 11, pp. 954–976, Nov. 2018, doi: 10.1016/S1474-4422(18)30322-3.

[5] J. C. S. Cho, D. W. Haun, N. W. Kettner, F. Scali, and T. B. Clark, "Sonography of the normal greater occipital nerve and obliquus capitis inferior muscle," *Journal of Clinical Ultrasound*, vol. 38, no. 6, pp. 299–304, Jul. 2010, doi: 10.1002/jcu.20693.

[6] M. Greher, B. Moriggl, M. Curatolo, L. Kirchmair, and U. Eichenberger, "Sonographic visualization and ultrasound-guided blockade of the greater occipital nerve: A comparison of two selective techniques confirmed by anatomical dissection," *Br J Anaesth*, vol. 104, no. 5, pp. 637–642, 2010, doi: 10.1093/bja/aeq052.

[7] J. H. Shim *et al.*, "Ultrasound-guided greater occipital nerve block for patients with occipital headache and short term follow up," *Korean J Anesthesiol*, vol. 61, no. 1, pp. 50–54, Jul. 2011, doi: 10.4097/kjae.2011.61.1.50.

[8] F. O. Walker, "Ultrasonography in Peripheral Nervous System Diagnosis," 2017, Accessed: Dec. 23, 2022. [Online]. Available: ContinuumJournal.com

[9] C. Skinner and S. Kumar, "Ultrasound-Guided Occipital Nerve Block for Treatment of Atypical Occipital Neuralgia," *Cureus*, Oct. 2021, doi: 10.7759/cureus.18584.

[10] G. R. Lauretti, S. W. R. O. Corrêa, and A. L. Mattos, "Efficacy of the Greater Occipital Nerve Block for Cervicogenic Headache: Comparing Classical and Subcompartmental Techniques," *Pain Practice*, vol. 15, no. 7, pp. 654–661, Sep. 2015, doi: 10.1111/papr.12228.

[11] E. Leinisch-Dahlke, T. Jürgens, U. Bogdahn, W. Jakob, & A. May, and A. May, "Greater occipital nerve block is ineffective in chronic tension type headache," 2005.

[12] S. M. Allen, F. Mookadam, S. S. Cha, J. A. Freeman, A. J. Starling, and M. Mookadam, "Greater occipital nerve block for acute treatment of migraine headache: A large retrospective cohort study," *Journal of the American Board of Family Medicine*, vol. 31, no. 2, pp. 211–218, Mar. 2018, doi: 10.3122/jabfm.2018.02.170188.

[13] T. Sprenger and C. L. Seifert, "Coma after greater occipital nerve blockade in a patient with previous posterior fossa surgery," *Headache*, vol. 53, no. 3, pp. 548–550, Mar. 2013, doi: 10.1111/head.12015.

[14] T. Bartsch and P. J. Goadsby, "Stimulation of the greater occipital nerve induces increased central excitability of dural afferent input," 2002.

[15] W. Young, B. Cook, S. Malik, J. Shaw, and M. Oshinsky, "The first 5 minutes after greater occipital nerve block," *Headache*, vol. 48, no. 7, pp. 1126–1128, Jul. 2008, doi: 10.1111/j.1526-4610.2008.01146.x.

[16] K. Kariya *et al.*, "Anatomical basis for simultaneous block of greater and third occipital nerves, with an ultrasound-guided technique," *J Anesth*, vol. 32, no. 4, pp. 483–492, Aug. 2018, doi: 10.1007/s00540-017-2429-9.

[17] D. Flamer *et al.*, "Comparison of two ultrasound-guided techniques for greater occipital nerve injections in chronic migraine: A double-blind, randomized, controlled trial," *Reg Anesth Pain Med*, vol. 44, no. 5, pp. 595–603, May 2019, doi: 10.1136/rapm-2018-100306.

[18] N. R. Kissoon *et al.*, "Comparative Effectiveness of Landmark-guided Greater Occipital Nerve (GON) Block at the Superior Nuchal Line Versus Ultrasound-guided GON Block at the Level of C2: A Randomized Clinical Trial (RCT)," *Clinical Journal of Pain*, vol. 38, no. 4, pp. 271–278, Apr. 2022, doi: 10.1097/AJP.0000000000001023.

Finito di stampare da
Logo s.r.l. – Borgoricco (PD) – Italia

IJAE
Italian Journal of Anatomy and Embryology
Vol. 127, N. 1 – 2023

€ 26,00 (for Italy)